Neuromicrophysiological systems with integrated electrodes for morphological and electrophysiological evaluations of 3D neuronal networks

Dissertation

zur Erlangung des Grades eines

Doktors der Naturwissenschaften

der Mathematisch-Naturwissenschaftlichen Fakultät

und

der Medizinischen Fakultät

der Eberhard-Karls-Universität Tübingen

vorgelegt

von

Fulya Ersoy

aus Konya, Türkei

2024

Tag der mündlichen Prüfung: 11.11.2024

Dekan der Math.-Nat. Fakultät: Prof. Dr. Thilo Stehle

Dekan der Medizinischen Fakultät: Prof. Dr. Bernd Pichler

1. Berichterstatter: Prof. Dr.Peter Loskill

2. Berichterstatter: Prof. Dr.Stefan Liebau

Prüfungskommission: Prof. Dr. Stefan Liebau

Prof. Dr. Peter Loskill

Prof. Dr. Simon J. Clark

Prof. Dr. Lena Smirnova

Erklärung / Declaration:

Ich erkläre, dass ich die zur Promotion eingereichte Arbeit mit dem Titel:

“Neuromicrophysiological systems with integrated electrodes for morphological and electrophysiological evaluations of 3D neuronal networks” selbständig verfasst, nur die angegebenen Quellen und Hilfsmittel benutzt und wörtlich oder inhaltlich übernommene Stellen als solche gekennzeichnet habe. Ich versichere an Eides statt, dass diese Angaben wahr sind und dass ich nichts verschwiegen habe. Mir ist bekannt, dass die falsche Abgabe einer Versicherung an Eides statt mit Freiheitsstrafe bis zu drei Jahren oder mit Geldstrafe bestraft wird.

I hereby declare that I have produced the work entitled “Neuromicrophysiological systems with integrated electrodes for morphological and electrophysiological evaluations of 3D neuronal networks”, submitted for the award of a doctorate on my own (without external help), have used only the sources and aids indicated and have marked passages included from other works, whether verbatim or in content, as such. I swear upon oath that these statements are true and that I have not concealed anything. I am aware that making a false declaration under oath is punishable by a term of imprisonment of up to three years or by a fine.

Tübingen, den ....

Datum / Date Unterschrift /Signature

SUMMARY

Neurological diseases are increasingly becoming a burden on society. Their prevalence is anticipated to grow as life spans increase, given that many neurodegenerative diseases are age-related. This research aims to develop platforms to study neurological diseases in vitro, facilitating a deeper understanding of their phenotypes. Additionally, the neuro-microphysiological systems (*NeuroMPS*) developed in this study provide platforms for conducting drug and neurotoxic screenings with multiple simultaneous readouts.

In this study, two *NeuroMPS*s were developed to investigate 3D neuronal networks in vitro. *NeuroMPS 1.0*, featuring 18 wells, is designed to study ECM-supported cultures, while *NeuroMPS 2.0*, with 9 wells, is intended to study neurospheres. Both *NeuroMPS*s are integrated with capped microelectrodes, which are novel tools enabling noninvasive electrophysiological readouts via neurites. The complete glass design aims for simultaneous morphological readouts, and the open-well design facilitates effluent analysis.

The validation process for *NeuroMPS 1.0* and *NeuroMPS 2.0* was thorough, ensuring the reliability and robustness of these platforms for studying neurological diseases. *NeuroMPS 1.0* was validated using co-cultures of neurons, astrocytes, and microglia derived from primary murine sources. *NeuroMPS 2.0* was validated with human neurospheres differentiated from neural progenitor cells. Morphological readouts were performed via immunocytochemistry, live imaging of GFP-transduced cells, and fluorescent dyes. The synaptic connections of neuronal circuits were confirmed using calcium imaging and electrophysiological recordings. Network functionality was evaluated using various antagonists (PTX, BIC, CNQX, APV), sodium channel blockers (TTX), and potassium channel blockers (4-AP). Rotenone, a neurotoxin, is used to highlight the sensitivity of the *NeuroMPS*s. The result of the neurotoxicity assay has shown that electrophysiological alterations were detected earlier than morphological and metabolic changes following toxin application. This indicates that *NeuroMPS*s provide early detection capabilities through electrophysiological readouts.

In conclusion, *NeuroMPS*s emerge as innovative tools for studying 3D neuronal networks, facilitating disease modeling, and screening drugs or toxins targeting the central nervous system. These platforms hold great promise for the future of neurological research, inspiring hope for more effective disease modeling and drug screening in the years to come.

The development of *NeuroMPS 1.0* was funded by the Baden Württemberg Stiftung GmbH under the grant agreement MIVT-7 (NEWRON-3D), and the development of *NeuroMPS 2.0* was funded by EUROSTARS under the grant agreement E!115217 (NEUROCHIP).

ZUSAMMENFASSUNG

Neurologische Erkrankungen werden zunehmend zu einer Belastung für die Gesellschaft. Ihre Häufigkeit nimmt mit steigender Lebenserwartung zu, da viele neurodegenerative Krankheiten altersbedingt sind. Ziel dieser Forschung ist die Entwicklung von Plattformen zur Untersuchung neurologischer Erkrankungen in vitro, um ein tieferes Verständnis ihrer Phänotypen zu ermöglichen. Darüber hinaus bieten die in dieser Studie entwickelten neuro-mikrophysiologischen Systeme (*NeuroMPS*) Plattformen zur Durchführung von Medikamenten- und Neurotoxizitäts-Screenings mit mehreren gleichzeitigen Readouts.

In dieser Studie wurden zwei *NeuroMPS* entwickelt, um 3D neuronale Netzwerke in vitro zu untersuchen. *NeuroMPS 1.0*, mit 18 Wells, ist zur Untersuchung von ECM-unterstützten Kulturen konzipiert, während *NeuroMPS 2.0*, mit 9 Wells, für die Untersuchung von Neurosphären gedacht ist. In beiden *NeuroMPS* sind gekappte Mikroelektroden integriert, die als neuartige Werkzeuge nicht-invasive elektrophysiologische Auslesungen über Neuriten ermöglichen. Das vollständige Glasdesign zielt auf gleichzeitige morphologische Readouts ab, und das Open-Well-Design erleichtert die Analyse von Effluenten.

Der gründliche Validierungsprozess für *NeuroMPS 1.0* und *NeuroMPS 2.0* stellte die Zuverlässigkeit und Robustheit dieser Plattformen zur Untersuchung neurologischer Erkrankungen sicher. *NeuroMPS 1.0* wurde unter Verwendung von Co-Kulturen aus Neuronen, Astrozyten und Mikroglia, die aus primären murinen Quellen stammen, validiert. *NeuroMPS 2.0* wurde mit menschlichen Neurosphären validiert, die aus neuralen Vorläuferzellen differenziert wurden. Morphologische Readouts wurden durch Immunzytochemie, Live-Imaging von GFP-transduzierten Zellen und fluoreszierende Farbstoffe durchgeführt. Die synaptischen Verbindungen neuronaler Schaltkreise wurden mittels Kalzium-Imaging und elektrophysiologischen Aufzeichnungen bestätigt. Die Netzwerkfunktionalität wurde unter Verwendung verschiedener Antagonisten (PTX, BIC, CNQX, APV), Natriumkanalblocker (TTX) und Kaliumkanalblocker (4-AP) gezeigt. Rotenon, ein Neurotoxin, wurde verwendet, um die Empfindlichkeit der *NeuroMPS* zu verdeutlichen. Die Ergebnisse zeigten, dass elektrophysiologische Veränderungen früher als morphologische und metabolische Veränderungen nach der Toxinapplikation erkannt wurden. Dies weist darauf hin, dass NeuroMPS frühzeitige Erkennungsmöglichkeiten durch elektrophysiologische Readouts bieten.

Zusammenfassend lassen sich *NeuroMPS* als innovative Werkzeuge zur Untersuchung von 3D neuronalen Netzwerken, zur Krankheitsmodellierung und zum Screening von Medikamenten oder Toxinen, die auf das zentrale Nervensystem abzielen, einsetzen. Diese Plattformen versprechen viel für die Zukunft der neurologischen Forschung und wecken

Hoffnungen auf effektivere Krankheitsmodelle und Medikamentenscreenings in den kommenden Jahren.

Die Entwicklung von *NeuroMPS 1.0* wurde von der Baden-Württemberg Stiftung GmbH im Rahmen des Fördervertrags MIVT-7 (NEWRON-3D) finanziert, und die Entwicklung von *NeuroMPS 2.0* wurde von EUROSTARS im Rahmen des Fördervertrags E!115217 (NEUROCHIP) finanziert.

ACKNOWLEDGMENTS

I want to thank Dr. Paolo Cesare for his supervision and for introducing me to neuro microphysiological systems. I am also immensely thankful to Dr. Laura Jentsch and Dr. Beatriz Martinez Molina for being outstanding colleagues and mentoring me in neuroscience. Their expertise and support have significantly contributed to my professional development. I want to thank Peter Heutink and Prof. Dr. Stefan Liebau for their guidance and being on my Advisory Board. I want to extend my sincere thanks to Prof. Dr. Katja Schenke-Layland for providing an excellent research environment at NMI. The facilities and resources available have greatly enhanced my research experience. Special thanks go to Dr. Peter Jones and Michael Mierjezewski for their insightful technical discussions regarding microfabrication. Their knowledge and willingness to help have been crucial in overcoming various challenges in my research. I also want to mention Emilio Pedro Gonzales and Jasmin Schäfer for their support during my electrophysiology experiments. I want to thank Lisa-Marie Erlandsdotter for providing the cells and for her support during my final year.

Joining MicroOrganoLab under Prof. Peter Loskill's guidance has been the most rewarding experience of my PhD. I am deeply grateful for his unwavering support, the opportunities he provided, and his invaluable guidance, which have significantly shaped my research journey. I am also deeply appreciative of the entire MicroOrganoLab team, especially Dr. Tanvi Shroff, Dr. Eduardo Bras, Katharina Schlünder, Alessia Moruzzi, Svenja Wingerter, and all other members of the team for their help, support, and friendship. Their camaraderie and encouragement have made my PhD journey a rewarding and enjoyable experience.

Last but not least, I want to thank Matthijs van der Moolen, who has been a fantastic teammate and a great friend throughout my PhD. We embarked on this PhD journey together, encouraging each other through good and bad days, especially during the pandemic and all the challenges we faced as a team. I also thank Marc Himmelbach and Monika Lam for their outstanding support and guidance throughout my PhD. Being a part of GTC was a privilege.

I am deeply thankful to Mülazlar: Bahar, Ayse, Kübra, Fazilet, Öznur, Kerem, and Ceyhun. Without their camaraderie and support, I wouldn’t have reached this point.

Tabii ki canım ailem, sizin desteğiniz olmadan bugün başardığım hiçbir şeyi başarmış olmazdım. İyi ki benim ailemsiniz. Canım anneciğim, babacığım ve de canım kardeşim Furkan, teşekkür ederim her an yanımda olduğunuzu hissettirdiğiniz için. Elbette ki, canım kocam Aziz Aykut’un varlığı olmadan bu son seneyi asla atlatmam mümkün olmazdı, iyi ki yanımdaydın, teşekkür ederim desteğin ve hayatımı kolaylaştırdığın için.

ABBREVIATIONS

2D	Two dimensional
3D	Three dimensional
AD	Alzheimer's disease
PD	Parkinson's disease
MEA	Microelectrode Array
MPS	Microphysiological System
CNS	Central Nervous System
ECM	Extracellular matrix
SEM	Scanning electron microscopy
mV	Millivolt
EPSP	Excitatory postsynaptic potential
IPSP	Inhibitory postsynaptic potential
GABA	Gamma-aminobutyric acid
RNA	Ribonucleic acid
iPSC	Induced pluripotent stem cell
PDMS	Polydimethylsiloxane
APTES	(3-Aminopropyl)triethoxysilane
HBSS	Hank's balanced salt solution
TUBB3	Tubulin beta 3
MAP2	Microtubule-associated protein 2
IBA1	Ionized calcium-binding adaptor protein 1
PFA	Paraformaldehyde
DPBS	Dulbecco's phosphate saline buffer
GFAP	Anti-glial-specific type-III intermediate filament protein
ICC	Immunocytochemistry
DMSO	Dimethyl sulfoxide
PAX-6	Paired box protein-6
SOX-2	Sex-determining region Y-box protein-2
NPC	Neuro progenitor cell
BDNF	Brain-derived neurotrophic factor
GDNF	Glial cell line-derived neurotrophic factor
EGF	Epidermal growth factor

FGF	Fibroblast growth factor
ICFC	Intracellular flow cytometry
FC	Flow cytometry
Hz	Hertz
ms	millisecond
s	second
h	hour
CμE	Capped microelectrode
MFR	Mean firing rate
BFR	Burst frequency rate
MBD	Mean burst duration
%SinB	Percentage of spikes in bursts
NBF	Network burst frequency
%BinNB	Percentage of bursts in network burst
PTX	Picrotoxin
TTX	Tetrodotoxin
BIC	Bicuculine
CTRL	Control
NMDA	N-methyl-D-aspartic acid
ATP	Adenosine triphosphate
GFP	Green fluorescent protein
AAV	Adeno-associated virus

TABLE OF CONTENTS

LIST OF TABLES

LIST OF FIGURES

1. INTRODUCTION

Neurological disorders, such as Alzheimer's disease (AD) and Parkinson's disease (PD), constitute significant global health challenges and rank as the second leading cause of death in Europe[1]. The complexity of these diseases, coupled with the intricate mechanisms of the brain, presents considerable obstacles for pharmaceutical research endeavors aimed at developing effective treatments. Traditional experimental models, including animal models and two-dimensional (2D) in vitro platforms, frequently fail to replicate human neurological characteristics accurately, resulting in limited predictive accuracy for clinical trials[2, 3].

Recent advancements have facilitated the development of three-dimensional (3D) microphysiological systems (MPS), which emulate brain-like neuronal structures in vitro[4-6]. These systems incorporate principles from molecular and cellular biology, bioengineering, material sciences, and computational modeling to mimic the complexity of the brain in 3D. By integrating multiple cell types, 3D histoarchitecture, and cell-to-cell interactions, these platforms surpass the capabilities of conventional monolayer cultures.

This research is centered on developing and validating a novel microphysiological system designed to study 3D neuronal circuits. The objective is to provide a more in vivo-like platform that closely recapitulates brain neuronal networks, thereby enhancing predictability in toxicology, drug screening, and disease modeling studies. The approach integrates various technologies, including 3D cell culture of primary murine and induced pluripotent stem cell (iPSC)-derived neuronal cultures, microfluidic techniques for system compartmentalization, and microelectrode arrays (MEA) for recording electrophysiological activity.

The interdisciplinary nature of this study enables simultaneous morphological and functional assessments of 3D neuronal circuits within a single device. The system facilitates detailed characterization of morphological properties at the subcellular level and quantification of released molecules, which is crucial for assessing neuronal function. Additionally, the device allows non-invasive recording of electrophysiological activities. The system offers enhanced throughput and reproducibility regarding cell culture and electrophysiological recordings and is compatible with functional, morphological, and metabolic readouts.

This thesis begins by describing fundamental neurophysiology concepts and the principal techniques utilized in neuroscience. It then introduces micro-physiological systems and their applications in central nervous system (CNS) studies, underscoring current challenges in the field. The thesis then presents two novel micro-physiological systems developed during this research, along with validation studies. The thesis concludes with a discussion of potential future applications and the advantages these systems offer to the field.

1.1. Neurophysiology

In the 19th century, advancements in microscopy and staining techniques allowed scientists to confirm that the brain, like other organs, comprises individual cells. The "cellular theory of the CNS," articulated by Ramón y Cajal[7] and Camillo Golgi[8], gained validation in the 20th century, culminating in both researchers being awarded the Nobel Prize in Medicine for their pioneering contributions. Subsequent research by Charles Sherrington further elucidated that neuronal communication occurs through electrical transmission[9, 10].

Today, it is well-established that the brain, in conjunction with the spinal cord, constitutes the central nervous system. This system functions as the central processing unit, receiving and coordinating information via electrical signals, thereby regulating all bodily functions. Despite this comprehensive understanding, numerous facets of neuronal communication and its dysfunctions in neurological diseases remain insufficiently explored. The brain comprises two types of cells: neurons, which are responsible for electrical signaling, and glial cells, which provide support, protection, and metabolic assistance to neurons. The human brain contains approximately 86 billion neurons[11], characterized by significant heterogeneity. Neurons are classified based on their morphology, postsynaptic action (inhibitory, excitatory, or modulatory), type of neurotransmitter secreted, and connectivity (interneuron or projection neuron)[12].

Neurons possess two primary compartments: the somatodendritic and axonal compartments. The somatodendritic region encompasses dendrites, which extend from the neuronal soma and serve as the principal locus for receiving signals from other neurons. These signals are received at dendritic spines, integrated, and summed at the axon hillock, the proximal somatic area. Depending on their function, neurons may have between one to 100,000 afferent connections[13]. The axonal compartment typically consists of a single projection with multiple branches, responsible for the rapid conduction of electrical signals by modulating the plasma membrane's electrical polarity. This compartment also transports essential proteins to the axon's distal part, known as the synaptic bouton or axon terminal, where neurotransmitters are encapsulated for release into the synaptic cleft[14].

Neurons maintain a membrane potential due to an unequal distribution of ions, with selective permeability to ions such as K^+, which is more concentrated intracellularly, and Ca^{2+}, Na^+, and Cl^-, which are more concentrated extracellularly[15]. The membrane voltage represents the difference between the internal and external surfaces of the neuronal membrane, with a resting potential of approximately -70 mV. Upon receiving synaptic input, the membrane either depolarizes or hyperpolarizes. If the summed signals at the axon hillock surpass the threshold

potential (typically -55 mV), an action potential is initiated, causing an abrupt depolarization of the membrane[14].

Voltage-gated channels play a crucial role in action potential transmission. When the membrane potential increases, sodium channels at the axon hillock open, allowing Na^+ ions to enter the cell. Subsequently, the slower-opening potassium channels permit K^+ ions to exit to the extracellular space. The influx of Na^+ elevates the cell's charge, depolarizing the membrane to approximately +40 mV. At this peak, Na^+ channels close, and K^+ channels remain open, leading to membrane hyperpolarization as K^+ ions continue to exit until these channels close. This phase is termed the refractory period, during which another action potential cannot be triggered. Na^+ and K^+ ions are then pumped back to reestablish the resting membrane potential. The action potential propagates along the axon, ensuring unidirectional signal transmission from the soma to the axon terminal[16, 17].

The amplitude of an action potential is invariant, adhering to the "all-or-none" principle, which implies that the frequency, rather than the amplitude, of action potentials encodes the response to a stimulus. Upon reaching the axon terminal, the electrical signal is transduced into chemical communication at the synapse. Most CNS synapses are chemical, with the synaptic cleft being the space between the presynaptic terminal and the postsynaptic neuron. The arrival of the action potential at the synaptic bouton opens voltage-gated Ca^{2+} channels, causing an influx of Ca^{2+} that triggers the release of neurotransmitters into the synaptic cleft[16]. These neurotransmitters bind to receptors on the postsynaptic neuron, resulting in either depolarization (EPSP) or hyperpolarization (IPSP), contingent on the neurotransmitter and receptor type[13, 15]. Common neurotransmitters include acetylcholine, glutamate, glycine, and GABA. Neurons can synthesize and release multiple neurotransmitters, with the synthesis occurring locally in the axon terminal, except for neuropeptides, which are produced in the cell body[18, 19].

Neurons form intricate networks with diverse firing patterns and rates, underpinning brain functions such as learning, memory, and decision-making. Understanding the formation, functionality, and alterations of these networks in disease remains a pivotal challenge in neuroscience.

1.2. Techniques employed in neuroscience research

The intricate nature of the brain has posed significant challenges in neurobiology. In recent decades, major progress in this field has largely stemmed from technological advancements, especially in optics and electronics, enabling modern neuroscientists to employ various techniques to study the central nervous system.

Neuroscientists have developed methods to study single neurons or neuron groups due to the complexity of neural networks. This targeted approach simplifies neurocircuit complexity, allowing for the correlation of specific brain regions or cultured neuron data with overall brain properties. In vitro systems in neurobiology often provide single-neuron resolution, yielding valuable insights not readily obtainable from in vivo models. This section emphasizes techniques utilized in neurobiology, including imaging, molecular analysis, transcriptomics, and electrophysiology, and details prevalent in vitro morphological and functional tools.

1.2.1. Imaging techniques

Imaging technologies have significantly advanced our ability to understand complex neuronal features. Modern imaging methods can be implemented as live imaging or post-fixation in culture. Visualization is enhanced through immunolabeling with antibodies or tracking with fluorescent proteins under cell-type-specific promoters.

Whole-brain imaging techniques, such as magnetic resonance imaging (MRI), computerized tomography (CT), and cerebral angiography, have been pivotal in structural brain studies in vivo. These methods, widely utilized in clinical neurology, facilitate identifying and monitoring vascular issues and neuronal disorders. Functional brain imaging techniques, including functional MRI, positron emission tomography (PET), and electroencephalography (EEG), enable observing brain activation in response to specific mental activities. However, these techniques primarily elucidate structural patterns rather than direct stimulus-response correlations, focusing on comparative analyses between healthy and pathological brain conditions.

Immunocytochemistry is the most prevalent in vitro technique for imaging 2D and 3D culture models. In this method, samples are fixed and labeled with marker-specific antibodies, then visualized with high resolution under a microscope. The advent of confocal microscopy has further enhanced image quality, facilitating the study of synaptic molecules with advanced imaging techniques. Live-cell imaging is conducted either with cytoplasmic dyes or fluorescent protein-containing viruses, which can target the desired cell type, resulting in fluorescence-expressing cells that are easily imaged with fluorescence microscopes.

1.2.2. Electrophysiology techniques

Electrical activity demonstrates synaptic connectivity within a neural network, indicating efficient communication flow. Electrophysiological activity can be explored using imaging techniques or electrode-based recording methods. Various Ca^{2+} indicators are employed for functional readouts, enabling the imaging of ion influx into neurons, which reflects alterations in cellular activity[20]. Notable Ca^{2+} influx occurs during chemical synapses in axon terminals,

making Ca^{2+} markers indispensable in optical microscopy for minimally invasive real-time observation of neural activity. This methodology allows the visualization of multiple neurons with high spatial resolution via fluorescence, confocal, or two-photon microscopy. Despite technological advances, capturing activity in three-dimensional neuronal cultures remains challenging, and the temporal resolution of fluorescence peaks is limited compared to electrode-based recordings. Moreover, because Ca^{2+} is involved in various cellular functions, such as intracellular signaling and synaptic plasticity, Ca^{2+} dyes act as surrogate indicators rather than direct measures of action potentials[21, 22].

Electrode-based recordings are fundamental for investigating neurons' electrical properties in vitro. Depending on electrode positioning, these recordings encompass patch-clamp, intracellular, and extracellular techniques. The patch-clamp technique involves close coupling of the electrode to the neuronal membrane. Intracellular recordings insert microelectrodes within neurons, while extracellular recordings position electrodes outside cells. Each method addresses specific research questions: patch-clamp is ideal for studying ion channel states, while extracellular recording is suited for capturing the activity of multiple neurons. Intracellular recordings, pioneered by Hodgkin and Huxley[23], measure voltage differences between intracellular electrodes and extracellular references, offering insights into single-channel mechanisms and neuronal voltage changes. Despite providing detailed information about single-channel and voltage changes, these techniques require precise electrode placement, limiting recordings to a few neurons per experiment.

Extracellular recordings are essential for simultaneously capturing multiple neurons' activity and studying neuronal circuit dynamics and plasticity. External electrodes measure rapid voltage changes during spikes. Micro-electrode arrays (MEAs), utilized for over two decades, record the electrical activity of neurons in brain slices or dissociated cultures[24]. MEAs facilitate simultaneous recording and electrical stimulation of multiple neurons, enabling studying neuronal network formation and properties. Extracellular recordings capture action potentials with varying waveforms, offering non-invasive, repeatable measurements on the same sample, thereby enhancing research productivity[25-27].

In conclusion, these advanced imaging and electrode-based techniques provide a comprehensive understanding of neuronal structure and function, delivering crucial insights into the complexities of brain activity and neurobiological processes.

1.2.3. Optogenetics

Optogenetics is a novel technique in neuroscience that enables the precise manipulation and observation of neuronal activity in both in vitro and in vivo settings. In vitro applications often involve cultured neurons (2D or 3D)[27, 28] or brain slices[29] that are genetically engineered

to express light-sensitive proteins like channelrhodopsins and halorhodopsins. This setup allows detailed analysis of synaptic transmission, neuronal connectivity, and fundamental neural properties under controlled conditions.

Optogenetics permits the modulation of neuronal activity within the intact brains of living organisms, offering insights into the functional organization of neural circuits and their roles in behavior and cognition. Using targeted light delivery systems, researchers can selectively activate or inhibit specific neuronal populations in freely moving animals, thereby elucidating the causal relationships between neuronal activity and complex behaviors. This technique has been crucial in studying various brain functions, such as sensory processing, motor control, and emotional regulation[30].

In conclusion, optogenetics bridges the gap between molecular neuroscience and behavioral studies, providing a comprehensive method to investigate the intricate workings of the nervous system with unmatched precision and specificity.

1.2.4. Transcriptomics

Transcriptomics is defined by Lowe et al.[31] as the study of RNA transcripts produced by the genome, studying these transcripts has incredibly advanced neuroscience research by providing comprehensive insights into gene expression in the brain. This field has transformed our understanding of gene regulation in neural development, function, and plasticity[32]. A major advance in neuroscience through transcriptomics is the ability to map the brain's cellular diversity. Single-cell RNA sequencing (scRNA-seq) allows researchers to explore the heterogeneity of neural cell populations, identifying different cell types and their unique gene expression patterns. This technique has revealed previously unknown neuron types and glial cells, deepening our understanding of the complexity and functionality of the brain[33, 34].

Transcriptomics has also illuminated the molecular mechanisms behind neurological disorders. By comparing the transcriptomes of healthy and diseased brains, researchers can pinpoint dysregulated genes and pathways involved in diseases such as Alzheimer's[35-37], Parkinson’s[37, 38], autism[39, 40], and schizophrenia[41, 42]. This knowledge is essential for developing targeted therapies and personalized medicine approaches. The data gained from transcriptomic analysis are also improving our understanding of how the brain responds to various stimuli, as well as learning and memory processes. Overall, transcriptomics has become a vital tool in neuroscience, advancing our understanding of brain biology and paving the way for new therapeutic strategies.

1.3. Microphysiological systems

A microphysiological system (MPS) is an in vitro model designed to replicate the complex physiological conditions of human tissues and organs. These systems integrate microfluidic technology with living cells, creating environments that closely mimic the specific conditions within human organs[43]. This allows for the detailed study of biological interactions and mechanical forces in a controlled setting. The significance of MPS lies in its superior ability to model human physiology compared to traditional cell cultures and animal models. Conventional 2D cell cultures lack the 3D structure and dynamic nature of actual tissues, and animal models often fail to predict human responses accurately due to interspecies differences. MPS addresses these limitations by providing a platform that closely simulates human organ functions, enabling more precise research into disease mechanisms, drug responses, and toxicology[44].

One major advantage of MPS is its potential to improve the predictability of preclinical testing. Many drug failures occur because current preclinical models do not reliably predict human reactions. By offering a more accurate and relevant model, MPS can enhance drug efficacy and safety assessment, potentially reducing the need for animal testing and accelerating the drug development process while cutting costs[45]. Additionally, MPS is invaluable for studying complex diseases that involve multiple organ systems or intricate cell interactions[46]. In cancer research, for instance, MPS can mimic the tumor microenvironment[47, 48], facilitating the study of cancer progression and metastasis under conditions that closely resemble those in the human body. Furthermore, MPS can model interactions between different organs, such as the liver, heart, and lung[49, 50], which is crucial for understanding systemic diseases and multi-organ toxicity[51]. MPS also holds promise for personalized medicine. By using patient-derived cells, these systems can model individual variations in disease and treatment responses, paving the way for more effective and customized therapies[52-54]. This is particularly beneficial for diseases with significant heterogeneity, like cancer and genetic disorders. MPS applications extend to brain models, including research on pain[55], neurotoxin screening[56-58], and disease modeling[59, 60].

In conclusion, microphysiological systems represent a groundbreaking approach to biomedical research, offering more accurate and human-relevant models for studying human physiology and disease. By bridging the gap between traditional in vitro models and animal studies, MPS has the potential to significantly enhance our understanding of disease mechanisms, improve drug development, and advance personalized medicine. As technology evolves, the applications and impact of MPS are expected to grow, further solidifying their role in advancing healthcare and biomedical research.

1.3.1. Neuro-micro physiological systems

Conventional 2D and animal models do not accurately represent in vivo conditions; thus, micro-physiological systems are essential to bridge the gap between in vitro research and clinical applications. In recent decades, the organ-on-chip concept has introduced a revolutionary approach to emulating neurophysiological conditions in vitro. By combining 3D culture techniques with microfluidic principles, researchers have been able to recreate the brain's microenvironment and provide a novel method for mimicking disease phenotypes in micro-physiological systems. The key components of neuro-microphysiological systems (*NeuroMPS*) include: i) the cell culture model, ii) the material of the *NeuroMPS*, and iii) integration with microelectrode arrays (MEAs).

1.3.1.1. Cell type

In vitro studies have traditionally utilized primary cell cultures derived from rodents despite the fact that chimpanzees exhibit the greatest anatomical and genetic similarities to humans[61]. The primary reason for this approach is the difficulty in obtaining cells from primates, given the ethical constraints and their limited availability. Rodents also share comparable neuroanatomy with humans and are more accessible than primates[62]. In recent decades, there has been a shift towards using human-originated cells to enhance the translatability of research findings. Despite this, animal-derived cells are still predominantly employed for proof-of-concept studies. While the data generated from these cells may not always be fully translatable to human pathologies, they remain valuable for the initial validation of systems. Nonetheless, the complexity of the rodent brain significantly differs from that of the human brain. In the long term, human-originated cells are likely to become the preferred source for the development of *NeuroMPS*.

Human cell sources can include primary human stem cells, which may be obtained from biopsies or postmortem samples. These cells have the ability to differentiate into various types of neurons and form synaptic connections[63, 64]. However, akin to primate research, ethical concerns and limited availability hinder the utilization of these cells. An alternative source is reprogrammed cells derived from fibroblasts, known as induced pluripotent stem cells (iPSCs), developed by Takahashi and Yamanaka[65, 66]. The advent of iPSCs in *NeuroMPS*[5, 6, 67, 68] has the potential to enable the creation of patient-specific models, allowing for precise in vitro modeling of neuronal disorders. Despite this, there are challenges associated with using iPSC-derived neurons. For instance, iPSCs may not fully preserve cellular functionalities and can exhibit significant differences depending on the differentiation technique employed. Additionally, reprogrammed cells may show genetic and protein variability, leading to reduced intra-cell type homogeneity[69].

1.3.1.2. Culture methods in *NeuroMPS*

In vitro models play a pivotal role in understanding CNS mechanisms. As the in vitro models develop, the culture systems employed in the models also vary depending on the application or the research question. 2D cultures, which are the traditional monolayers, have been very well-established in recent decades and are still heavily utilized due to their high throughput applications and lower experimental variability in contrast to in vivo models [70-72]. However, despite their ease of application in recording electrophysiological activity, 2D neuronal cultures lack the physiological complexity of the brain architecture, such as the vasculature, spatiotemporal architecture, and extracellular matrix. These shortcomings limit inter- and intra-cellular interactions, potentially leading to altered gene expression and neuronal activity compared to 3D models[73-76].

3D cell cultures, despite their challenges, hold great promise in replicating brain processes with greater accuracy. The incorporation of an extracellular matrix, although complex, is a hurdle that can be overcome. Hydrogels, such as Matrigel, provide ECM-like support and have been shown to enhance neuron viability[77, 78]. While the undefined nature of Matrigel complicates reproducibility, ongoing research is focused on overcoming these limitations. Even with these challenges, 3D cell cultures are a step forward in our quest to better emulate the intricate structure of the brain.

An alternative to hydrogel-supported 3D cultures is the use of assembled cell structures known as neurospheres or brain organoids. These 3D constructs originate from either induced pluripotent stem cells (iPSCs)[79] or neural progenitor cells[67] and undergo differentiation into neuronal and glial populations. The 3D structures offer a complexity comparable to in vivo conditions, making them particularly suitable for studying brain properties. Neurospheres facilitate the examination of disease phenotypes within a controlled environment while maintaining sufficient complexity. Additionally, the more sophisticated brain organoids, such as cerebral organoids[79, 80] and midbrain organoids[81-83], enable the investigation of the central nervous system's complexity and functionality.

While all culture systems are valuable for investigating pathophysiological processes, assembled cells (neuropheres and brain organoids) provide a distinctive interface between in vitro and in vivo neurobiology, showcasing advanced cell composition, maturation, and tissue architecture. Nevertheless, obtaining readouts from neurospheres and brain organoids is more restricted than hydrogel-supported 3D cultures. Assessing the morphology of organoids or neurospheres remains challenging, as does acquiring functional information from these structures. However, advances in imaging and clearing methods are improving the quality of readouts. Additionally, 3D cultures often suffer from inadequate or uneven cell nourishment,

leading to increased internal cell death. This issue is being addressed through improved design and the perfusion of *NeuroMPS*s, where nutrient diffusion is more efficient.

1.3.1.3. Technical approaches and material choice for *NeuroMPS*

Microphysiological system technology has been employed in neuroscience research for over two decades. The initial generation of *NeuroMPS*s predominantly utilized polydimethylsiloxane (PDMS), a silicon-based material that can be shaped through soft lithography[84-87]PDMS is highly valued for its flexibility, transparency, and air permeability, which facilitate high-resolution optical imaging. These properties have made PDMS a preferred material for more than a decade. However, PDMS chips have notable limitations, including non-reusability and incompatibility with certain hydrophobic compounds. These challenges have driven researchers to explore alternative materials for *NeuroMPS* applications that meet the requirements for high-quality imaging, throughput, reusability, and seamless integration with sensors and electrodes for in situ analysis.

Thermoplastics, such as polycaprolactone, have been employed to create 3D-printed nervous systems on chips for studying viral infections in the nervous system[88]. More recently, thermoplastic polyurethane has also been used to 3D print MPSs[89], demonstrating biocompatibility, durability, and flexibility comparable to PDMS. The advantages of thermoplastics include diverse fabrication methods, cost-effectiveness, and availability. However, MPSs produced with thermoplastics are still single-use, although they are more suitable for large-scale production compared to PDMS-based MPSs.

An alternative to PDMS and thermoplastic-based MPSs is glass-based MPSs[27, 90]. Glass-based systems enable high-quality morphological analysis as they do not suffer from compound absorption issues, thus providing reliable data for drug and toxin screenings. Additionally, their washability and autoclave compatibility make these systems reusable. Furthermore, the integration of sensors and electrodes on glass substrates is well-established and straightforward.

1.3.1.4. Integration of electrophysiological readouts to the *NeuroMPS*s

Neurons predominantly communicate via electrical signals, which poses a considerable challenge in evaluating the feasibility of functional readouts within neuronal culture systems. Section 1.2.2 elaborates on various methodologies for obtaining these readouts. To achieve the desired electrophysiological readout, the design of MPSs must be meticulously tailored. Specific modifications are necessary for techniques such as extracellular recording, patch-clamp, or calcium imaging. Researchers frequently utilize MEAs integrated into the platform substrate, calcium imaging, or occasionally a combination of both. These designs often incorporate compartmentalized structures interconnected by microchannels, which are

advantageous for examining axonal transport, unidirectional axonal growth, axonal regeneration, or the characteristics of neuronal networks in neurological disorders[25, 78].

Recording electrodes can be situated within the microchannels or within the tissue compartments[25]. Positioning the electrodes in the microchannels increases signal impedance, thereby enhancing the accuracy of electrical activity recordings from neurites rather than somas. This approach is also applicable to 3D *NeuroMPS*[27, 77, 78]. Brain organoids or neurospheres can be monitored from their surfaces or invasively to acquire information regarding ion channels in neuronal cells. Although techniques such as patch-clamp can obtain core electrical data from organoids, they have limitations, including low reproducibility and the requirement for high levels of expertise.

To overcome these challenges, Shin et al.[4] developed a 3D high-density multifunctional multi-shaft MEA to capture the internal structures of a human spinal cord organoid. Despite its advanced capabilities, the system exhibited low reproducibility. Alternatively, Park et al.[91] introduced a high-throughput 3D 'multifunctional mesoscale scaffold' for more extensive studies of neuronal assemblies, enabling non-invasive electrophysiological recording and optogenetic neuromodulation. Another innovative approach involved growing organoids around a mesh MEA to maintain electrodes at the organoid core[90]. Despite its potential, this technique also encountered low throughput and reproducibility issues. Soscia et al. utilized 3D vertically positioned microelectrodes within a hydrogel scaffold to record neuronal activity, but this method also demonstrated low reproducibility rates and a low likelihood of recording.

These technical advancements aim to provide more comprehensive insights into neuronal assemblies and circuits, potentially facilitating studies of central nervous system disorders. In this research, two *NeuroMPS*s with integrated electrodes for hydrogel-supported single-cell cultures and assembled neuronal cultures have been developed to address these challenges.

2. MATERIALS AND METHODS

2.1. Neuro micro physiological system (NeuroMPS)

NeuroMPS consists of a monolithic quartz glass piece and MEA. The monolithic glass piece is designed with Autodesk Inventor Software (Autodesk Inc., CA, USA) and produced by FEMTOprint SA (Switzerland). MEAs are designed with CleWin CAD software (WieWeb, Netherlands). Photomasks are ordered from Deltamask (Netherlands), and MEAs are produced by NMI TT (Reutlingen, Germany).

2.2. Microfabrication of capped microelectrodes on MEAs

MEAs are cleaned in hot DI water in an ultrasonic bath, then rinsed with isopropanol and dried in an oven (Heraus) under nitrogen at 120°C for 30 min. MEAs are treated with oxygen plasma (Piccolo, Plasma electronic GmbH, Germany) for 120 s before the process and then are baked at 150°C for 1 h to dehydrate the surface. Before spin coating, the substrates are equilibrated to room temperature for approximately 15 minutes. The MEAs are then placed on a spin coater (1001 S, CONVAC GmbH), and to obtain 3 µm thick micro tunnels, 1 ml SU-8 2002 (Kayaku Advanced Materials, USA) is dispensed with a pipette onto the plasma-treated MEA surface. The MEAs are spun at 500 rpm for 10 s, then accelerated to 1000 rpm and spun another 30s. They are followed by a soft bake at 95 °C for 2 min to evaporate the solvent and stabilize the photoresist on the surface. Once the MEAs are cooled to room temperature, the SU-8 is exposed using a SÜSS MA6 mask aligner (Süss Microtec SE, Germany) at 150 mJ/cm^2 through a photomask with an i-line filter that filters the UV light to achieve a wavelength of 365 nm. Immediately after the exposure, the MEAs are placed on a hotplate for post-exposure bake. The MEAs are ramped up to 95 °C at 3°C/min, baked for 2 minutes, then cooled down to room temperature. The structures are developed in mr-DEV 600 (Micro resist technology GmbH, Berlin, Germany) for 15 s and then rinsed in isopropanol. Before processing the second layer, the MEAs with SU-8 structures are baked at 150°C for 30 minutes (ramped 2°C/min) to prevent overdevelopment of the SU-8 during the next development steps of the fabrication process.

ADEX^{TM} TDFS A20, a dry film photoresist produced by DJ Microlaminates Inc. (Boston, USA), is used for the second layer. ADEX comes covered in PET cover foil and carrier foil. The cover foil is removed from the ADEX sheets with a tweezer and a pouch laminator (GMP Photonex@325, EF02015) used to laminate ADEX over SU-8 micro tunnels at 3 mm/s speed and 75 °C. The MEAs are rested at room temperature for approximately 10 minutes, and then the carrier foil is removed from the laminated ADEX sheets and exposed through the photomask. The exposed MEAs are immediately placed on a hot plate, ramped up to 65 °C at a speed of 3°C/min, and baked for an hour at 65°C for the post-exposure bake. The MEAs are

then cooled down to room temperature before development. The ADEX layer is developed in cyclohexanone for about 8 min and then rinsed in isopropanol. Once the capped microelectrodes are fabricated, the structures are placed in an oven, ramped up to 175 °C at 0.5 °C/min, baked for 30 minutes, and cooled down to room temperature.

2.3. Assembling the neuro micro physiological system

The monolithic quartz pieces are treated with (3-Aminopropyl)triethoxysilane (APTES) (440140, Sigma Aldrich). Briefly, the monolithic quartz pieces are treated with oxygen plasma (Piccolo, Plasma Electronic GmbH, Germany) for 120 s. Then APTES is deposited to the surface via vapor phase for 20 min under vacuum. The substrates are baked for 20 min at 120 °C to stabilize the deposition on the surface. EPOTEK 301-2FL (Epoxy Technology, MA, USA) is an epoxy-based adhesive used to assemble the monolithic quartz piece and the MEA. EPOTEK 301-2FL consists of two components, and prior to the assembly, they are mixed vigorously and degassed to ensure no bubbles. Then, the adhesive is dispersed onto the treated surface of the monolithic quartz pieces using a glue dispenser with 45 mPa pressure. Once the entire surface is covered with EPOTEK 301-2FL, the monolithic glass piece and the MEA are aligned using Fineplacer ® lambda (Finetech GmbH, Germany), and the monolithic quartz piece is placed on MEA. The assembled *NeuroMPS* was then placed in an oven, ramped up to 80°C at 0.5 °C/min, baked for 3 hours, and cooled down to room temperature.

2.4. Reusing the *NeuroMPSs*

In case of contamination, *NeuroMPS* can be sterilized in a dry oven, ramping up to 150°C at 0.5 °C/min, baked for 45 minutes, and cooled to room temperature. After culturing, *NeuroMPS*s are soaked overnight in 1% Terg-a-zyme ® (Z273187, Sigma-Aldrich) in deionized water. They are then rinsed with water and dried under the bench. They are plasma-treated for two minutes prior to use.

2.5. Primary murine hippocampal neurons and astrocytes

The Swiss strain (RjOrl: Swiss) pregnant mice are provided by Janvier Labs (France). The pregnant mouse is sacrificed with euthanasia (CO_2) at E16/E17 based on previously published protocols [92, 93]. The mouse is sprayed with 70% ethanol before transferring it under the sterile bench. Then, the pre-natal mice are removed from the uterus with a mid-ventral cut and moved into a petri dish containing pre-cooled Hank's balanced salt solution (HBSS) -/- (14170112, Thermo Fisher Scientific, MA, USA). Then, the pups are removed from the amniotic sack and decapitated with sterile scissors. The heads are then transferred into a fresh pre-cooled HBSS -/- containing petri dish, and under the dissecting microscope (SMZ-171, Motic, Hong Kong), the brain is dissected by making a posterior-anterior cut through the skull and pulling the brain ventrally using tweezers. These steps are repeated for all pups; then, the

brains are collected in a fresh pre-cooled HBSS -/- containing petri dish. The cerebellum is removed with a scalpel (0205, scalpel blades No.15, Swann-Morton, UK) before making a transversal cut through hemispheres to visualize the hippocampus. The meninges are removed with the help of micro tweezers for better visualization of the dark and curved shape of the hippocampus. Once the area is cleaned, the hippocampus is extracted from the surrounding tissue with micro tweezers and collected in a 15 ml tube containing fresh pre-cooled HBSS -/- to continue with enzymatic digestion. The Neural Dissociation Kit (T) (130-093-231, Miltenyi Biotec GmbH, Germany) is used to dissociate hippocampal tissue. After enzymatic digestion, the cell solution is strained with 70 µm MACS SmartStrainer (130-098-462, Miltenyi Biotec GmbH, Germany) using a filtering medium (**Table 1**), then centrifuged at 300g for 5 min. The cells are then resuspended in culturing medium (**Table 2**). The medium is switched to maturation medium (**Table 3**) after 4 DIV.

Table 1. Filtering medium composition

Filtering Medium	Working Concentration	Product info
Neurobasal Plus™ Medium		A3582901, Gibco, Thermo Fisher Scientific, MA, USA
Foetal Bovine Serum	10 %	10082139, Thermo Fisher Scientific, MA, USA
Penicillin/Streptomycin	500 U/ml	P4333, Sigma-Aldrich, Merck KGaA, Germany

Table 2. Culturing medium composition

Culturing Medium	Working Concentration	Product info
Neurobasal Plus™ Medium		A3582901, Gibco, Thermo Fisher Scientific, MA, USA
SM1 Neuronal Supplement	2 %	5711, STEMCELL Technologies Inc., Germany
Penicillin/Streptomycin	500 U/ml	P4333, Sigma-Aldrich, Merck KGaA, Germany

Table 3. Maturation medium composition

Maturation Medium	Working Concentration	Product info
BrainPhys™ Medium		5790, STEMCELL Technologies Inc., Germany
SM1 Neuronal Supplement	2 %	5711, STEMCELL Technologies Inc., Germany
Penicillin/Streptomycin	500 U/ml	P4333, Sigma-Aldrich, Merck KGaA, Germany

2.6. Primary murine microglia

2.6.1. Preparing conditioned media with L929 fibroblasts for microglia stimulation

L929 murine fibroblasts (kindly provided by H. Ehrenreich's Laboratory at the Max Planck Institute of Experimental Medicine, Göttingen; L929/R (ECACC 04102001)) are plated at a density of 470,000 cells per flask and supplemented with 55 ml fibroblast culturing medium (**Table 4**). The cells are incubated for 7 days at 37°C and 5 % CO_2, during which time no media addition or refreshment occurs. At the end of the 7th day, the media from the flasks is harvested, filtered through 0.22 µm filters (431229, Corning), and stored at -20 °C until used.

Table 4. Fibroblast Culturing Medium Composition

Fibroblast Culturing Medium	Working Concentration	Product info
DMEM, high glucose		41965039, Gibco, Thermo Fisher Scientific, MA, USA
Fetal Bovine Serum	10 %	10082139, Thermo Fisher Scientific, MA, USA
Penicillin/Streptomycin	100 U/ml	P4333, Sigma-Aldrich, Merck KGaA, Germany

2.6.2. Coating of the flasks

T75 flasks are coated with 50 µg/ml poly-D-lysine (PDL) (P7280, Sigma Aldrich) for 30 minutes at 37°C and 5% CO_2. Then, the PDL solution is washed with distilled water once, and the flasks are dried for 2 hours under the sterile bench. 10 ml of microglia culturing medium is then added to the flasks and incubated at 37°C and 5% CO_2 until the cells are ready to be plated.

2.6.3. Microglia isolation

Microglia isolation from newborn mice (day 1 or 2) is obtained following the previously published protocol by Garcia-Agudo et al.[94]. The mice are decapitated, and the heads are transferred into pre-cooled HBSS -/-. The brains are removed from the skull and cleaned out of meninges and then minced with a scalpel and transferred into trypsin-EDTA (0.05%) (25300054, Thermo Fisher Scientific, MA, USA) (2 brains in 5 ml trypsin-EDTA) in 50 ml falcon tubes. Falcons were then incubated in a 37°C water bath for 2 x 5 minutes with vortexing (MS1 mini shaker, IKA Works Inc., Wilmington, North Carolina, USA) for 15 seconds between and after the incubation to improve dissociation and eliminate the neuronal survival. Enzymatic digestion is stopped with the microglia culturing medium (**Table 5**) containing 400 IU/ brain DNAse I (LS002139, Cell Systems). Samples were then incubated for another 3 minutes in a 37°C water bath to enhance enzymatic dissociation and followed by physically triturated using a 5 ml serological pipette (606-160, Greiner Bio-One GmbH, Germany). Then, the cells are centrifuged at 150 g for 10 min, resuspended in a microglia culturing medium, plated into the pre-coated T75 flasks, and incubated at 37°C and 5% CO_2. The medium is completely refreshed at 1 DIV and 2 DIV with microglia culturing medium; at 4DIV, 1/3 of the medium is removed and replaced with the conditioned medium, and at 7DIV, the complete medium is refreshed with microglia stimulation medium (**Table 6**). Cells were harvested at 9 DIV. The harvested cells are purified using the MidiMACS™ Cell separation kit (130-042-302, Miltenyi Biotec, Germany) with LS columns (130-042-401, Miltenyi Biotec, Germany) using CD11b microbeads (130-093-636, Miltenyi Biotec, Germany) following the manufacturer's protocol. Briefly, cells are stained with CD11b microbeads; the stained cells are held in the LS column under a magnetic field, and then the LS column is freed from the magnetic field and purged into a 15 ml tube with microglia culturing medium and centrifuged at 150 g for 10 minutes. Microglia are then mixed with neurons and astrocytes and plated into *NeuroMPS 1. 0*.

Table 5. Microglia Culturing Medium Composition

Microglia Culturing Medium	Working Concentration	Product info
DMEM, high glucose		41965039, Gibco, Thermo Fisher Scientific, MA, USA
Horse Serum	10 %	26050070, Thermo Fisher Scientific, MA, USA
Penicillin/Streptomycin	50 U/ml	P4333, Sigma-Aldrich, Merck KGaA, Germany

Table 6. Microglia Stimulation Medium Composition

Microglia Stimulation Medium	Working Concentration
Microglia Culturing Medium	2:3
Conditioned Medium	1:3

2.7. 3D culturing in *NeuroMPS 1.0*

Matrigel® (356230, Corning Inc., NY, USA) is used as a hydrogel for 3D seeding of the cells. Matrigel® is liquid between 4-6°C and starts polymerizing above 8°C. Thus, the cell seeding solution and all the *NeuroMPS 1.0* are kept on ice and handled as quickly as possible. Cell solution is prepared at 4X concentration in the culturing medium, and just before plating, it is mixed with Matrigel® with a 1:4 ratio (75% Matrigel). The *NeuroMPS 1.0* is placed on a cold metal block, and the wells are seeded with Matrigel-containing cell solution under the microscope (SMZ-171, Motic, Hong Kong). Once all the wells are seeded, the *NeuroMPS 1.0* is flipped in a petri dish to ensure equal cell distribution in the wells and incubated at 37°C for 10 min. Once the Matrigel is polymerized, the cells are supplemented with culturing medium, and the *NeuroMPS 1.0* is incubated at 37°C and 5% CO_2. Half of the medium is refreshed every other day, and on day 4, the medium switches to maturation medium and continues refreshing with it every other day.

2.8. Immunocytochemistry (ICC)

ICC stainings are performed in two different ways. For dissociated cells, the cells are fixed in a fixing solution (**Table 7**) at room temperature for 30 minutes and then washed with washing buffer (**Table 9**) 5 times. Then, the cells are permeabilized with permeabilization buffer (**Table 9**) for 1 hour at room temperature on a rocker (InfinityRocker™ Pro, Next Advance, NY, USA). This was followed by washing cells 5 times with a washing buffer and subsequently blocking the buffer employed on the cells, which were placed on a rocker overnight at 4°C. The next day, the blocking buffer is aspirated, and primary antibodies (**Table 10**) in the antibody buffer are applied to the cells and incubated on a rocker overnight. TUBB3 stained axons and dendrites, MAP2 stained dendrites, GFAP stained astrocytes, and IBA1 stained microglia. The following day, the cells were washed with a washing buffer 5 times and left in the washing buffer overnight. The next day, the cells were washed with a washing buffer 5 times, and then the secondary antibodies (**Table 11**) in the antibody buffer were applied to the cells and incubated on a rocker overnight at 4°C. Afterward, the cells were washed with a washing buffer 5 times and left in the washing buffer overnight at 4°C. The following day, the cells were washed with a washing buffer 5 times, and then the buffer was replaced with SlowFade™

Diamond Antifade mountant (S36967, Thermo Fisher Scientific, MA, USA). Mounted samples can be kept at 4°C for up to 3 months. All the washing steps are performed by replacing half of the total volume.

Table 7. Fixing Solution Composition

Fixing Solution	Concentration	Product info
Dulbecco`s phosphate-buffered saline		14190144, Thermo Fisher Scientific, MA, USA
Paraformaldehyde	4 % (w/v)	P6148, Sigma-Aldrich, Merck KGaA, Darmstadt, Germany
Sucrose	4 % (w/v)	S0389, Sigma-Aldrich, Merck KGaA, Darmstadt, Germany

Table 8. Ingredients for ICC Solutions

Ingredients for ICC solutions	Product info
Dulbecco's phosphate-buffered saline (DPBS), no calcium, no magnesium	14190094, Gibco, Thermo Fisher Scientific, MA, USA
Fish skin gelatine	G7765, Sigma-Aldrich, Merck KGaA, Germany
Triton X-100	T9284, Sigma-Aldrich, Merck KGaA, Germany
Normal donkey serum	017-000-121, Dianova GmbH, Germany

Table 9. The Composition of ICC Solutions

ICC Solutions	Composition	Concentration
Washing Buffer	DPBS Fish skin gelatine	 0.2 % (w/v)
Permeabilization Buffer	Washing Buffer Triton X-100	 0.3 % (w/v)
Blocking Buffer and Antibody Buffer	Washing Buffer Permeabilization buffer Normal donkey serum	 0.1 % (v/v) 0.2 % (v/v)

Table 10. Primary Antibodies for Primary Murine Culture

Primary antibodies	Host	Product info
Purified anti-tubulinβ3 (TUBB3)	Mouse	801201, BioLegend CNS Inc, CA, USA
Anti-microtubule-associated protein 2 (MAP2)	Chicken	NB300-213, Novus Biologicals, CO, USA
Anti-glial-specific type-III intermediate filament protein (GFAP)	Mouse	173011, Synaptic Systems GmbH, Germany
Anti-calcium binding adaptor molecule 1 (Iba1)	Rabbit	019-19741, FUJIFILM Wako Chemicals, Japan

Table 11. Secondary Antibodies

Secondary antibodies	Reactivity	Host	Product info
Alexa Fluor 488- conjugated AffiniPure Donkey Anti-Mouse IgG	Mouse	Donkey	715-545-150, Dianova GmbH, Germany
Alexa Fluor 488- conjugated AffiniPure Donkey Anti-Mouse IgG	Rabbit	Donkey	711-545-152, Dianova GmbH, Germany
Alexa Fluor 594- conjugated AffiniPure Donkey Anti-Mouse IgG	Chicken	Donkey	703-585-155, Dianova GmbH, Germany
Goat anti-Rabbit IgG (Heavy Chain), Superclonal™ Recombinant Secondary Antibody, Alexa Fluor™ 555	Rabbit	Goat	A27039, Invitrogen, Thermo Fisher Scientific, MA, USA
Alexa Fluor 647- conjugated AffiniPure Donkey Anti-Chicken IgG	Chicken	Donkey	703-605-155, Dianova GmbH, Germany
Alexa Fluor 647- conjugated AffiniPure Donkey Anti-Rat IgG	Rat	Donkey	712-605-153, Dianova GmbH, Germany

A different ICC staining method is employed for neurospheres. Neurospheres are fixed in a fixing solution (**Table 7**) for 1 hour at room temperature and then washed with Dulbecco's phosphate-buffered saline(DPBS) (14190144, Thermo Fisher Scientific, MA, USA) 3 times for 5 minutes. The neurospheres are dehydrated with serial solutions (**Table 12**). Briefly, the neurospheres are incubated in solution-1 for 15 minutes, then switched to solution-2 for another 15 minutes, then continued with solution-3 for 15 minutes, and again incubated with solution-1 for another 15 minutes, followed by washing with DPBS for 15 minutes. After that, the neurospheres are permeabilized in solution-4 for 30 minutes. Then, the neurospheres are transferred into the penetration buffer (HSB-BK, Visikol, NJ, USA) and incubated for 30

minutes with shaking at 300 rpm. Up until this step, all the incubations are employed at room temperature. It is continued with incubation in blocking buffer (HSB-BK, Visikol, NJ, USA) at 37°C for 1 hour with shaking at 300 rpm. After blocking, the neurospheres are incubated with primary antibodies (**Table 13**) prepared in the antibody buffer (HSB-BK, Visikol, NJ, USA) overnight at 37°C, shaking at 300 rpm, then another 48 hours at 4°C (no shake). They are followed by washing 3 times for 15 minutes in the washing buffer (HSB-BK, Visikol, NJ, USA) at 37°C with shaking at 300 rpm. Secondary antibodies (**Table 11**) and the nuclear dye (**Table 13**) are prepared in the antibody buffer, and neurospheres are transferred into this solution. They are incubated at 37°C for 90 minutes with shaking at 300 rpm. The secondary antibodies are washed again 3 times for 15 minutes in the washing buffer at 37°C with shaking at 300 rpm. Then, the neurospheres are brought to room temperature, and the washing buffer is switched with DPBS, incubated for 10 minutes at room temperature, and then cleared in Scale S4 solution (**Table 14**) at 4°C for 48-72 hours. Before imaging, the neurospheres are mounted in SlowFade™ Diamond Antifade mountant (S36967, Thermo Fisher Scientific, MA, USA).

Table 12. Neurosphere Dehydration Solutions for ICC

Neurosphere dehydration solutions	Solution Recipe	Product info
Ingredients		
Methanol		5.89596, Sigma-Aldrich, Merck KGaA, Darmstadt, Germany
Dimethyl sulfoxide (DMSO)		D2438, Sigma-Aldrich, Merck KGaA, Darmstadt, Germany
Triton X-100		X100, Sigma-Aldrich, Merck KGaA, Darmstadt, Germany
Solutions		
Solution 1	50 % Methanol in water	
Solution 2	100 % Methanol	
Solution 3	20% DMSO in methanol	
Solution 4	1 % Triton X-100 in PBS	

Table 13. Primary Antibodies and dyes for neurospheres

Primary antibodies and dyes	Host	Product info
Purified anti-tubulinβ3 (TUBB3)	Mouse	801201, BioLegend CNS Inc, CA, USA
Anti-microtubule-associated protein 2 (MAP2)	Chicken	NB300-213, Novus Biologicals, CO, USA

Anti-glial fibrillary acidic protein (GFAP)	Rabbit	GA52461-2, DAKO Omnis, Agilent CA, USA
Anti-Neurofilament heavy polypeptide antibody	Chicken	ab4680, abcam Inc., UK
Anti-Nestin Antibody	Mouse	MAB1259, R&D Systems Inc., MN, USA
Anti-Pax-6 Antibody	Rabbit	901301, BioLegend CNS Inc, CA, USA
Anti-Sox2 Antibody	Rabbit	AB5603, Sigma-Aldrich, Merck KGaA, Darmstadt, Germany
4′,6-Diamidino-2-phenylindole dihydrochloride (DAPI)		D8417, Sigma-Aldrich, Merck KGaA, Darmstadt, Germany
Hoechst 33342 Solution (20 mM)		62249, Thermo Fisher Scientific, MA, USA

Table 14. The Composition of Scale S4 Solution

Scale S4 solution	Concentration	Product info
D-Sorbitol	40 % (w/v)	S3889, Sigma-Aldrich, Merck KGaA, Darmstadt, Germany
Glycerol	10 % (w/v)	G2025, Sigma-Aldrich, Merck KGaA, Darmstadt, Germany
Urea	4 M	51456, Sigma-Aldrich, Merck KGaA, Darmstadt, Germany
Triton X-100	0.2 % (w/v)	X100, Sigma-Aldrich, Merck KGaA, Darmstadt, Germany
DMSO	15 % (w/v)	D2438, Sigma-Aldrich, Merck KGaA, Darmstadt, Germany
Ultrapure water		

2.9. Culturing neuro progenitor cells

This study uses two neuro progenitor cell (NPC) lines: i) a commercial line (ax0018, AXOL Bioscience, Easter Bush, UK) and ii) an in-house iPSC-derived NPC line. NPCs are derived from the KOLF2.1J iPSC line (JIPSC1000, The Jackson Laboratory, CT, USA) at Microorgano Lab (Tübingen, Germany) by Lisa–Marie Erlandsdotter following the protocol based on Reinhardt et al., 2013 [95].

The culture plates are coated with 5 µg/ml laminin (LN521, Biolamina) in DPBS +/+ overnight at 4°C. NPCs are plated at a concentration of 50,000 cells/cm^2 and cultured in NPC Culturing medium (**Table 15**) at 37°C and 5% CO_2. Medium is refreshed every other day until 80 % confluency is reached.

Table 15. NPC Culturing Medium Composition

NPC Culturing Medium	Working Concentration	Product info
Neurobasal™ Medium	1:1 with DMEM/F12 medium	21103049, Gibco, Thermo Fisher Scientific, MA, USA
DMEM/F-12, GlutaMAX™ supplement	1:1 with Neurobasal™ medium	31331028, Gibco, Thermo Fisher Scientific, MA, USA
B-27™ Supplement (50X), minus vitamin A	1X	12587010, Gibco, Thermo Fisher Scientific, MA, USA
N-2 Supplement (100X)	1X	17502048, Gibco, Thermo Fisher Scientific, MA, USA
Penicillin-Streptomycin (10,000 U/ml)	100 U/ml	15140122, Gibco, Thermo Fisher Scientific, MA, USA
2-mercaptoethanol (50 mM)	50 µM	31350010, Gibco, Thermo Fisher Scientific, MA, USA
Human/Mouse/Rat BDNF, Animal-Free Recombinant Protein, PeproTech®	20 ng/ml	AF-450-02, Gibco, Thermo Fisher Scientific, MA, USA
Human FGF-basic (FGF-2/bFGF) (154 aa), Animal-Free Recombinant Protein, PeproTech®	10 ng/ml	AF-100-18B, Gibco, Thermo Fisher Scientific, MA, USA
Recombinant Human EGF Protein, CF	10 ng/ml	236-EG, R&D Systems Inc., MN, USA

2.10. Flow cytometry of NPCs

The quality of NPCs is evaluated using flow cytometry. Cells are initially stained with surface antibodies/dyes (**Table 16**) in PBS (-/-) for 10 minutes at room temperature in the dark. The FOX-P3 Buffer Kit (130-093-142, Miltenyi Biotec) is employed for intracellular staining (**Table 16**). Cells are fixed and permeabilized with the kit's permeabilization/fixation solution for 30 minutes at 4°C in the dark, followed by incubation with the intracellular antibody solution in the kit's permeabilization solution for another 30 minutes at 4°C. After each step, cells are centrifuged at 300g for 4 minutes and washed with AutoMACS running buffer (130-091-221, Miltenyi Biotec). The cells are then resuspended in AutoMACS running buffer and maintained at 4°C until acquisition.

An unstained control is included in all analyses. Samples are acquired using the BD LSRFortessa™ Cell Analyzer (BD Biosciences), and data analysis is performed using FlowJo software (version 10).

Table 16. Flow Cytometry antibodies and dyes

Flow Cytometry Antibodies and dyes	Clone	Conjugate	Application	Product info
PAX-6 Antibody, anti-human, REAfinity™	REA507	APC	ICFC	130-123-267, Miltenyi Biotec GmbH, Germany
Nestin Antibody, anti-mouse/rat, REAfinity™	REA575	PE	ICFC	130-119-799, Miltenyi Biotec GmbH, Germany
Sox2 Antibody, anti-human/mouse, REAfinity™	REA320	Vio Bright V423	ICFC	130-131-077, Miltenyi Biotec GmbH, Germany
Zombie Aqua™ Fixable Viability Kit			Surface	423101, , BioLegend CNS Inc, CA, USA

2.11. Neurosphere generation and culture

Before plating NPCs, the AggreWell™ 800 (34815, STEMCELL Technologies) is conditioned with anti-adherence rinsing solution (07010, STEMCELL Technologies). A volume of 500 µl of the solution is added to each well, and the plate is centrifuged at 1300g for 5 minutes. The wells are then washed twice with NPC culturing medium without growth factors (**Table 15**).

NPC cultures with 80-90% confluency are used for neurosphere formation. The cells are incubated with StemPro™ Accutase™ Cell Dissociation Reagent (A1110501, Gibco, Thermo

Fisher) for 5 minutes at 37°C with 5% CO_2. Once the cells are detached, Accutase™ is neutralized with the NPC culturing medium without growth factors, and the cells are centrifuged at 300g for 5 minutes. The cells are then resuspended in NPC culturing medium and plated in AggreWell™ 800 at a concentration of 1.5 x 10^6 cells per well. The plate is centrifuged at 100g for 3 minutes. After confirming even cell distribution, the plate is incubated at 37°C with 5% CO_2 for 48 hours.

After 48 hours, the media in the AggreWell™ 800 is replaced with the neurosphere culturing medium (**Table 17**). The neurospheres from each well are then transferred to individual wells of a 6-well plate. Each well is supplied with 2 ml of neurosphere culturing medium, and the plate is incubated on an orbital shaker at 90 rpm at 37°C with 5% CO_2. The culture medium is refreshed every other day with the neurosphere culturing medium for 3 weeks, after which it is switched to the neurosphere maturation medium.

Table 17. Neurosphere Culturing Medium Composition

Neurosphere Culturing Medium	Working Concentration	Product info
Neurobasal™ Medium		21103049, Gibco, Thermo Fisher Scientific, MA, USA
B-27™ Supplement (50X), serum-free	1X	17504044, Gibco, Thermo Fisher Scientific, MA, USA
GlutaMAX™ Supplement (100X)	1X	35050038, Gibco, Thermo Fisher Scientific, MA, USA
Penicillin-Streptomycin-Glutamine (100X)	1X	10378016, Gibco, Thermo Fisher Scientific, MA, USA
Human/Mouse/Rat BDNF, Animal-Free Recombinant Protein, PeproTech®	10 ng/ml	AF-450-02, Gibco, Thermo Fisher Scientific, MA, USA
Recombinant Human GDNF Protein	10 ng/ml	212-GD, R&D Systems Inc., MN, USA

Table 18. Neurosphere Maturation Medium Composition

Neurosphere Maturation Medium	Working Concentration	Product info
BrainPhys™ Medium		5790, STEMCELL Technologies Inc., Germany
B-27™ Supplement (50X), serum-free	1X	17504044, Gibco, Thermo Fisher Scientific, MA, USA
GlutaMAX™ Supplement (100X)	1X	35050038, Gibco, Thermo Fisher Scientific, MA, USA
Penicillin-Streptomycin-Glutamine (100X)	1X	10378016, Gibco, Thermo Fisher Scientific, MA, USA
Human/Mouse/Rat BDNF, Animal-Free Recombinant Protein, PeproTech®	10 ng/ml	AF-450-02, Gibco, Thermo Fisher Scientific, MA, USA
Recombinant Human GDNF Protein	10 ng/ml	212-GD, R&D Systems Inc., MN, USA

2.12. Characterization of neurosphere's physical properties

Neurospheres are examined for their circularity and diameter change over time. For that, bright field images are acquired with an EVOS FL digital fluorescence microscope (Thermo Fisher Scientific) every two weeks. Five random regions are imaged in each well in a 6-well plate. The images are analyzed with an ImageJ macro. The images are first converted to binary and then to masks. The "Analyze particle" option is employed with the following parameters: size= 30,000-infinity μm2, include holes, and exclude on the edges. The shape of neurospheres is approximated to a circle, and the diameter is calculated using the formula below where d indicates diameter and A indicates area:

$$d = 2\sqrt{A/\pi}$$

The circularity of the neurospheres is calculated using the formula below, where A indicates area and P indicates perimeter:

$$C = 4\pi(\frac{A}{P^2})$$

2.13. Live/Dead Staining

Neurospheres are transferred into 96-well plates for the assay. The neurospheres generated from the commercial NPC line are stained using the LIVE/DEAD™ Cell Imaging Kit (R37601, Thermo Fisher Scientific) according to the manufacturer's protocol. Briefly, the live cell dye solution (Calcein AM) and dead cell dye (BOBO™-3 Iodide) are mixed, and 20 µM Hoechst (62249, Thermo Fisher Scientific) is added. The neurospheres are then incubated in the staining solution for 30 minutes at 37°C with 5% CO_2.

For the neurospheres generated from KOLF2.1J NPCs, staining is performed with 1:2000 CellTox™ Green (G8741, Promega GmbH) and 20 µM Hoechst. The dye solution is prepared in the neurosphere culturing medium, and the neurospheres are incubated in the staining solution for 30 minutes at 37°C with 5% CO_2.

Following incubation, the neurospheres are imaged using fluorescence microscopy (Cell Observer® with spinning disc head, Zeiss).

2.14. CellTiter-Glo

The neurospheres are transferred into a 96-well plate prior to the assay. CellTiter®-Glo 3D Cell Viability Assay(G7570, Promega GmbH) is performed according to the manufacturer's instructions. Briefly, the reagent is added to the wells 1:1 dilution. Then, the plate is spun at 800 rpm for 5 minutes on a thermomixer (ThermoMixer C, Eppendorf) to enhance the lysis, followed by 25 minutes of incubation at room temperature in the dark. Following incubation, the luminescence measurement is acquired with the TECAN Spark plate reader.

2.15. Dynamic Cytotoxicity Assay

The neurospheres are stained with 1:2000 CellTox™ Green for 30 minutes, then rotenone is applied to them. The neurospheres are imaged with the Image Xpress Micro-Confocal High Content Imaging System (Molecular Devices). For analysis, data is normalized to untreated samples.

2.16. Ca^{+2} Imaging

The neurospheres were incubated with 2 µM Cal-520®, AM (21130, AAT Bioquest) in the culturing medium for one hour at 37°C in a 5% CO_2. After incubation, the neurospheres were washed three times with pre-warmed Tyrode's buffer (T2397, Sigma Aldrich). The imaging of the neurospheres was then performed in Tyrode's buffer with a fluorescence microscope (Cell Observer® with spinning disc head, Zeiss).

2.17. Electrophysiological Recordings

The *NeuroMPSs* are recorded one device at a time. After they are placed on the MEA2100-System (Multi Channel Systems), the incubator is placed on top of the *NeuroMPS*, and the device is allowed to be acclimatized for 10 minutes before recording. Spontaneous activity is always recorded before the compound application (

Table *19*).

Table 19. Compounds applied to neurospheres

Compound	Product info	Description
Picrotoxin (PTX)	1128, Tocris Bioscience, Bristol, UK	GABA antagonist
Tetrodotoxin (TTX)	1078, Tocris Bioscience, Bristol, UK	Sodium channel blocker
Bicuculine methchloride (BIC)	B7686, Sigma-Aldrich, Merck KGaA, Darmstadt, Germany	GABA antagonist
CNQX disodium salt hydrate	C239, Sigma-Aldrich, Merck KGaA, Darmstadt, Germany	Non-NMDA receptor antagonist
APV	A8054, Sigma-Aldrich, Merck KGaA, Darmstadt, Germany	NMDA receptor antagonist
4- aminopyridine (4-AP)	A78403, Sigma-Aldrich, Merck KGaA, Darmstadt, Germany	Potassium channel blocker

The electrophysiological recordings are analyzed using NeuroExplorer software (version 5.1, Nex Technologies, Littleton, MA, USA). The analysis encompasses conversion, filtering, spike detection, burst analysis, and evaluation of network synchronicity. Spike detection and burst analysis are conducted using scripts provided by the software. However, custom Python scripts supplied by Nex Technologies are utilized for network burst analysis to ensure precise and thorough examination.

Initially, electrodes are grouped according to their respective wells to identify burst and network burst activity in each well. Spike detection for each electrode uses a 4th-order band-pass filter with a frequency range of 60 Hz to 6000 Hz. Action potentials are identified using a threshold crossing algorithm set at 4*σn for *NeuroMPS 1.0* and 4.75*σn for *NeuroMPS 2.0*, where σ represents a critical standard deviation value used to determine the background noise level. The formula for this calculation[96], where x signifies the band-pass filter signal, is:

$$\sigma n = median(\frac{|x|}{0.6745})$$

Burst analysis involves applying an interval algorithm to define burst periods within a spike train. Specific parameters are set[97], including a minimum duration of 10 ms for an event train to be classified as a burst. Each burst has to contain at least five spikes, with maximum time intervals of 170 ms between the initial two spikes and 300 ms between spikes within the burst. For two bursts to be considered a single burst, the minimum interval between them is 200 ms. These parameters facilitate the export of data for further analysis.

Network bursts (NB), defined as bursts occurring simultaneously across most electrodes in a well, are examined to analyze synchronicity. The analysis employs a customized NeuroExplorer script based on Poisson's surprise method[98], a widely recognized algorithm for burst detection. This method distinguishes trains of spikes from baseline neuronal firing and defines bursts as deviations from expected neuronal activity following Poisson's distribution. The surprise (S) levels calculated by this method evaluate the likelihood of a burst being a random occurrence using the following formula:

$$S = -loglog(P)$$

$$P = e^{-rT} \sum_{i=n}^{\infty} \frac{(rT)^i}{i!}$$

Here, P is the probability that a time interval T contains n or more spikes, with r representing the mean firing rate.

Although this approach proved unreliable for detecting bursts following drug application, it was adequate for network burst analysis. At least 33% of electrodes needed to fire a burst synchronously to qualify as a network burst. The start of an NB was marked by the first spike in a burst within the NB, and its end was defined by the last spike of any burst within the NB, with the surprise level fixed at 3. The raw data were then exported for additional analysis.

The analysis focused on several key variables indicative of network activity, including the mean firing rate (MFR), burst frequency rate (BFR), mean burst duration (MBD), percentage of spikes in bursts (%SinB), Network Burst Frequency (NBF) and percentage of bursts in network bursts (%BinNB). These metrics (**Table 20**) provided a detailed understanding of the neuronal activity and synchronicity within the network.

Table 20.Parameters analyzed for electrophysiological recordings

Parameter	Unit	Description
Mean firing rate (MFR)	Hz	Number of spikes per second during the recording
Burst frequency rate (BFR)	Hz	Number of bursts detected per second during the recording
Percentage of spikes in bursts (% SinB)	%	percentage of detected spikes takes place in a burst
Mean burst duration (MBD)	s	The average time between the first and last spike in a burst
Network burst frequency (NBF)	Hz	Number of network bursts detected per second during the recording
Percentage of bursts in network bursts (% BinNB)	%	Percentage of detected bursts takes place in network burst

2.18. Statistical analysis

The data is analyzed using GraphPad Prism Software (version 9.3.1). The sample size is always reported in the figure caption. The basal values of each condition are first examined for outliers utilizing the ROUT method (ROUT=5 %). The normality of the data is tested with the Shapiro-Wilk test, and student t-test or one-way ANOVA is performed between two or more groups. When a statistical test is employed, it is indicated in the figure caption. The error bars always represent the standard error of the mean (SEM). Significant differences are represented with asterisks (*p-value<0.05; **p-value<0.01; ***p-value<0.001) unless indicated otherwise.

3. RESULTS

3.1. Fabrication of Neuro micro-physiological systems

NeuroMPSs are designed as user-friendly, multi-functional devices to study 3D neuronal networks in vitro, facilitating a deeper understanding of neuronal diseases and pathological phenotypes. The *NeuroMPS* combines a microelectrode array (MEA) and a monolithic quartz glass piece. Since it is entirely transparent, *NeuroMPS* allows users to employ imaging readouts. Moreover, it has open wells enabling facile effluent collection. At the bottom of the device, an MEA with capped microelectrodes (CμEs) allows electrophysiological readouts from 3D cultures in a non-invasive manner. The innovation of the *NeuroMPS* is capturing electrical activity from neurites via CμEs regardless of where the cell body is located.

The two key components of *NeuroMPS 1.0* are: i) a custom-designed microelectrode array featuring capped microelectrodes (**Figure 2**) and ii) a tailored quartz microwell module featuring 18 individual wells (**Figure 1**). Each well comprises a tissue compartment with 14 CμEs and a media reservoir. The footprint of the MEA is based on the commercially available 256-electrode MEA “MEA2100-System” (Multi Channel Systems GmbH). 256 electrodes are allocated into 18 wells as 14 recording electrodes. Each well also includes a reference electrode, with every six wells connected to one another and to a single contact pad.

NeuroMPS 1.0 is designed to facilitate the 3D culture of single cells embedded in a gel matrix. Additionally, the wells are designed according to 384 well plate footprints for possible integration with automation systems.

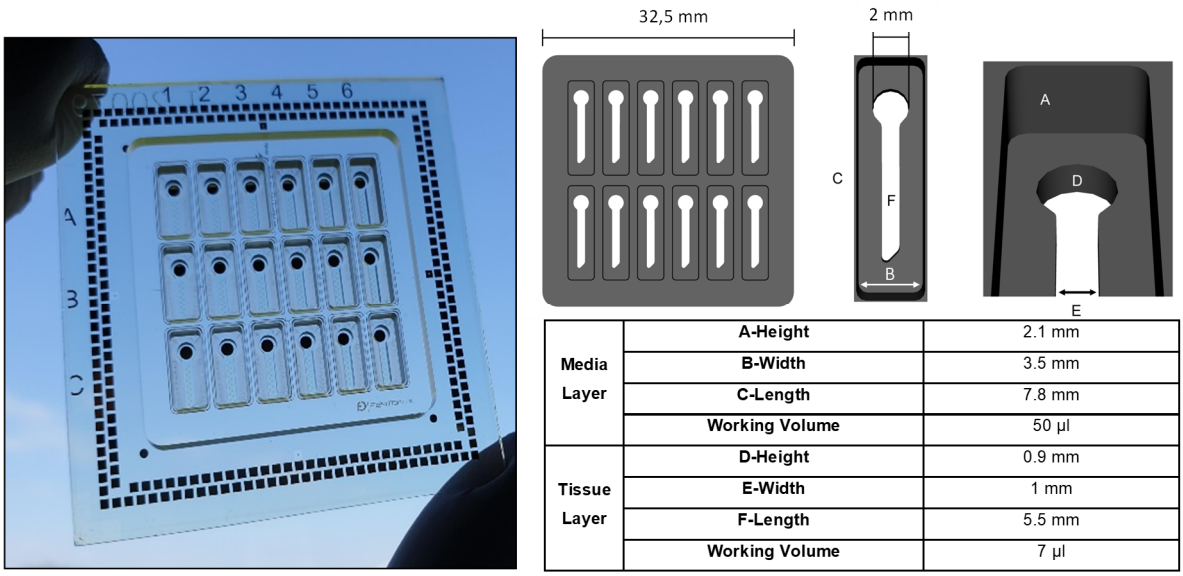

Media Layer	A-Height	2.1 mm
	B-Width	3.5 mm
	C-Length	7.8 mm
	Working Volume	50 µl
Tissue Layer	D-Height	0.9 mm
	E-Width	1 mm
	F-Length	5.5 mm
	Working Volume	7 µl

Figure 1. NeuroMPS 1.0. Transparent MPS comprises a custom-designed MEA and a tailored glass microwell module with 18 wells **(left**).Dimensions of the media and tissue layers of the well (**right**). Reproduced from reference[27] (CC BY 4.0) © IOP Publishing.

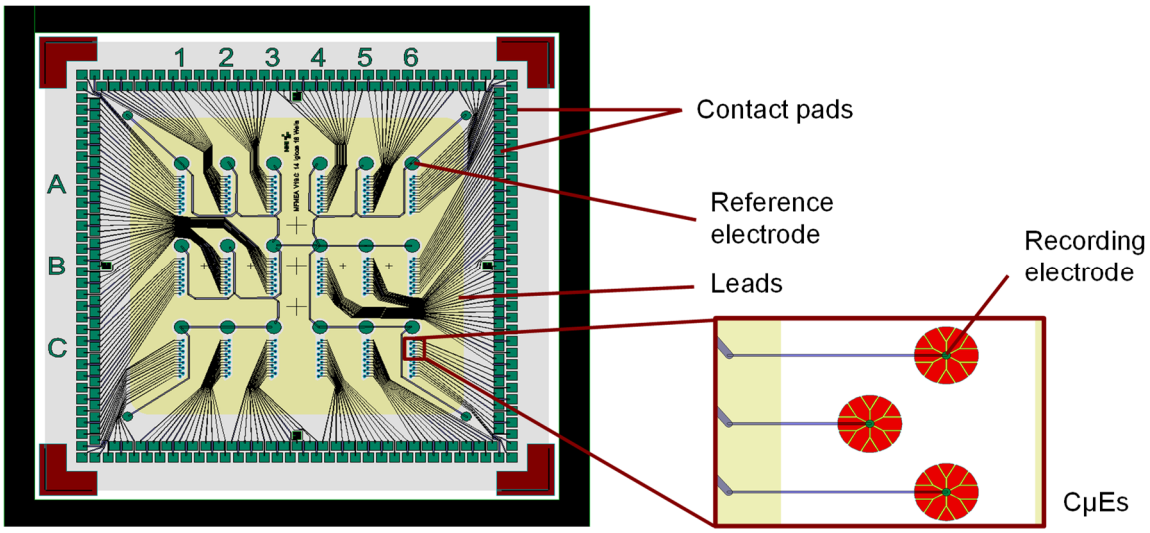

Figure 2. MEA and CµE design of NeuroMPS 1.0

NeuroMPS 2.0 is designed to facilitate the multi-parameter study of neurospheres, allowing for the simultaneous acquisition of morphological, metabolic, and functional data. The system comprises a quartz microwell module featuring nine individual wells (**Figure 3** and **Figure 6**), alongside a custom-designed MEA with CµEs (**Figure 4**). Custom MEA design follows the footprint of the commercially available 120-electrode MEAs for MEA2100-System (Multi Channel Systems GmbH). 120 electrodes are distributed into 9 wells as 13 recording

electrodes, and one reference electrode. Each three reference electrode is connected to the other and to one contact pad. Each well is equipped with small pins to maintain neurospheres suspended in the tissue compartment (**Figure 5**). The pins are designed specifically to hold the neurospheres suspended in a gel matrix while allowing them to extend neurites toward the CμEs. Furthermore, the microwell module has the footprint of a 96-well plate to integrate *NeuroMPS 2.0* into automated workflows.

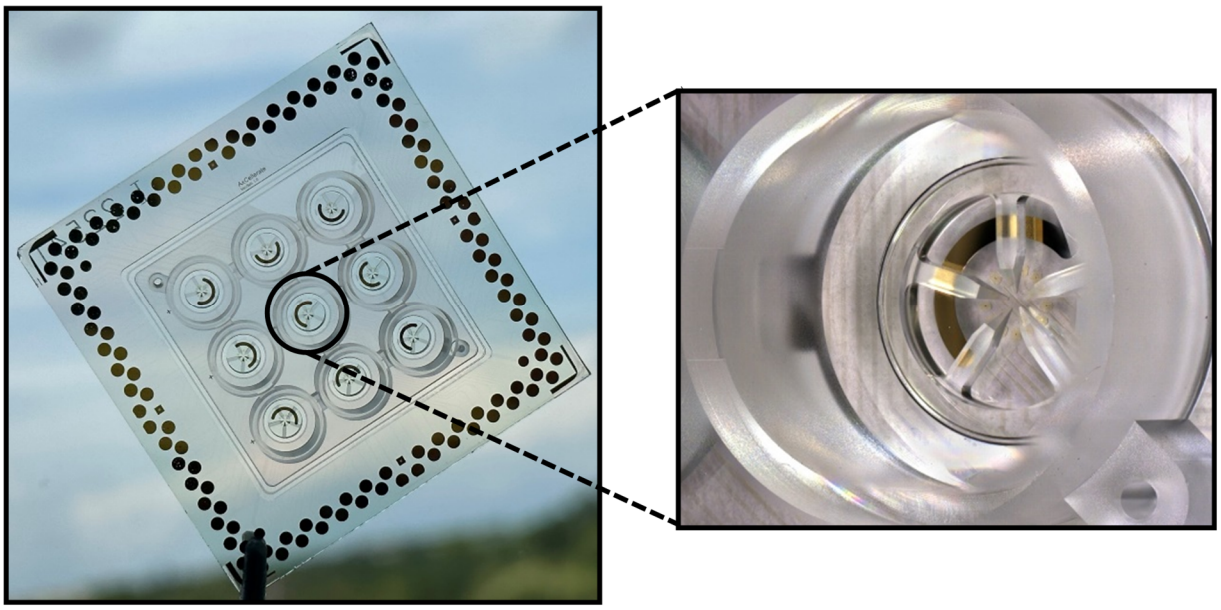

Figure 3. NeuroMPS 2.0. A neuro microphysiological system designed for neuronal neurospheres. A novel well design to accommodate neurospheres in gel (**right**).

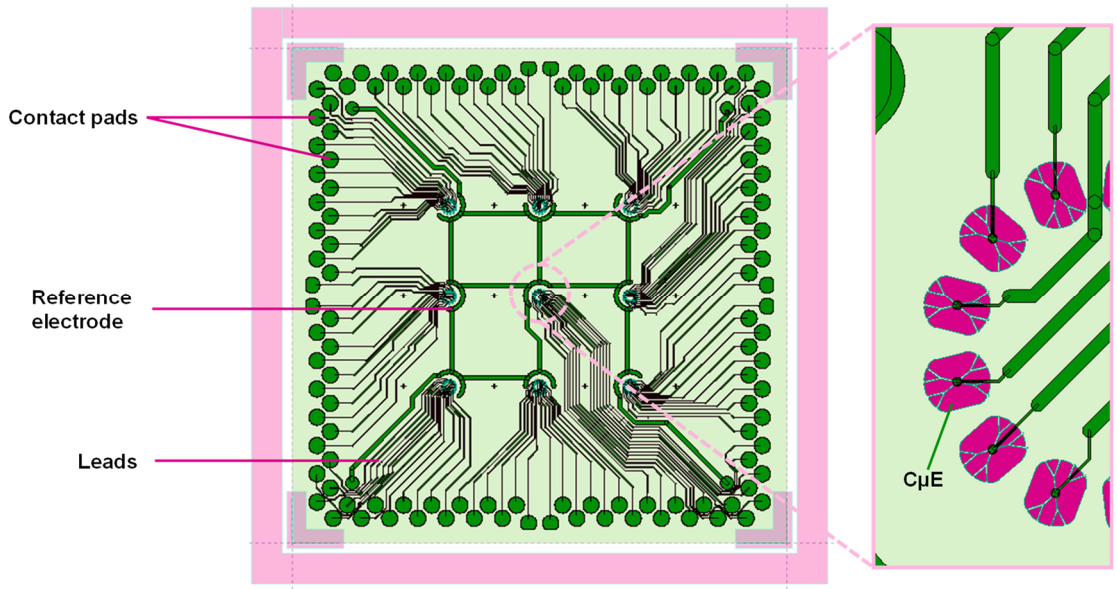

Figure 4.MEA and CμE design of NeuroMPS 2.0

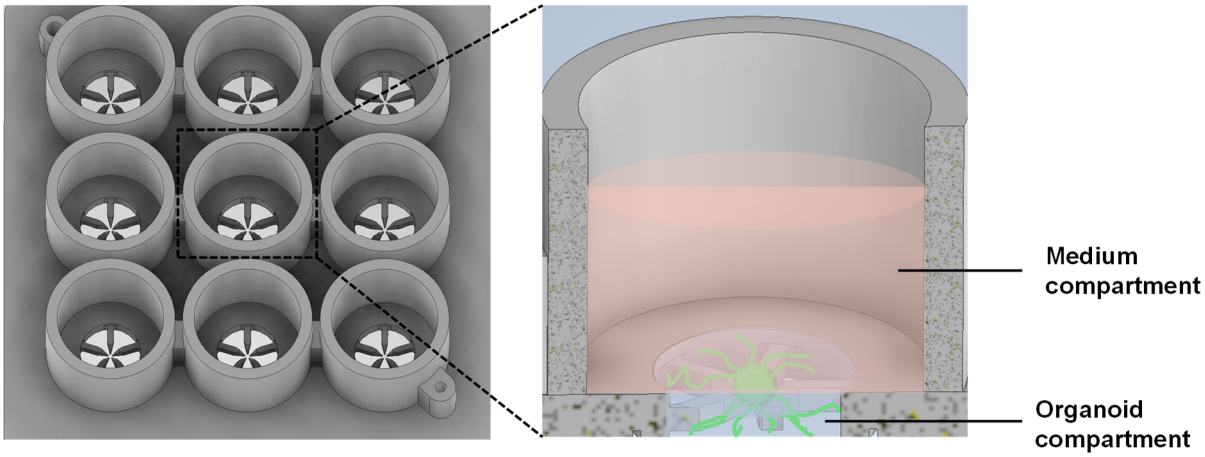

Figure 5. Schematic of quartz microwell module of NeuroMPS 2.0. The wells have a spheroid compartment with five pins holding spheroids 300 µm above the bottom. The medium compartment supplements the neurospheres with the required nutrition.

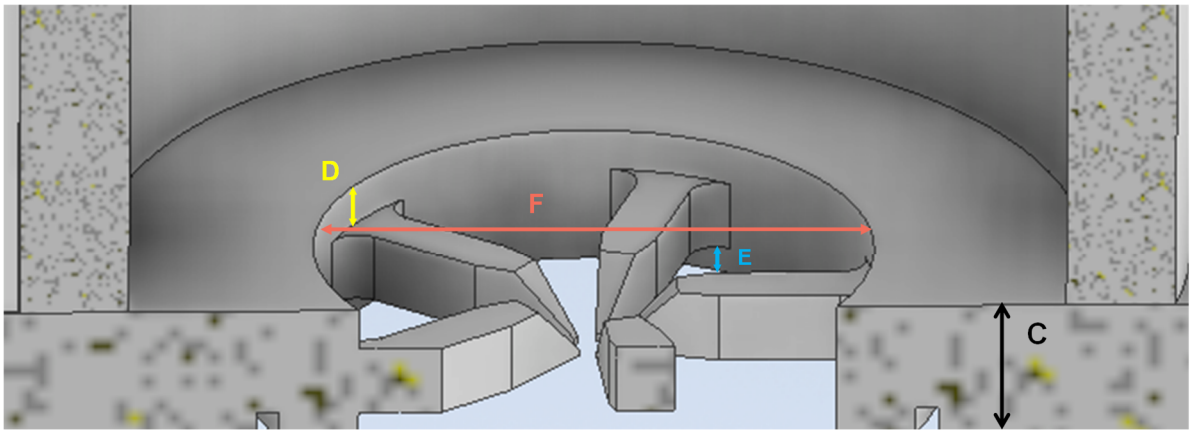

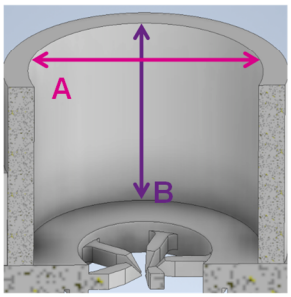

A	7 mm
B	5.8 mm
C	1 mm
D	0.2 mm
E	0.3 mm
F	4 mm
Volume of medium compartment	180 µl
Volume of organoid compartment	12 µl

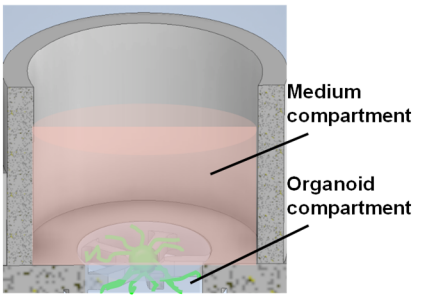

Figure 6. Dimensions of *NeuroMPS 2.0*

3.1.1. Relevance of the capped microelectrodes

Electrophysiology is a critical aspect of neurophysiological events, and monitoring it in vitro with neuronal models is essential. While 3D cultures provide a more physiologically relevant structure, capturing electrical activity in 3D volumes poses significant challenges. In these cultures, neuronal somas are suspended within the 3D volume, and recording electrodes are typically placed at the bottom of the culture device or plate. This placement reduces the likelihood of capturing signals due to the distance between soma and the electrodes in 3D cultures. Some models integrate electrodes within the 3D volume[4, 5], but the probability of the electrodes aligning next to a neuronal soma remains low. Research by Martinez Molina and Jentsch et al.[27] indicates that neuronal somas must be within 15 µm of the electrode to capture electrical activity effectively; otherwise, the signal is lost in the noise. CµEs have been designed to address this issue, allowing recordings from neurites instead of neuronal somas (**Figure 7**).

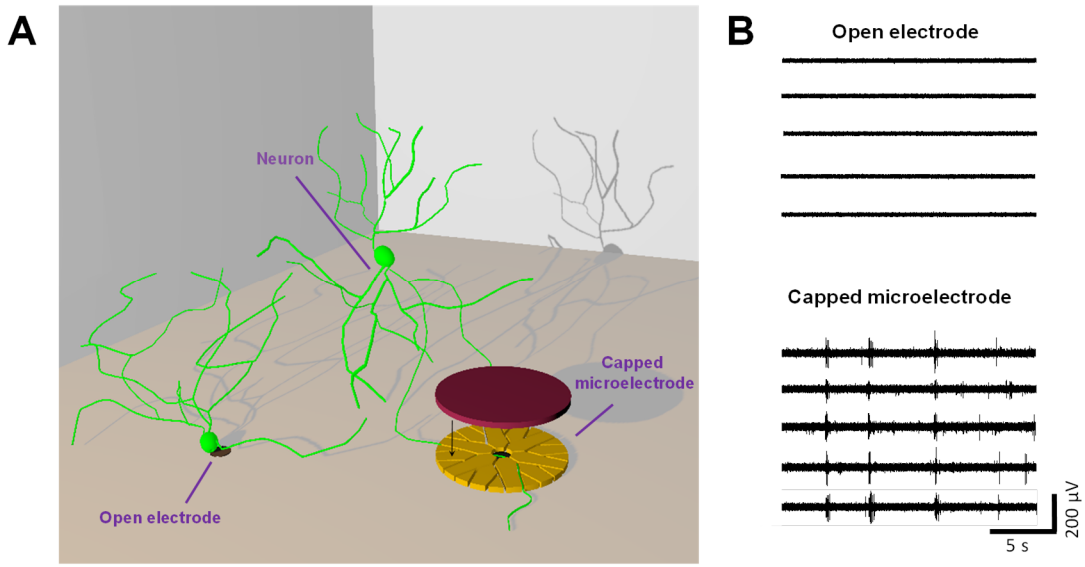

Figure 7. Significance of CµEs. Schematic of spatial distribution of neurons in 3D and recording methods with open and capped electrodes (A). Trace plots of the recordings in 3D with open electrodes and capped microelectrodes. Reproduced from reference[27] (CC BY 4.0) © IOP Publishing.

CµEs are composed of an electrode, micro tunnels, and a sealing cap and are manufactured using photolithography techniques (**Figure 8**). The tunnels and caps are made from epoxy-based photoresists that are both biocompatible and durable in culture mediums. Designed for neurites to grow into them, CµEs capture electrophysiological information even when the electrodes are positioned at the bottom of the culture device and the neuronal somas are in a

3D volume. As the electrophysiological activity is recorded from the neurites grown into CμEs, the readout is performed non-invasively, enabling continuous monitoring of the same culture.

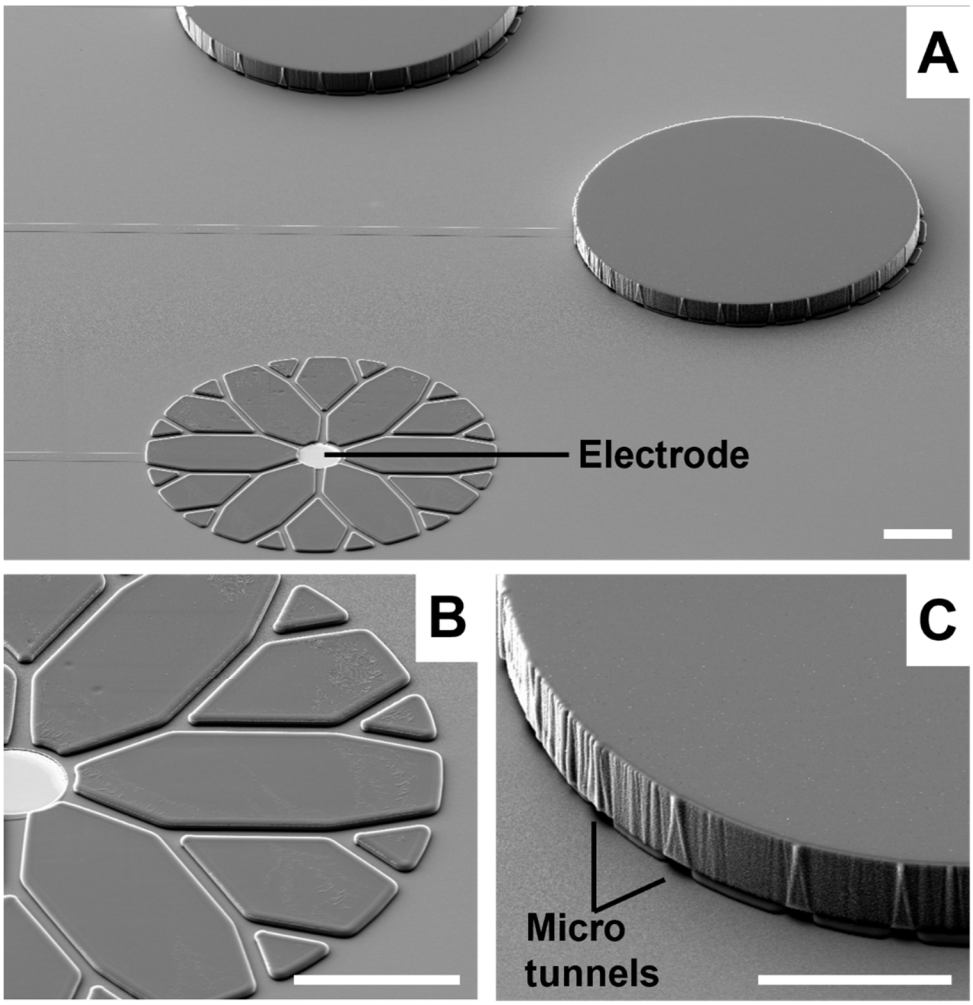

Figure 8. SEM Images of the CμEs. Recording electrode, micro tunnel structures, and capped microelectrodes (A). 5 μm wide micro tunnels for neurite growth towards electrode (B). Side view of the CμE, entrance of micro tunnels (C). Scale bars, 50 μm.

3.2. Neuro-micro physiological system 1.0

Validation of *NeuroMPS* 1.0 involves morphological and electrophysiological assays, predominantly utilizing primary murine cells. Unless specified otherwise, experiments entail primary murine neuron-astrocyte co-cultures embedded in Matrigel.

The culture composition and the morphology of the cells are evaluated via immunocytochemistry. Electrophysiological activity has been assessed by investigating the effects of cell concentration, culturing methods, culture composition, and handling. *NeuroMPS 1.0* is further characterized by pro-inflammatory compounds and rotenone, a neurotoxin.

3.2.1. Primary murine neuronal culture

The cells for co-culture are isolated from prenatal mouse hippocampal tissue, yielding a mixture of neurons and astrocytes, while microglia are isolated from postnatal mouse brain. Two different cell compositions are evaluated: i) neurons and astrocytes isolated from prenatal mice and ii) triple-culture with microglia.

Following isolation, cells are embedded in Matrigel and plated in the *NeuroMPS.* The viability of the culture is monitored for 10 days in vitro, demonstrating viability exceeding 75% (**Figure 9**). After 7 days in vitro (DIV), the cells are immunostained for the neuronal (TUBB3, axons, and dendrites), astroglial (GFAP), and microglial (IBA1) markers. The cells are distributed equally in matrigel, and neurites protrude in all directions (**Figure 10**). Therefore, *NeuroMPS* accurately replicates physiological morphology, which is crucial for establishing proper network formation. Neurons demonstrate partite synaptic morphology with astrocytes and microglia, and all three types of cells exhibit protrusions into the 3D matrix (**Figure 11**).

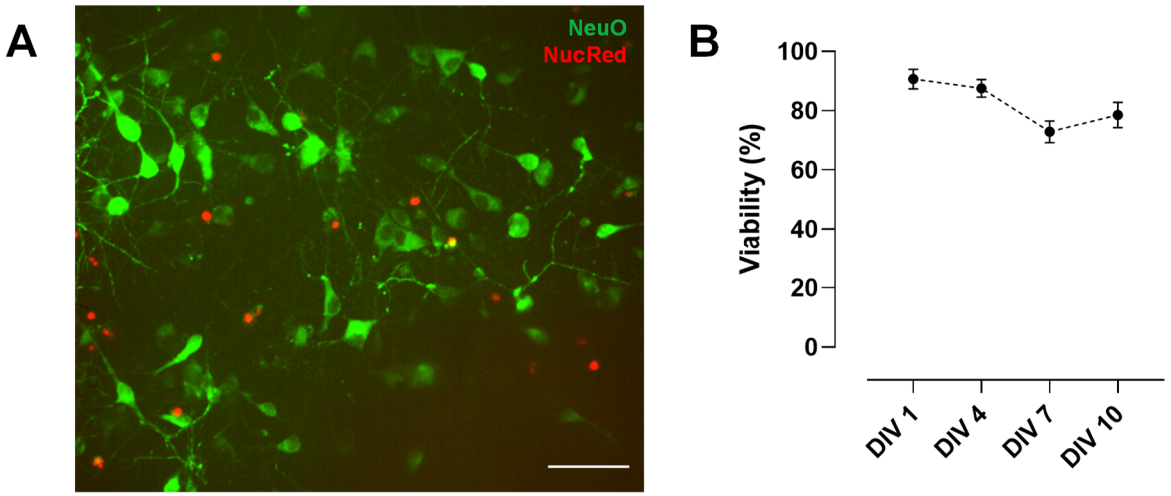

Figure 9.Viability assessment of primary murine cells in vitro in neuroMPS 1.0. Representative image of primary murine neuronal culture at 10 DIV. Live neurons are stained with NeuroFluor™ NeuO and dead cells are stained with NucRed. Scale bar, 50 µm (A). The primary murine culture is viable through 10 days in vitro (DIV). The calculations are performed in triplicates.(B). Reproduced from referencence[27] (CC BY 4.0) © IOP Publishing.

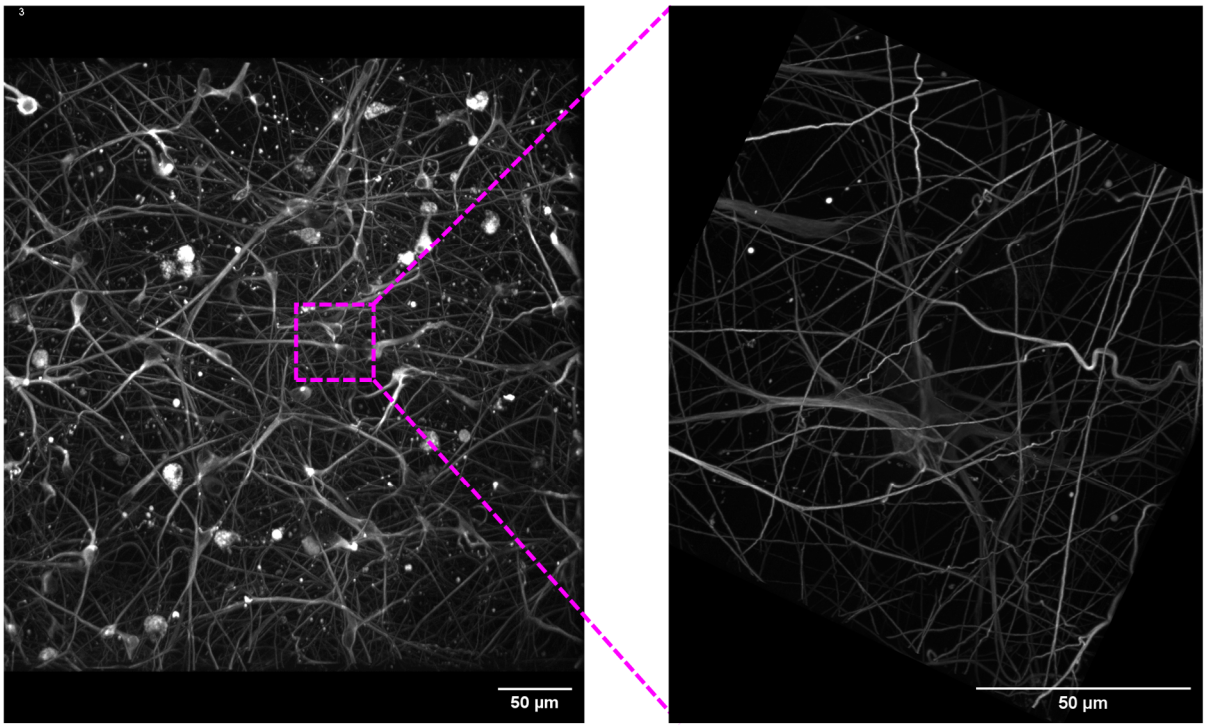

Figure 10. Immunocytochemistry of primary murine neurons in 3D. Neurons are stained with TUBB3. Maximum intensity projection (MIP) of 400 µm thick culture (**left**), 3D reconstruction of neurons stained with TUBB3 in the Matrigel (**right**).

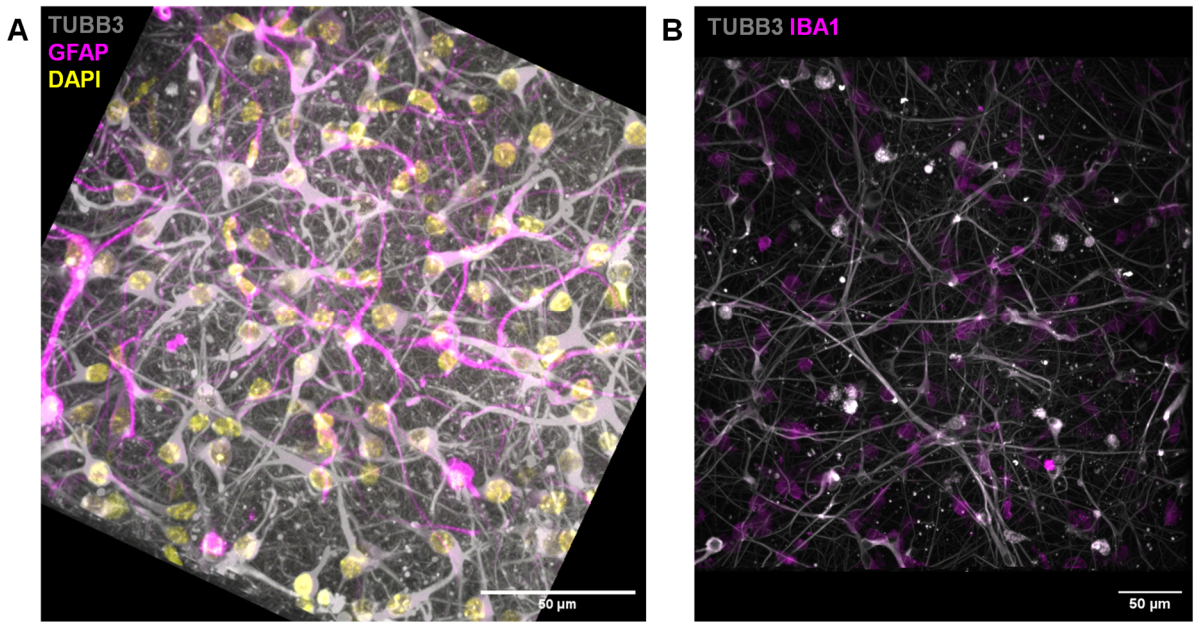

Figure 11. Immunocytochemistry of primary murine culture. A 3D reconstruction of the culture demonstrates how cells are distributed in Matrigel. Neurons were stained with TUBB3, astrocytes were stained with GFAP, and nuclei were stained with DAPI (A). A maximum intensity projection of a 400 µm thick culture demonstrates neurons stained with TUBB3 and microglia stained with IBA1 (B).

3.2.2. Neurons protrude into capped microelectrodes and develop network activity

The growth of the neurites into the micro tunnels of the capped microelectrodes is assessed to characterize the functional readouts. It is shown that at 4 DIV, the neurites are already protruding into the micro tunnels of the CμEs. The neurite growth is monitored for 10 days, and the abundance of the neurites in the tunnels increases over time. In parallel, the development of network activity is investigated. The activity is first evaluated using raster plots to observe the spike abundance over time (**Figure 12**).

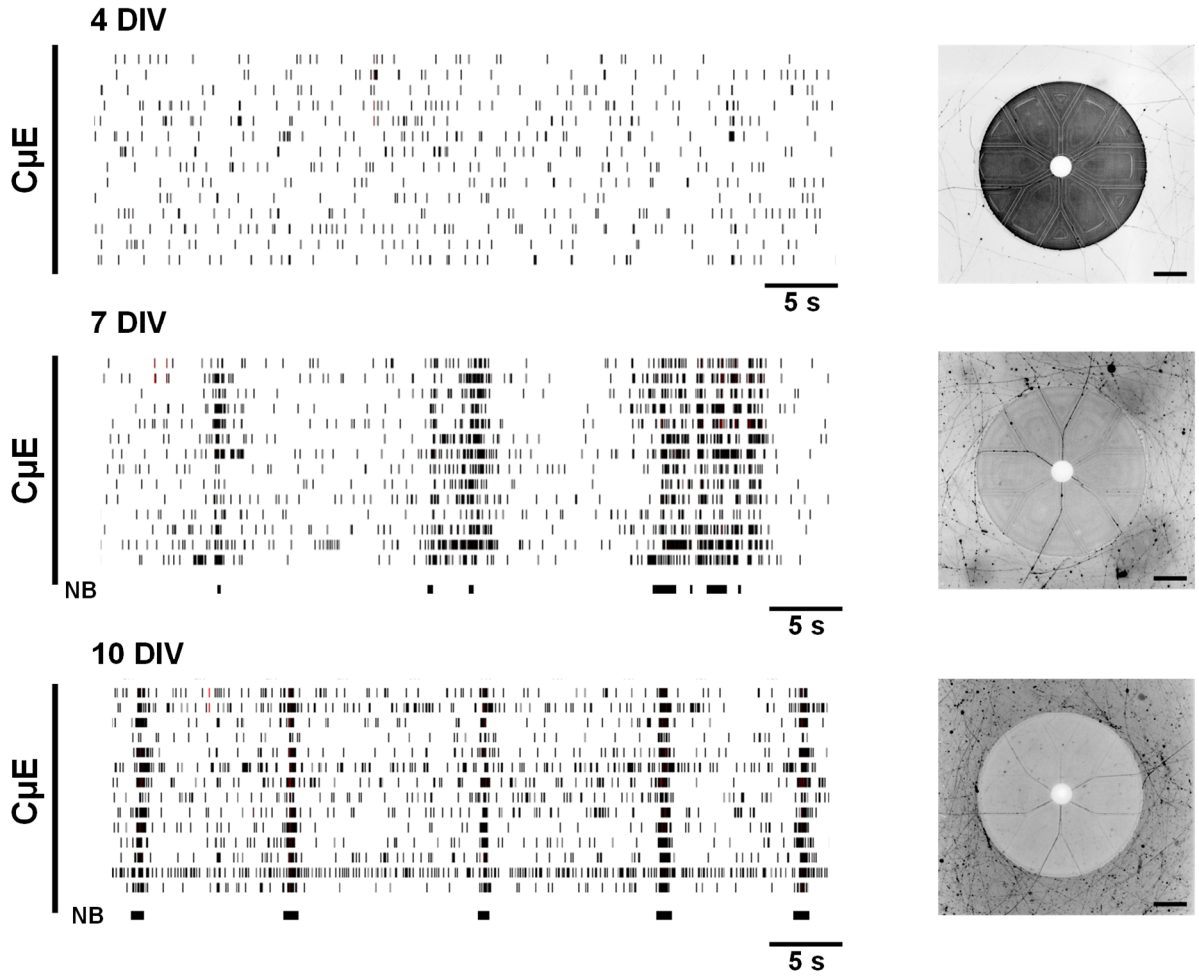

Figure 12. Network activity development of the primary murine culture in Matrigel. Neuronal protrusion into capped microelectrodes and the network activity development were assessed at 4DIV, 7 DIV, and 10 DIV. Raster plots demonstrate how the activity pattern develops towards burst activity, and NB stands for network burst (left). Protrusion of neurite into the micro tunnels imaged using GFP transduced primary murine neurons. Scale bar, 50 μm (right). Reproduced from reference[27] (CC BY 4.0) © IOP Publishing.

Then, mean firing rate (MFR), burst frequency rate (BFR), network burst frequency (NBF), and percentage of bursts in network bursts (%BinNB) are determined from the recordings. Network burst is the parameter that indicates that neurons build a network with their synaptic connections and is a sign of the maturation of the network. Recordings from 4, 7, and 10 DIV reveal that at 4DIV, neurites grow into the CμEs and are electrophysiologically active, but the culture does not exhibit a network activity until 7 DIV. At 10 DIV, most of the burst activity occurs in network bursts (**Figure 12** and **Figure 13**).

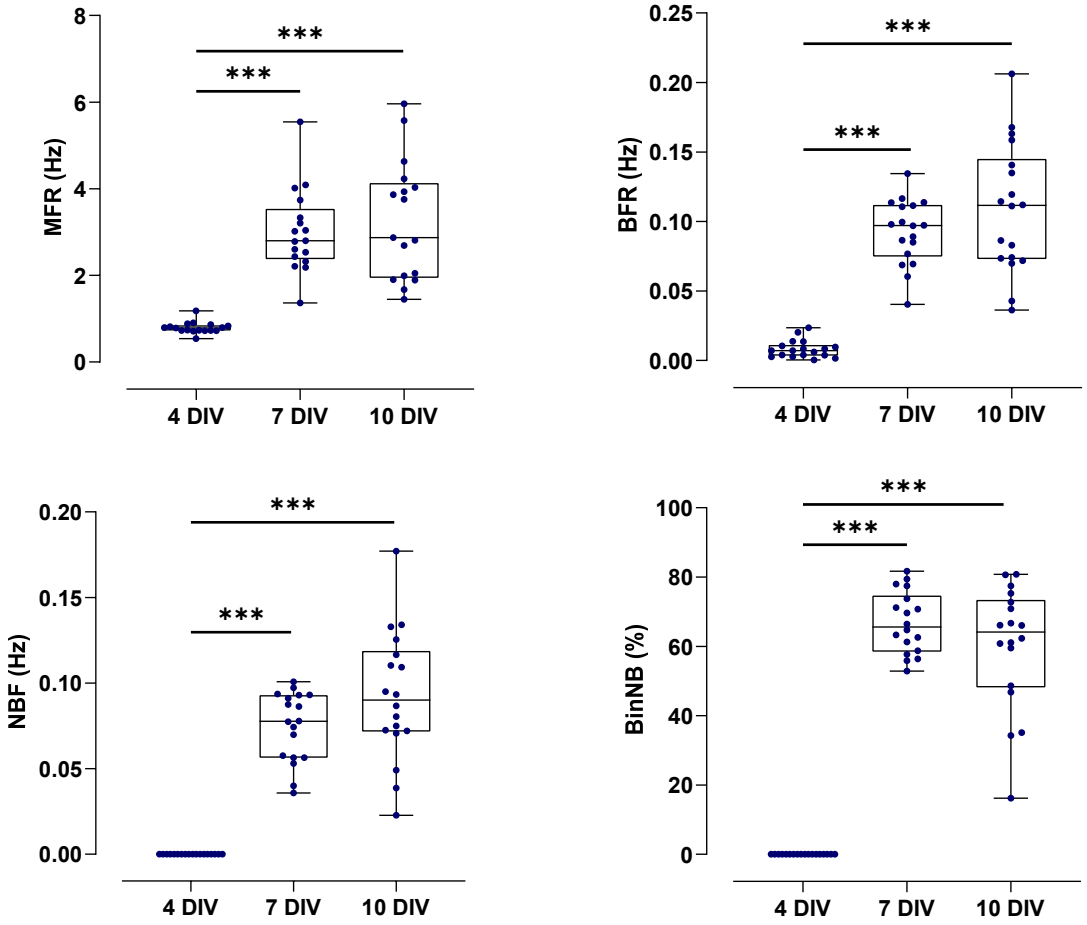

Figure 13. Recording analysis of the primary murine neurons for network activity development. Recordings are conducted from the same devices at 4 DIV, 7 DIV, and 10 DIV. The box plots display the median and quartiles, while the whiskers represent individual wells. Comparisons to control values are made using one-way ANOVA. Asterisks represent the significance. Reproduced from reference [27] (CC BY 4.0) © IOP Publishing.

3.2.3. Cell concentrations in *NeuroMPS 1.0* affect the activity development.

Higher cell concentrations facilitate network formation due to increased synaptic connections. However, *NeuroMPS 1.0* is supplemented with static media, and if the concentration is too high, the cells may experience stress from the accumulation of waste, which negatively impacts electrophysiological activity. *NeuroMPS 1.0* is tested with cell concentrations of 3,000 cells/µl, 4,000 cells/µl, and 5,000 cells/µl to determine the optimal cell concentration to form network activity while maintaining culture health. As network activity develops at 7 DIV (**Figure 12**), electrophysiological activity is assessed at 8 DIV and 9 DIV. The activity is analyzed for parameters including MFR, BFR, MBD, and NBF (**Figure 14**).

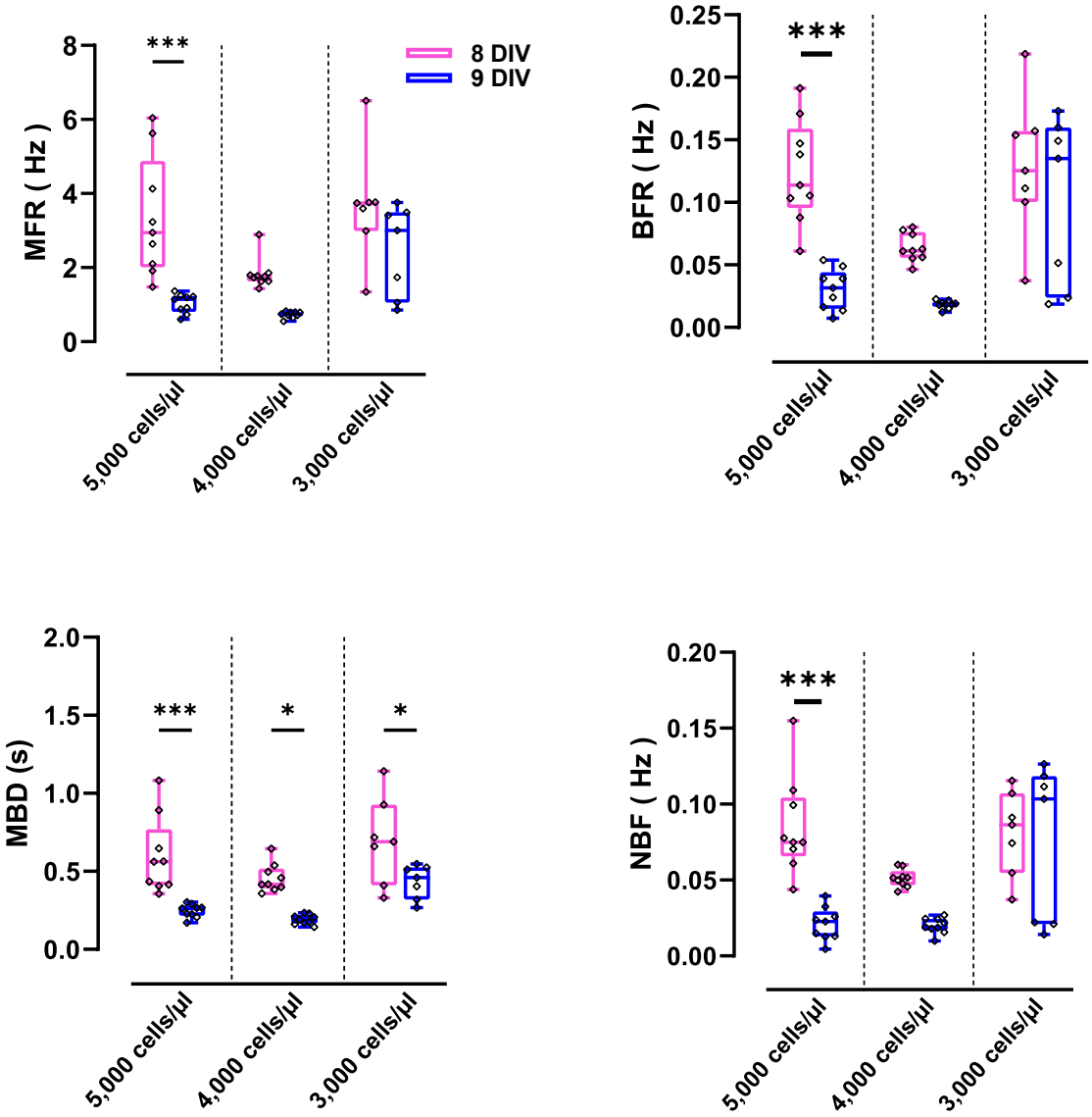

Figure 14. Investigation of optimum cell concentration for electrophysiological readouts. The cells are plated in *NeuroMPS 1.0* at 3,000 cells/µl, 4,000 cells/µl, and 5,000 cells /µl. The activity is

recorded at 8 DIV and 9 DIV. Box plots represent the median and its quartiles. Whiskers demonstrate minimum and maximum values. The activity between 8 DIV and 9 DIV is compared using one-way ANOVA, N=7-9. Asterisks represent the significance.

The wells plated with 5,000 cells/µl exhibit higher median values compared to those plated with 4,000 cells/µl; however, the median for the wells plated with 3,000 cells/µl is similar to that of the 5,000 cells/µl wells. All wells tend to show a decline in activity at 9 DIV, with the most significant drop observed in wells with the highest cell concentration and the smallest drop in wells with the lowest concentration. Despite the similar values for 5,000 cells/µl and 3,000 cells/µl, both exhibit higher variability than the 4,000 cells/µl wells. Additionally, the activity decline at 9 DIV is less severe in the 4,000 cells/µl wells compared to the other concentrations.

The activity is further explored by focusing on 4,000 cells/µl. MFR, BFR, %SinB, MBD, NBF, and %BinNB are determined from the recordings (**Figure *15***). The recordings at 8, 9, and 10 DIV revealed that activity remained relatively stable, with similar variability across all time points. A decrease in activity at 9 DIV is observed only for MBD and %BinNB. At 10 DIV, there is a decline in %SinB, MBD, MFR, and % BinNB values, yet significant drops are noted only in % BinNB and MBD.

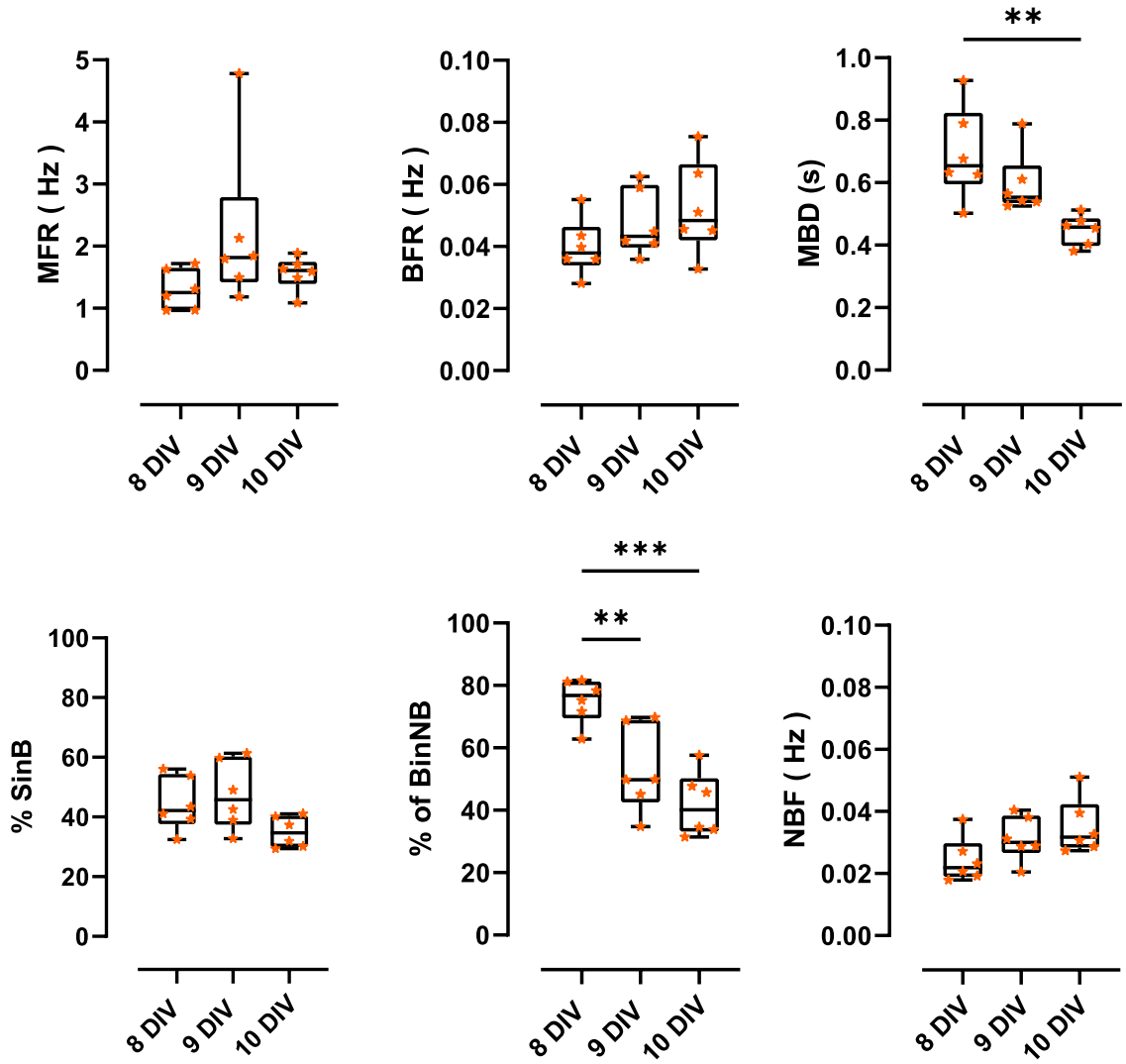

Figure 15. Electrophysiological activity of the wells plated with 4,000 cells/µl. The activity is recorded at 8 DIV, 9 DIV, and 10 DIV. Box plots represent the median and its quartiles; whiskers demonstrate the minimum and maximum values. The data is analyzed using one-way ANOVA, N= 6. Asterisks denote the significance.

3.2.4. Culturing methods can be substituted in *NeuroMPS 1.0*

NeuroMPS 1.0 consists of a gel layer where dissociated cells are embedded in a hydrogel, and on top of this layer, the media layer is supplemented to the culture. Although the hydrogel provides support for building the 3D architecture that recapitulates the physiological conditions, when it comes to compound applications or disease modeling, this might be a limitation due to the penetration of the compounds into the hydrogel. Different culturing methods are investigated to address this issue and assess neuronal activity (**Figure 14**).

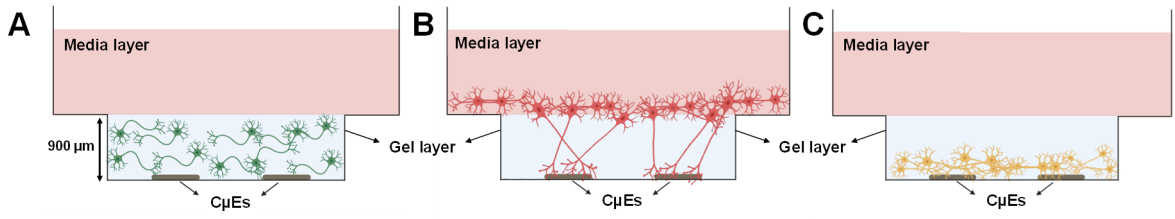

Figure 16. The schematic of tested culturing methods. The cells are embedded in Matrigel and cured immediately to achieve equal distribution—method-1 (**A**). The cells are plated on top of a 900 µm matrigel layer, and neurites are grown into a gel layer—method-2 (**B**). The cells are embedded in matrigel; however, before curing, the device is kept cold to allow cells to sink down to the bottom 100 µm part—method-3 (**C**). The figure is created with Biorender.com.

Two different cell concentrations (28,000 cells/well and 35,000 cells/well) are utilized across three different culturing methods. Electrophysiological activity is recorded at 4 DIV, 6 DIV, 8 DIV, and 10 DIV. The data is analyzed for MFR and NBF (**Figure 17**, **Figure 15** and **Figure 16**). Results indicate that wells with the higher cell concentration tend to lose activity by 10 DIV, except in method 2. This exception in method 2 may be due to the constant contact with the media interface, which potentially facilitates better cell waste removal. In contrast, insufficient waste removal through the gel in methods 1 and 3 likely contributes to the observed activity drop. Across different culturing methods, MFR and NBF exhibit similar trends for wells with lower cell concentrations. Therefore, depending on the study's requirements, any of these methods can be employed to achieve reliable results.

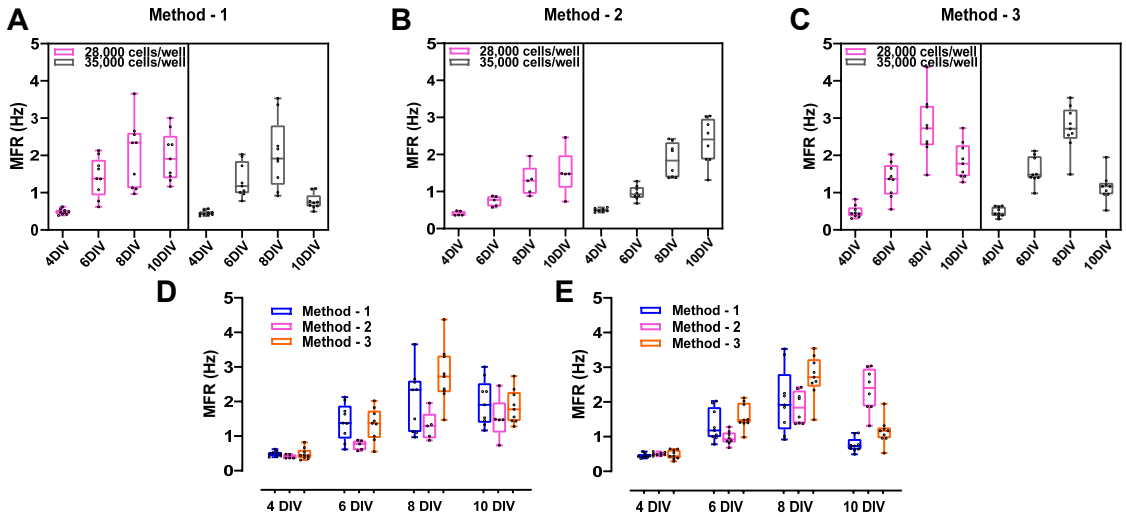

Figure 17. Testing different culturing methods for electrophysiological activity development - MFR. 28,000 cells/ well and 35,000 cells / well are plated into neuro MPS 1.0, and activity is recorded at 4, 6, 8, and 10 DIV. Data is analyzed for MFR. Different cell concentrations per method are plotted in panels **A**, **B**, and **C**. Different methods per time point for 28,000 cell / well are plotted in panel **D** and for

35,000 cell/well in panel **E**. Bar graphs represent the median and its quartiles, and whiskers demonstrate minimum and maximum values, N= 5-9 wells.

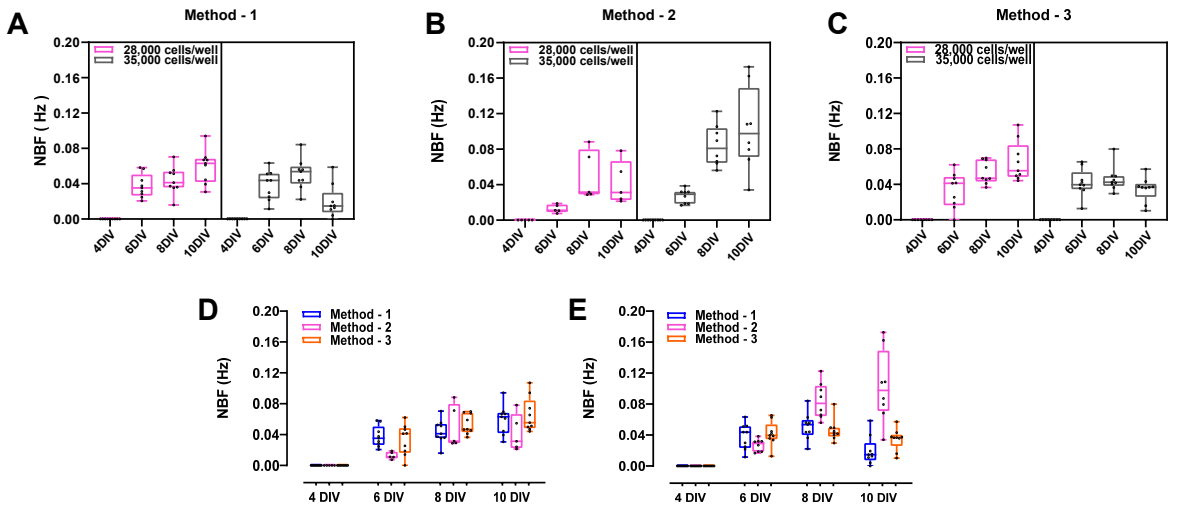

Figure 18. Testing different culturing methods for electrophysiological activity development - NBF. 28,000 cells/ well and 35,000 cells / well are plated into neuro MPS 1.0, and activity is recorded at 4, 6, 8, and 10 DIV. Data was analyzed for network burst frequency (NBF). Different cell concentrations per method are plotted in panels **A**, **B**, and **C**. Different methods per time point for 28,000 cell / well are plotted in panel **D** and for 35,000 cell/well in panel **E**. Bar graphs represent the median and its quartiles, and whiskers demonstrate minimum and maximum values, N= 5-9 wells.

3.2.5. Spontaneous activity recovery after handling and pipetting

Electrophysiology is a sensitive readout, and network activity may vary due to any disturbances in the cultural environment. Handling and pipetting also contribute to fluctuations in network activity. It is essential to determine the earliest time at which the culture recovers from environmental and pipetting disruptions. Recovery is assessed at both the well and electrode levels, with data analyzed for MFR, BFR, % SinB, and MBD.

NeuroMPS 1.0 is plated with primary murine neurons and astrocytes at a concentration of 4,000 cells/µl to assess the effect of handling. Spontaneous network activity is recorded, and the devices are returned to the incubator. To determine the impact of pipetting along with handling, media is applied to the wells following the recording of spontaneous activity, simulating compound application. Recovery is evaluated by comparing the relative change in activity to the initial spontaneous activity after 30 minutes, 1 hour, and 2 hours, aiming for minimal change. The data shows that the culture fully recovers from handling disturbances after 2 hours, with minimal recovery occurring after 30 minutes and 1 hour (**Figure 19**). Conversely, the culture exhibits a notably rapid recovery from disturbances caused by

pipetting and handling; across all parameters, activity shows signs of recovery within one hour (**Figure *20***).

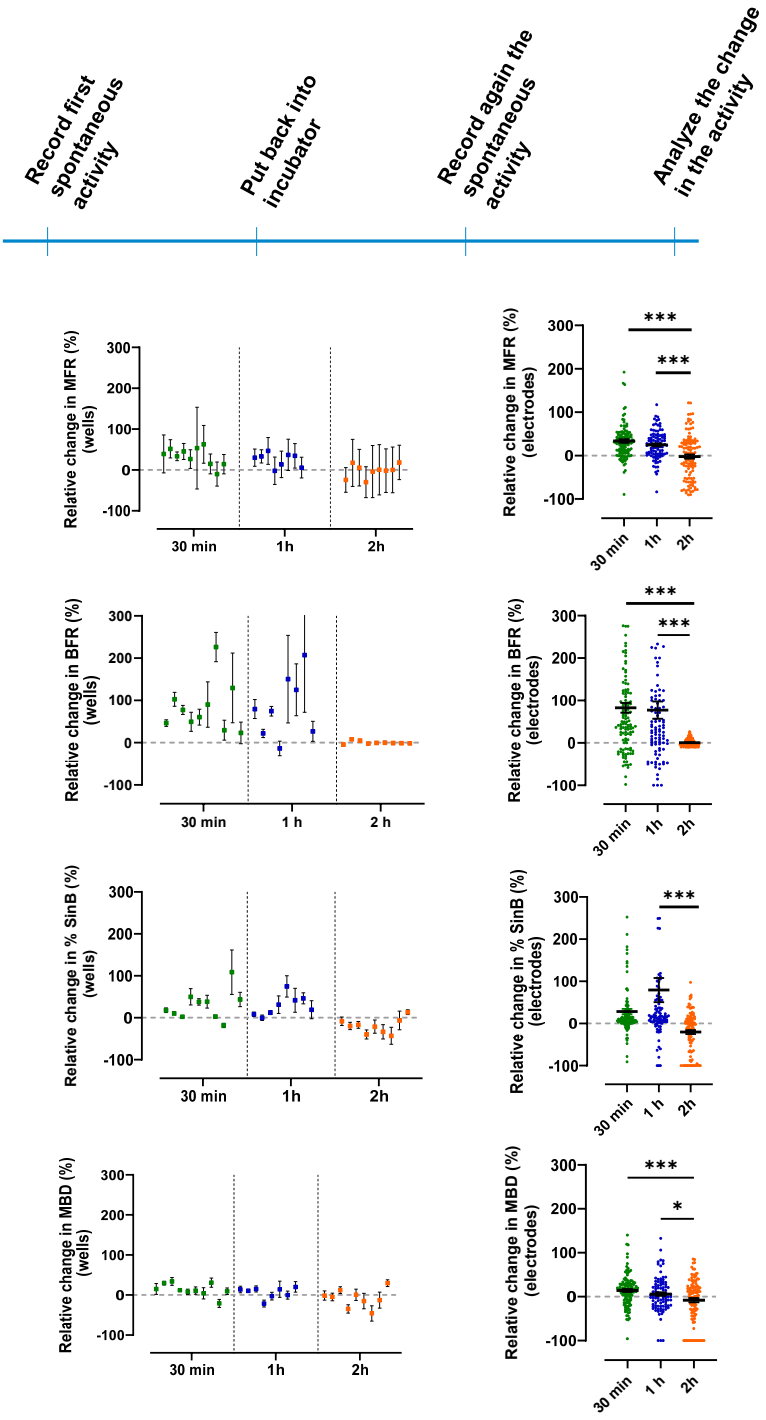

Figure 19. Electrophysiological activity recovery from handling the NeuroMPS 1.0. The devices are brought to the recording set-up, the spontaneous activity is recorded, and they are returned to the incubator. The activity is recorded after 30 minutes, 1 hour, and 2 hours to assess the recovery, and the relative change to spontaneous activity is plotted. The data are analyzed for MFR, BFR, %SinB, and MBD. In the graphs that demonstrate the data at the well level, the dots represent the mean value of the well, which has 14 electrodes, and error bars indicate SEM. In the graphs illustrating the data at the

electrode level, the dots represent the values recorded from each electrode, the horizontal line indicates the mean value. The electrode level data is analyzed using one-way ANOVA, N= 126. Asterisks denote the significance.

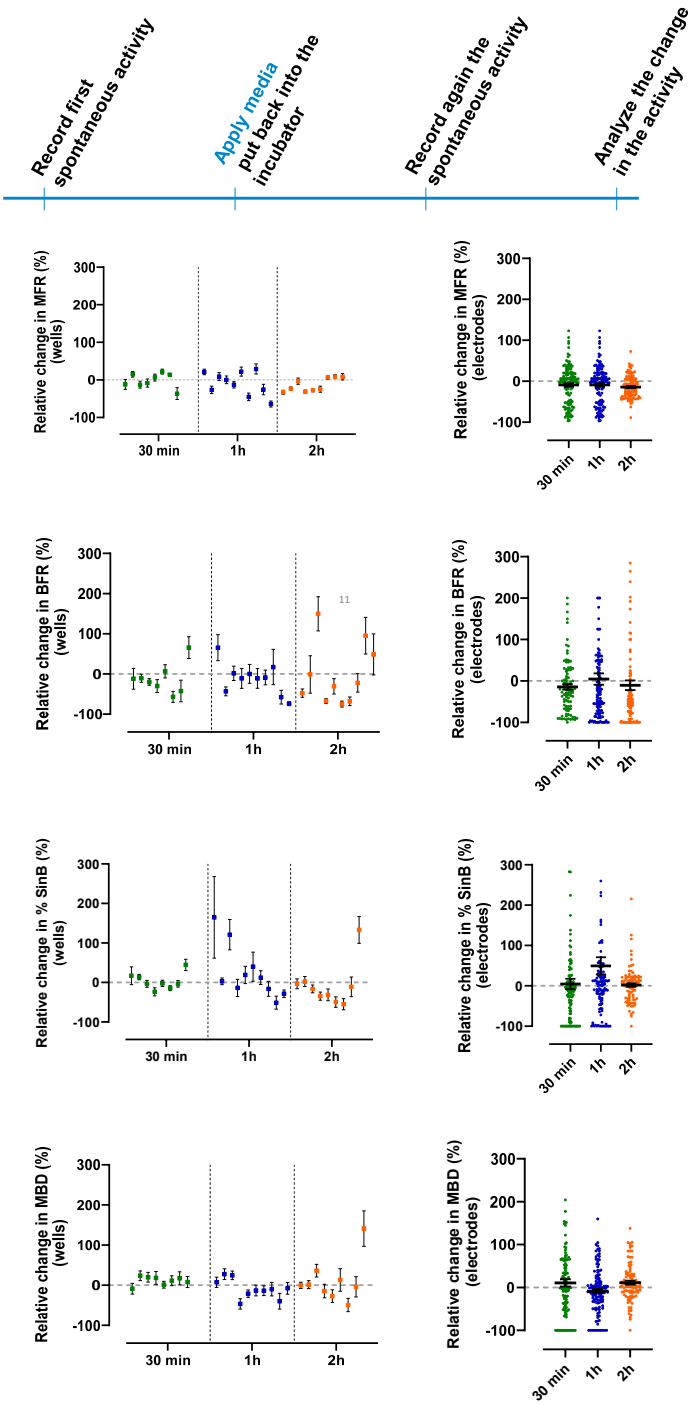

Figure 20. Electrophysiological activity recovery from handling and pipetting in the neuroMPS 1.0. The devices are brought to the recording set-up, the spontaneous activity is recorded, and then media is applied to each well and returned to the incubator. The activity is recorded after 30 minutes, 1 hour, and 2 hours to assess the recovery, and the relative change to spontaneous activity is plotted. The data are analyzed for MFR, BFR, %SinB, and MBD. In the graphs that demonstrate the data at the

well level, the dots represent the mean value of the well, which has 14 electrodes. In the graphs illustrating the data at the electrode level, the dots represent the values recorded from each electrode, the horizontal line indicates the mean value. The electrode level data is analyzed using one-way ANOVA, N= 126. Asterisks denote the significance.

3.2.6. Culture compositions affect the network activity.

NeuroMPS 1.0 is cultured with two different culture compositions. First, it is cultured with neurons and astrocytes, and for the following composition, microglia are added to the culture with a 1:8 ratio to the rest of the cells in the culture. It is known from the literature that microglia support neuronal network maturation[99]. The activity was analyzed for mean firing rate, burst frequency rate, % of spikes in bursts, and mean burst duration. For further exploration, pro-inflammatory compounds interferon-gamma (IFN-γ) and tumor necrosis factor-alpha (TNF-α) have been applied to the culture, and their effect is investigated. The network activity begins to develop by 7 DIV, with network bursts appearing in primary murine culture (**Figure 12**). Therefore, 8 DIV cultures serve as the starting point for this study. Initial (basal) activity is recorded, followed by applying pro-inflammatory compounds to the wells. Subsequent recordings from *NeuroMPS 1.0* devices are taken after 24 and 48 hours of incubation. The final data is normalized to the basal activity recorded at 8 DIV, aiming to provide a more accurate evaluation of relative changes over time. Additionally, different media are used for the culture compositions (

Table *21*).

Table 21. Culture groups. Groups are categorized according to the cell composition, cytokine treatments, and pro-inflammatory compound applications. +: compound added, -: compound is not added.

Groups	Cultures	IL-34 and TGFβ2	IFNγ and TNFα
A	Neurons+Astrocytes (N+A)	**-**	**-**
B	Neurons+Astrocytes (N+A)	**-**	**+**
C	Neurons+Astrocytes (N+A)	**+**	**-**
D	Neurons+Astrocytes (N+A)	**+**	**+**
E	Neurons+Astrocytes+Microglia (N+A+M)	**+**	**-**
F	Neurons+Astrocytes+Microglia (N+A+M)	**+**	**+**

Microglia are incorporated into the culture to enhance its physiological relevance. Since cytokines are vital for microglia survival and health, IL-34 and TGFβ2 are added to the media for groups E and F. These cytokines are also included in group C to investigate their potential effects on neuronal or astroglial populations. Pro-inflammatory compounds are applied to groups B, D, and F. Groups B, C, and D, which contain only neurons and astrocytes, do not show significant differences compared to the untreated group (A) in any parameters. The presence of cytokines does not produce a significant effect either. However, cultures containing microglia exhibit a tendency for rapid decreases in activity compared to group A (untreated). The application of pro-inflammatory compounds activates the microglia, and the significant reductions in MFR and BFR suggest that activated microglia substantially influence neuronal circuits and disrupt the network (**Figure 21**). When comparing group D (neurons and astrocytes) with group F (neurons, astrocytes, and microglia), group F shows a more significant decrease in activity after stimulation with pro-inflammatory compounds. This confirms that microglia activation significantly impacts network activity. Additionally, group E (non-stimulated, microglia-containing culture) shows significant decreases, suggesting the possibility that the matrigel cultural conditions themselves may activate the microglia.

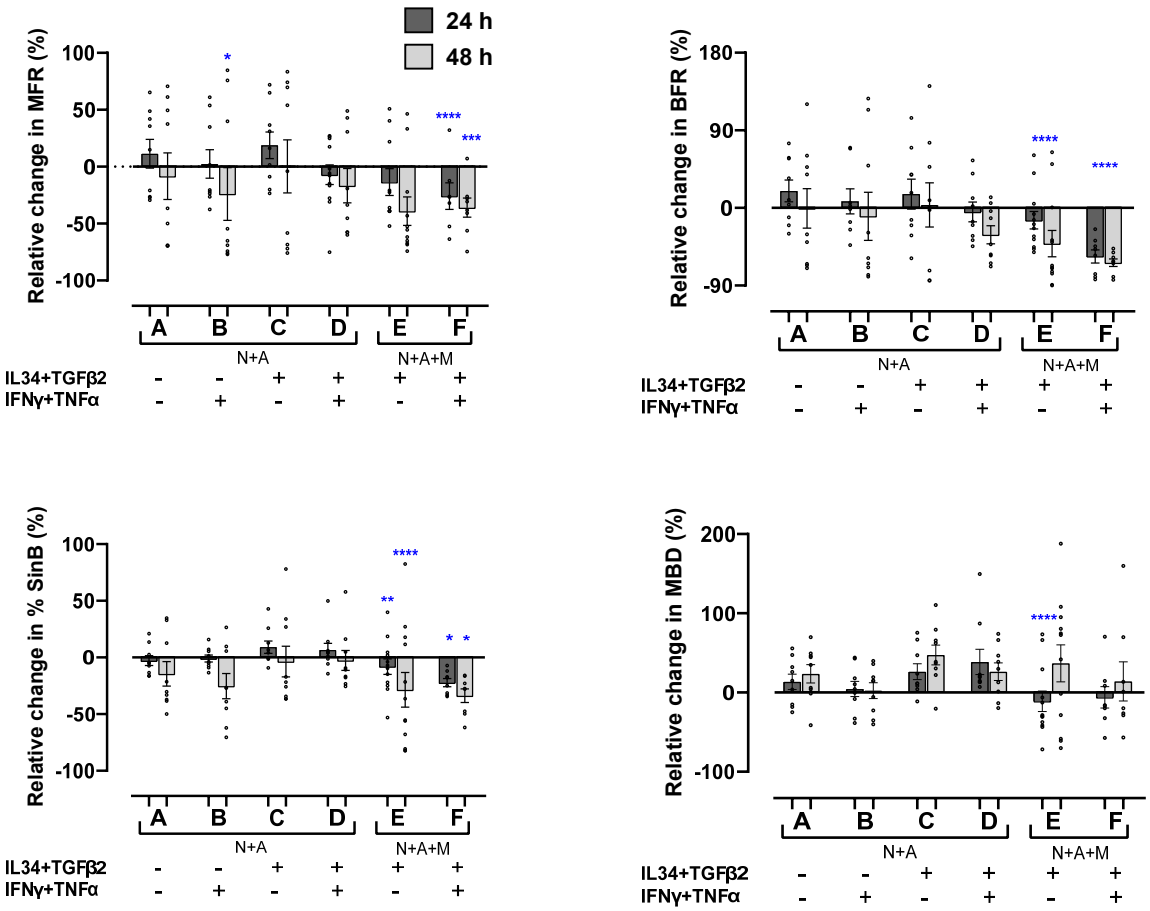

Figure 21. Stimulation of different culture conditions with pro-inflammatory compounds. Recording data was analyzed and plotted as a relative change to recordings performed at 8 DIV (T=0). The data compared was acquired at T= 24 h and T= 48 h after pro-inflammatory compound application. Data are plotted as bar graphs where bars indicate mean value, dark grey bars, and whiskers represent T=24h, while light grey bars and whiskers represent t=48h. The data was analyzed using one-way ANOVA against a non-treated sample (group A). Blue asterisks represent the significance level between group A and the different conditions. Tables under the graphs illustrate the presence (+) or the absence (-) of cytokines (IL34 and TGFβ2) and pro-inflammatory compounds (IFNγ and TNFa). Culture groups are explained in

Table **21**.

A neurotoxin study has been conducted using *NeuroMPS 1.0* with primary murine cells. Rotenone, a pesticide that disrupts the complex I pathway in mitochondria[100], has been used as a neurotoxin. The study utilizes a tri-culture of neurons, astrocytes, and microglia. Endpoint analyses include morphological readouts and electrophysiological measurements. Morphological readouts have been performed exclusively on neurons after transducing them with eGFP proteins. Images of the neurons have been acquired 20 minutes, 6 hours, and 24 hours following rotenone application. The earliest dissociation of neurites has been observed

after 24 hours and only in samples subjected to high concentrations of rotenone (1 µM, 0.5 µM, and 0.1 µM).

The tri-culture has also been assessed for its electrophysiological response to rotenone. Five concentrations were applied to the tri-culture, and electrophysiological activity has been recorded 10 minutes after application. The recordings were analyzed for MFR, BFR, and MBD. A significant decrease in both MFR and BFR has been observed at all concentrations. However, the response in MBD is not significant at the 0.01 µM rotenone concentration (**Figure 22**). The electrophysiological effects of rotenone were observed rapidly, in contrast to the morphological changes, which took up to 24 hours and were only significant at higher concentrations of rotenone (**Figure 23**).

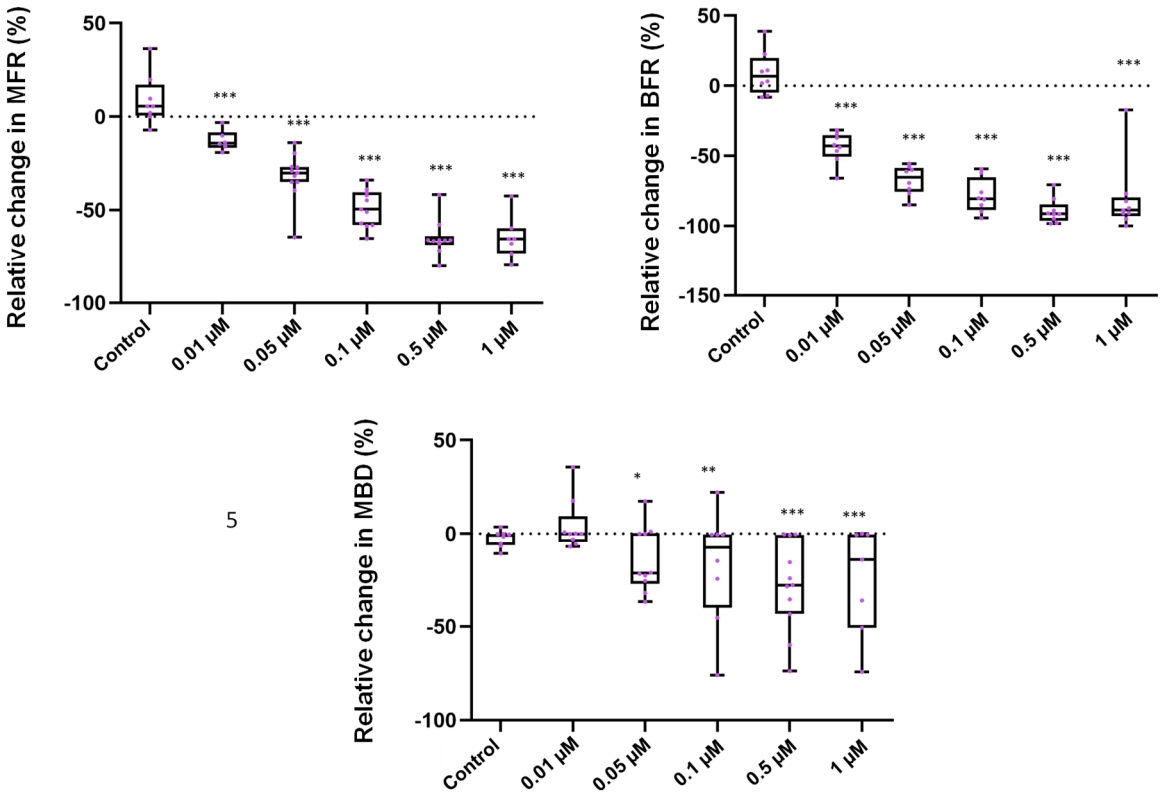

5

Figure 22. Electrophysiological response of primary murine cells to rotenone. 8 DIV neuron, astrocyte, and microglia tri-culture is treated with rotenone for 10 minutes, and the electrical activity is recorded. Recordings are analyzed for MFR, BFR, and MBD; bar graphs represent the median and its quartiles. Whiskers demonstrate individual recordings and N= 8-10 wells. Data was analyzed with one-way ANOVA against the control group, and asterisks represent the significance.

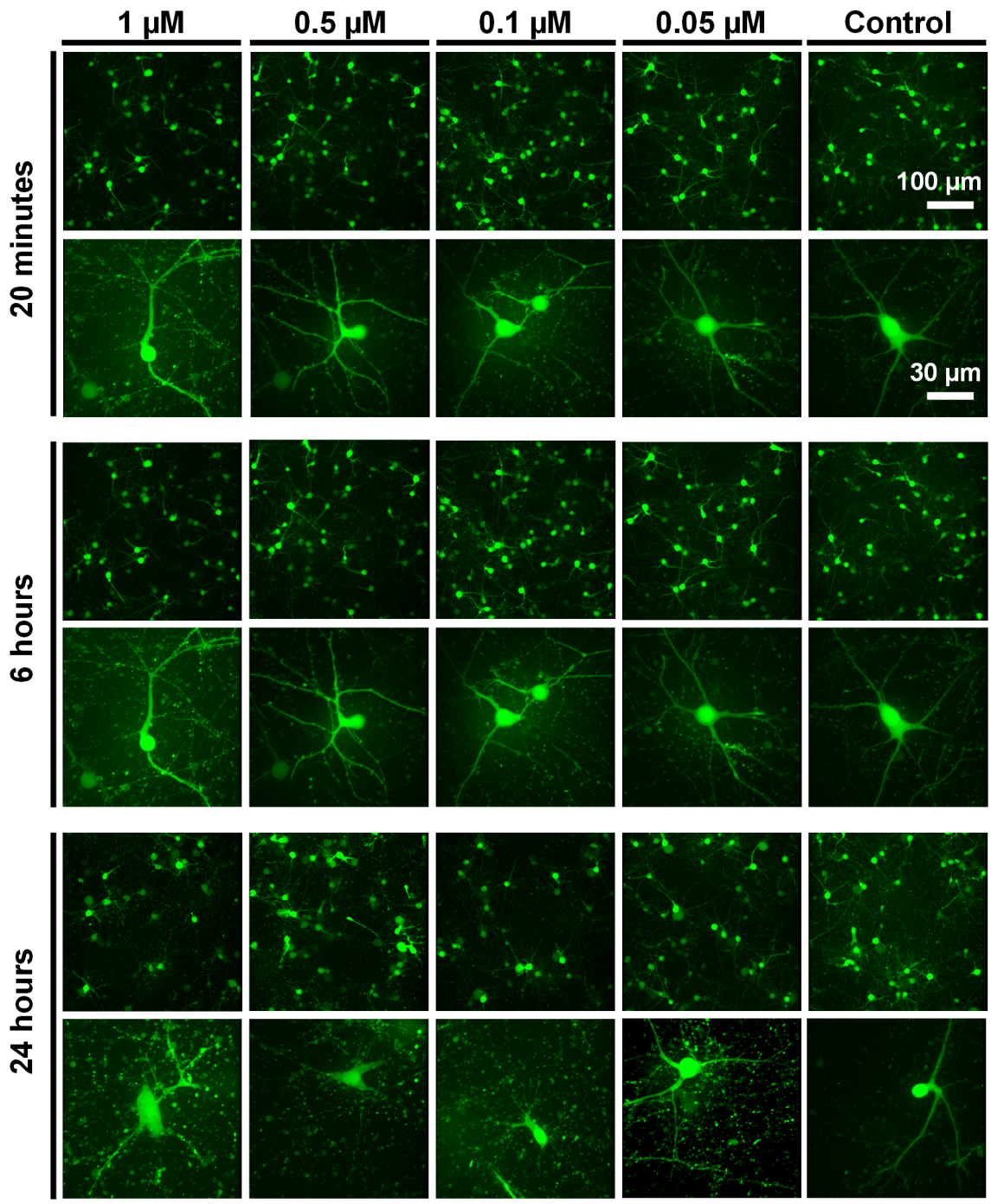

Figure 23. Morphological changes in neurons in response to Rotenone application. Primary murine neurons are transduced with eGFP protein. Four different concentrations of rotenone are applied to 8 DIV culture and the culture is imaged after 20 minutes, 6 hours and 24 hours of incubation. The images are MIP of 300 µm thick stacks.

3.3. Neuro-micro physiological system 2.0

Neurospheres derived from induced pluripotent stem cells (iPSCs) hold promise for exploring human-specific molecular, cellular, and genetic events similar to those observed in the human brain, potentially shedding light on neuronal functions in healthy or dysfunctional states.

Numerous research teams currently assess neurosphere culture's advantages and challenges by investigating how the cells derived in neurospheres represent natural human brain growth across the genetic expression, protein composition, shape, electrical activity, architecture, and functionality. So far, research into neurospheres has primarily been devoted to confirming and enhancing the accuracy of these models, though efforts to identify characteristics relevant to intricate illness mechanisms are underway. Despite neurospheres evolving to exhibit distinct and vigorous characteristics, they are still very basic compared to the brain's complex structure.

3D cultures are achieved either with a hydrogel scaffold, which aims to imitate ECM structure and give cells support, or the cells are assembled as spheroids and secrete their ECMs. Neuronal cultures require a specific stiffness, and the hydrogel must support neurite growth throughout its matrix to form a comprehensive neuronal network. Selecting an appropriate hydrogel that meets these criteria presents a significant challenge. To overcome this issue, neuronal cultures tend to move towards assembled cultures. These cultures generally start from pre-differentiated neuro precursor stages, and the cells are guided into spheroid structures. Spheroids are then differentiated into neurons and glial cells. As the brain consists of neuronal and glial populations, getting these populations in spheroids is also desired. The goal is to use these neurospheres for in vitro screenings and achieve better predictability before transferring the results to the clinics.

3.3.1. Neurosphere model

It is still quite challenging to achieve an active neuronal network in neurospheres. Here, I modified the protocol from Pamies et al.[67] to enhance the network formation and obtain an electrophysiological activity. The protocol begins with neural progenitor cells, which are induced to form spheroids and subsequently cultured in suspension with constant shaking throughout the differentiation period. (**Figure 24**). This is a relatively simple differentiation method in which the cells are pushed towards neuronal and glial cells with only two growth factors: brain-derived neurotrophic factor (BDNF) and glial cell line-derived neurotrophic factor (GDNF). Synaptic network formation is enhanced with a base medium switch at week 3, and differentiation and network formation are characterized by 8 weeks.

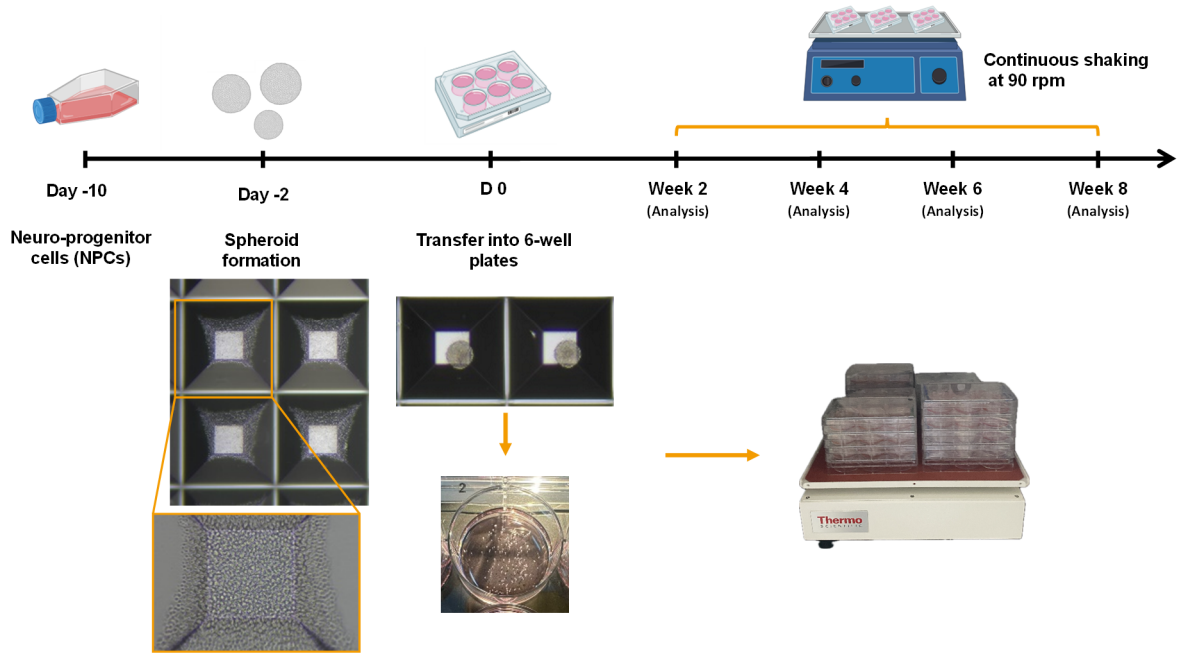

Figure 24. Schematic of neurosphere generation. Created with Biorender.com

3.3.2. Characterization of the neuro progenitor cells

The brightfield images of AX18 and KOLF2.1J cell lines showed the typical rosette structure of the NPCs (**Figure 25**). The cells are stained for PAX-6, SOX2, and nestin, which are the marker proteins for neuronal progenitor cells[101]. The flow cytometry results showed that at least 80 % of the population is positive for the NPC markers for AX18 (**Figure 26- A**) and 60 % for KOLF2.1J **Figure 27 - A**) lines. The immunocytochemistry showed the co-localization of nestin/SOX2 and nestin/PAX6 in the cells (**Figure 26 – B** and **Figure 27 – B**)

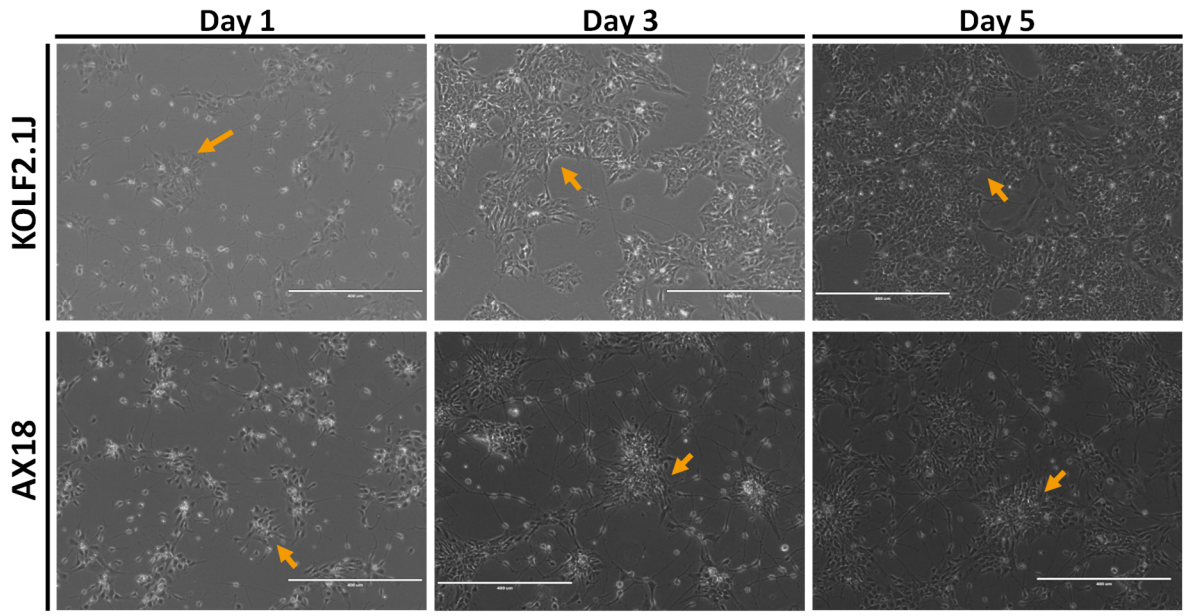

Figure 25. Brightfield images of AX18 and KOLF2.1J NPC lines. Brightfield images are taken on days 1, 3, and 5. The arrows show the rosette structures of the NPCs. Both NPC lines show the typical morphology of the neuro progenitor cells. The scale bar is 400 µm.

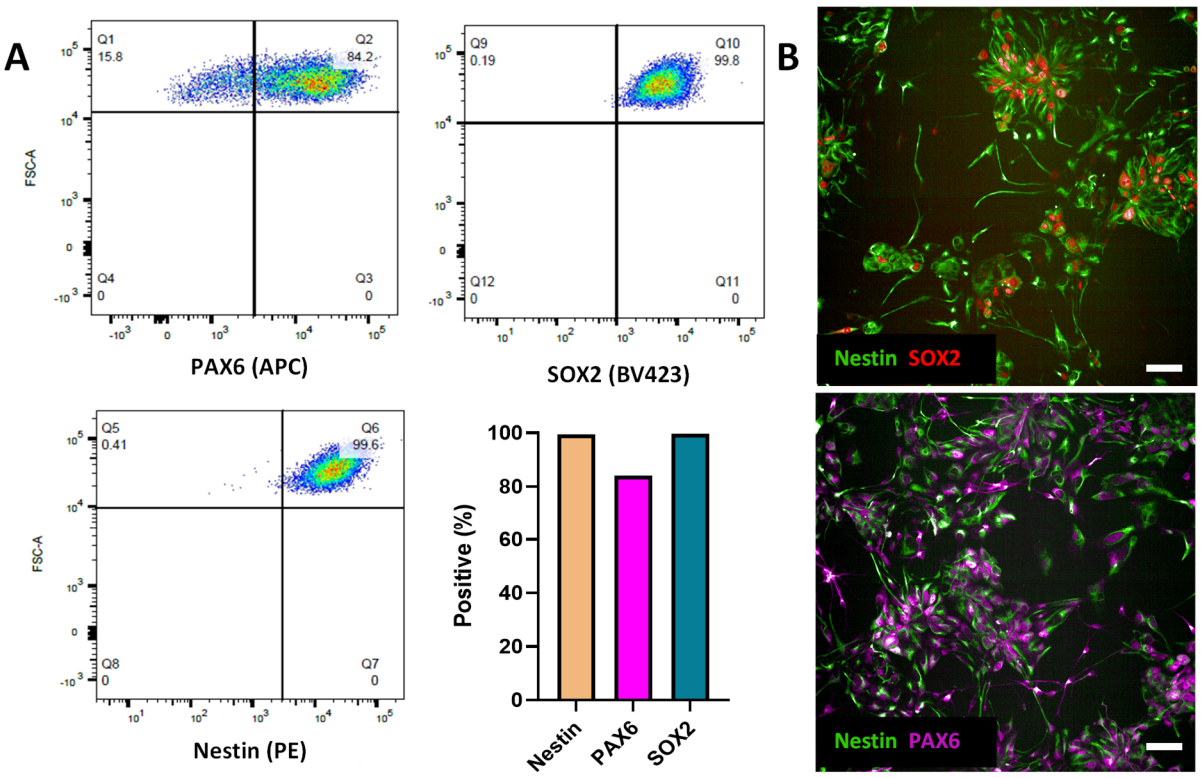

Figure 26. Characterization of AX18 NPC line. Flow cytometry data of the AX18 line for PAX6, SOX2 and nestin. More than 80 % of the cells are positive for all the markers **(A)**. Immunocytochemistry of the AX18 line showed the co-localization of the nestin and SOX2 (top), nestin and PAX-6 (bottom). The scale bars are 50 µm **(B)**.

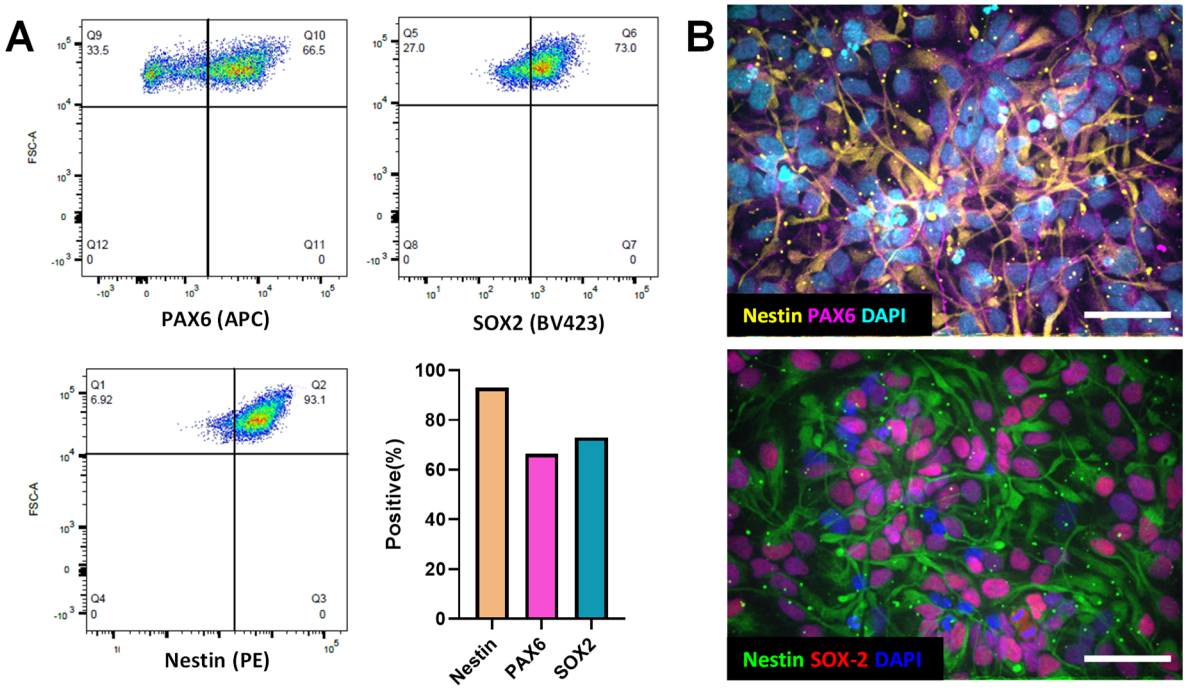

Figure 27. Characterization of neuro progenitor cells from KOLF2.1J line. Flow cytometry data of the KOLF2.1J NPCs for PAX6, SOX2 and nestin. More than 60 % of the cells are positive for all the markers **(A)**. Immunocytochemistry of the KOL2.1J line showed the co-localization of the nestin and PAX-6 (top), nestin and SOX2 (bottom). The nuclei were stained with DAPI. The scale bars are 50 µm **(B)**.

3.3.3. Viability assessment of the neurospheres

The viability is examined every two weeks. Nuclei stained with Hoechst, the dead cells in AX18 neurospheres are stained with BOBO™-3 iodide and dead cells in KOLf2.1J neurospheres are stained with Celltox Green. AX18 neurospheres have more dead cells than KOLF2.1J neurospheres over time. At week 8, AX18 neurospheres have developed a larger necrotic core compared to the KOLF2.1J neurospheres (**Figure 28**). In addition to staining, the viability is assessed by CellTiter-Glo® 3D Viability Assay (G9681, Promega GmbH, Germany) every two weeks (**Figure 29**). AX18 neurospheres demonstrate decreasing viability over time.

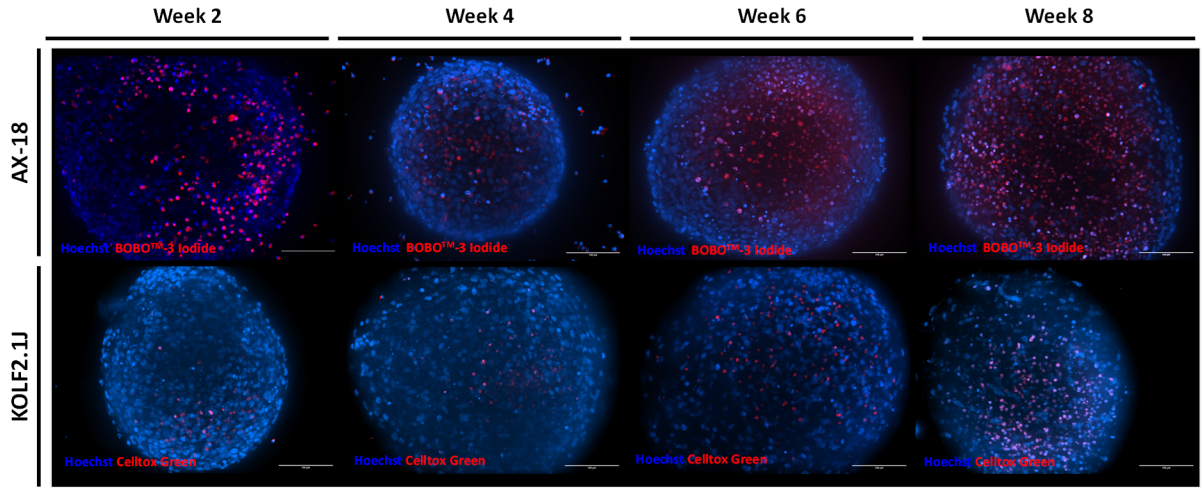

Figure 28. Representative images of AX18 and KOLF2.1J neurospheres for viability assessment. The nuclei of the cells are stained with Hoechst (blue). Dead cells in AX18 neurospheres are stained with BOBO™-3 iodide (red) and in KOLF2.1J neurospheres with Celltox Green (red). Scale bar, 100 µm.

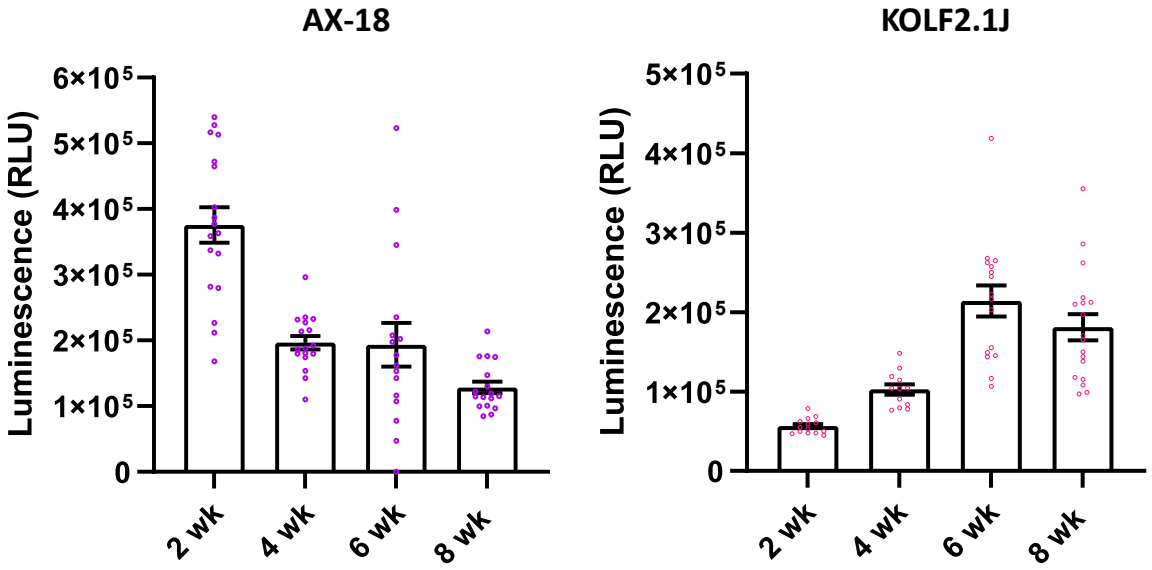

Figure 29. Viability assessment of the neurospheres over time. Viability is assessed based on the present ATP activity, which indicates the metabolically active cells. A direct relationship exists between the luminescence measured and the ATP activity. AX18 neurospheres have showed decreased ATP activity over time, resulting in decreased viability (left). In contrast, KOLF2.1J neurospheres have followed an increasing ATP activity until week 6; however, the activity has dropped at week 8 (right).

3.3.4. Characterization of the neurospheres

NPCs are guided towards neurons and glial cells with neurosphere culturing medium (**Table 17**) and neurosphere maturation medium(**Table 18**). Immunocytochemistry staining is used to characterize the differentiation of the NPCs towards these populations. The neurospheres are stained for axons (TUBB3, NFH), dendrites (MAP2), astrocytes (GFAP), and upper (SABT2) and lower (CTIP2) layer markers (**Figure 30-33**). Neurospheres are also stained for dopaminergic neurons (TH), inhibitory neurons (Parvalbumin), and pre-synaptic molecules (Synapsin1, Synaptophysin1) (**Figure 34**).

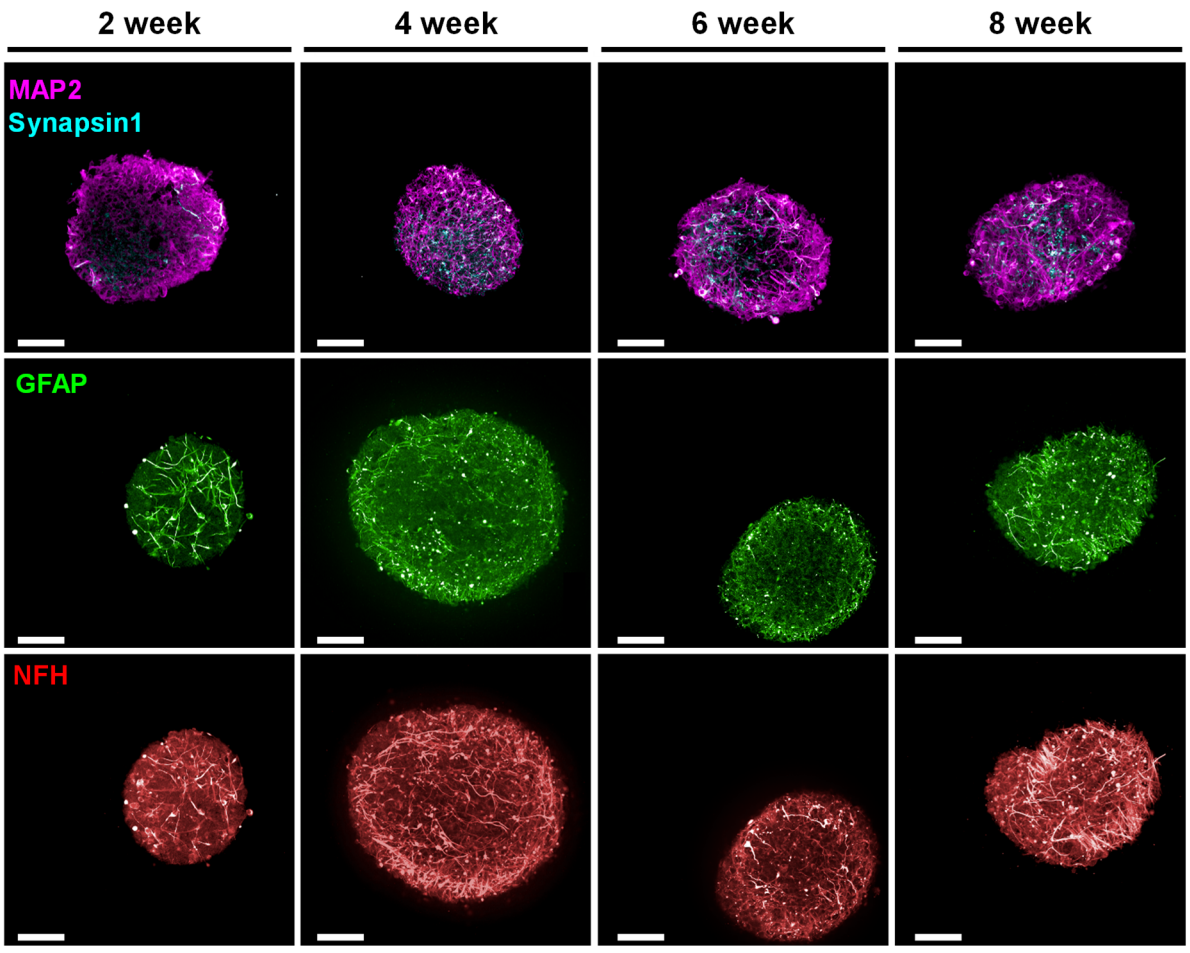

Figure 30. Immunocytochemistry of AX18 neurospheres. Neurospheres are stained for dendrites (MAP2), astrocytes (GFAP), Axons (NFH), and pre-synaptic proteins (Synapsin1). The images are maximum intensity projections of stacks that scanned 300 µm. Scale bar, 100 µm.

Both AX18 and KOLF2.1J neurospheres develop neurons and astroglia. The astrocyte population starts to form within two weeks of differentiation and continues to increase over time. Dendritic and axonal markers are present at week 2, and the neurofilament heavy chain

(NFH) marker starts at week 2 and increases in abundance over time (**Figure 30** and **Figure 31**). KOLF2.1J neurospheres are further assessed for the presence of markers from variable layers of the brain. Upper- and lower-layer markers are positive for the 6-week-old neurospheres (**Figure 33**). The presence of the markers from different brain layers indicates that the neurospheres recapitulate a better phenotypic representation of the brain.

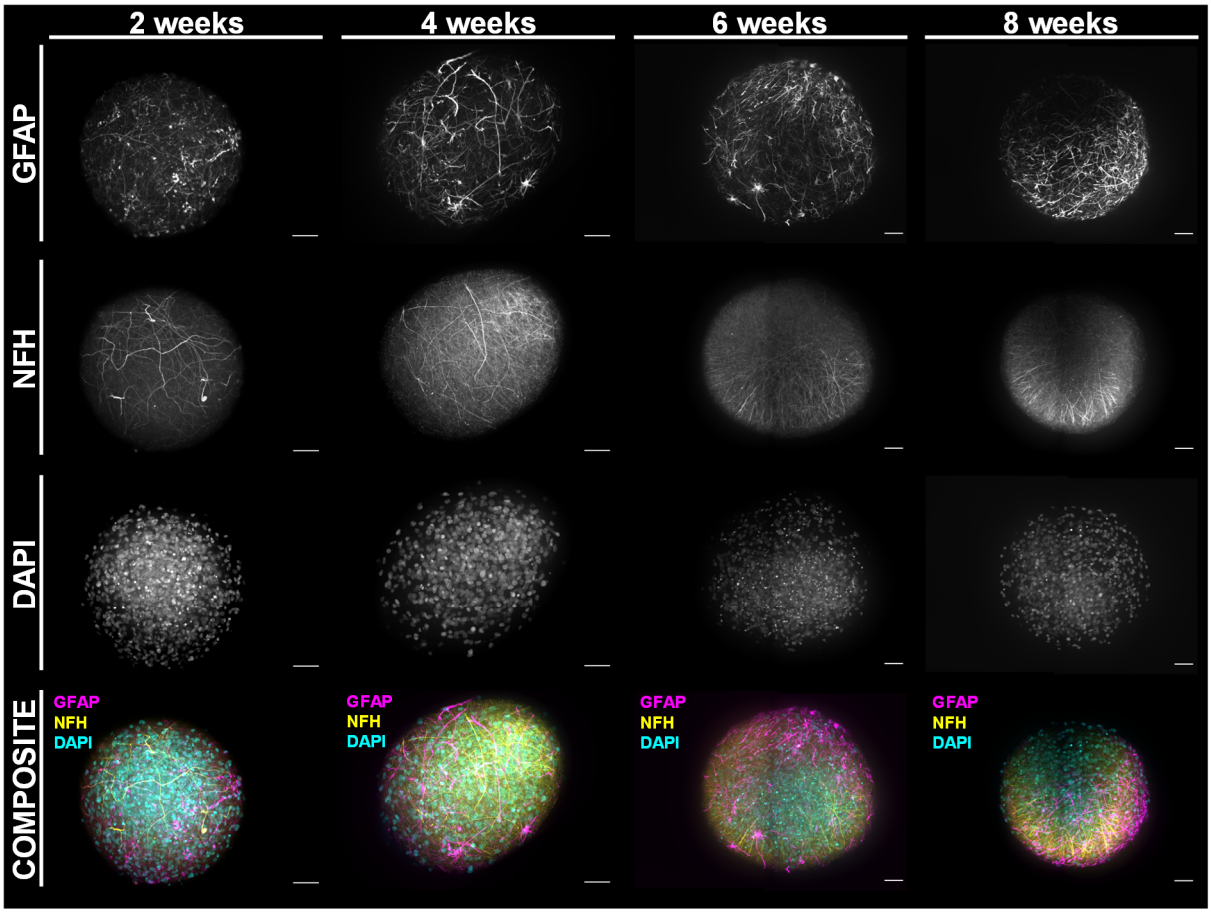

Figure 31. Immunocytochemistry of KOLF2.1J neurospheres. Neurospheres are stained for astrocytes (GFAP), Axons (NFH), and nuclei (DAPI). The images are maximum intensity projections of stacks that scanned 300 µm. Scale bar, 50 µm.

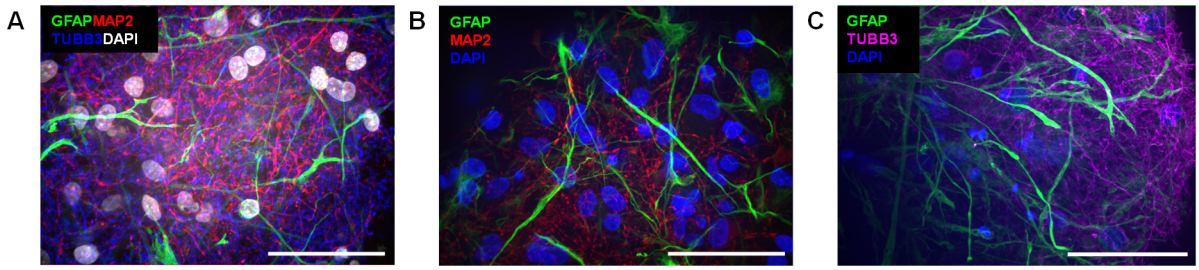

Figure 32. Immunocytochemistry of KOLF2.1J neurospheres imaged with higher magnification. Astrocytes are labeled with GFAP (green), dendrites are labeled with MAP2 (red), Axons are labeled with TUBB3, and nuclei are labeled with DAPI (white). The stained neurosphere is 6 weeks old **(A)**. Astrocytes (GFAP) are shown in green; dendrites (MAP2) are shown in red, and nuclei (DAPI) are shown in blue. The stained neurosphere is 6 weeks old **(B)**. Astrocytes (GFAP) are shown in green, axons (TUBB3) are shown in magenta, and nuclei (DAPI) are shown in blue. The stained neurosphere is 8-week-old **(C)**. Scale bar, 50 µm.

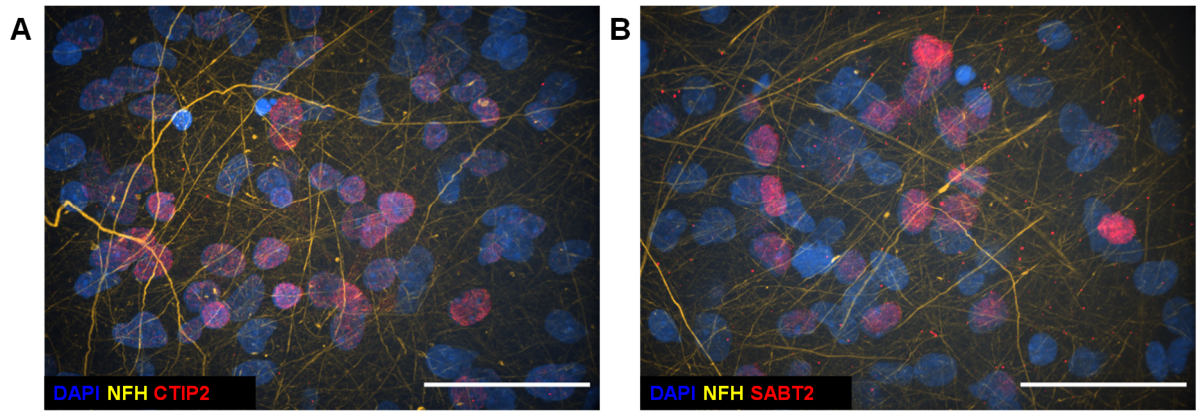

Figure 33. Immunocytochemistry of KOLF2.1J neurospheres for specific brain region markers. A 6-week-old neurosphere is stained for neurites (NFH), nuclei (DAPI), and cerebral cortex lower layer (layer V and VI) marker (CTIP2) **(A)**. A 6-week-old neurosphere is stained for neurites (NFH), nuclei (DAPI), and cerebral cortex upper layer (SABT2) **(B).** Scale bar, 50 µm.

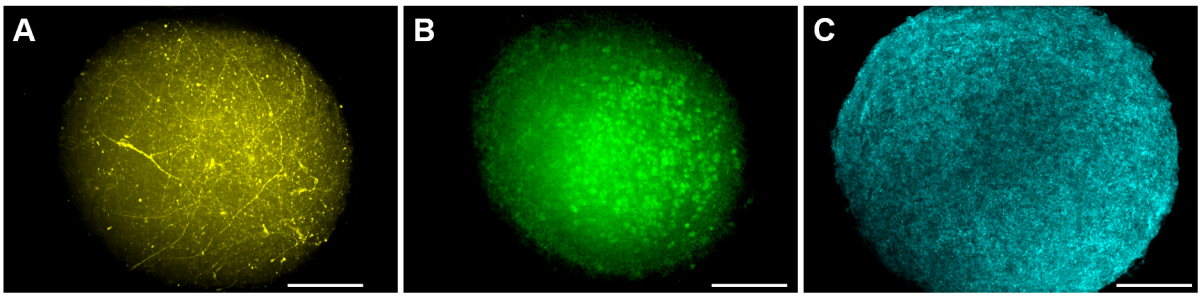

Figure 34. Immunocytochemistry of 6-week-old KOLF2.1J neurospheres for different neuron types and pre-synaptic vesicles. Dopaminergic neurons are stained with tyrosine hydroxylase (TH) **(A).** Inhibitory (GABAergic) neurons are stained with parvalbumin **(B)**. Pre-synaptic vesicles are stained with synaptophysin1 **(C)**. Scale bar, 100 µm. The images are maximum intensity projection of 300 µm scan.

3.3.5. Characterization of the physical properties of the KOLF2.1J neurspheres

KOLF2.1J neurospheres are used to assess the physical properties of the neurospheres over time, and the changes in diameter and circularity of the neurospheres are examined. As explained in detail in section 2.12, the brightfield images are taken every two weeks, and the diameter and circularity values are plotted (**Figure 35**). More than 50 neurospheres are analyzed, and the mean value of the diameter is calculated as 423.1 ± 57.5 µm (standard deviation) at week 2, 492.3 ± 53.4 µm at week 4, 538.4 ± 61.8 µm at week 6 and 698.5 ±109.7 µm at week 8. The diameter plot reveals that the diameters of the neurospheres increase over time; however, while the standard deviation remains similar for the first three time points, on week 8, the standard deviation value doubles, and the variability of the diameter increases. The circularity of the neurospheres is stable with low variability, with a mean value of 0.8 ± 0.02 (standard deviation) until week 8. However, the circularity value drops to 0.7, and the standard deviation increases fivefold to 0.1 at week 8.

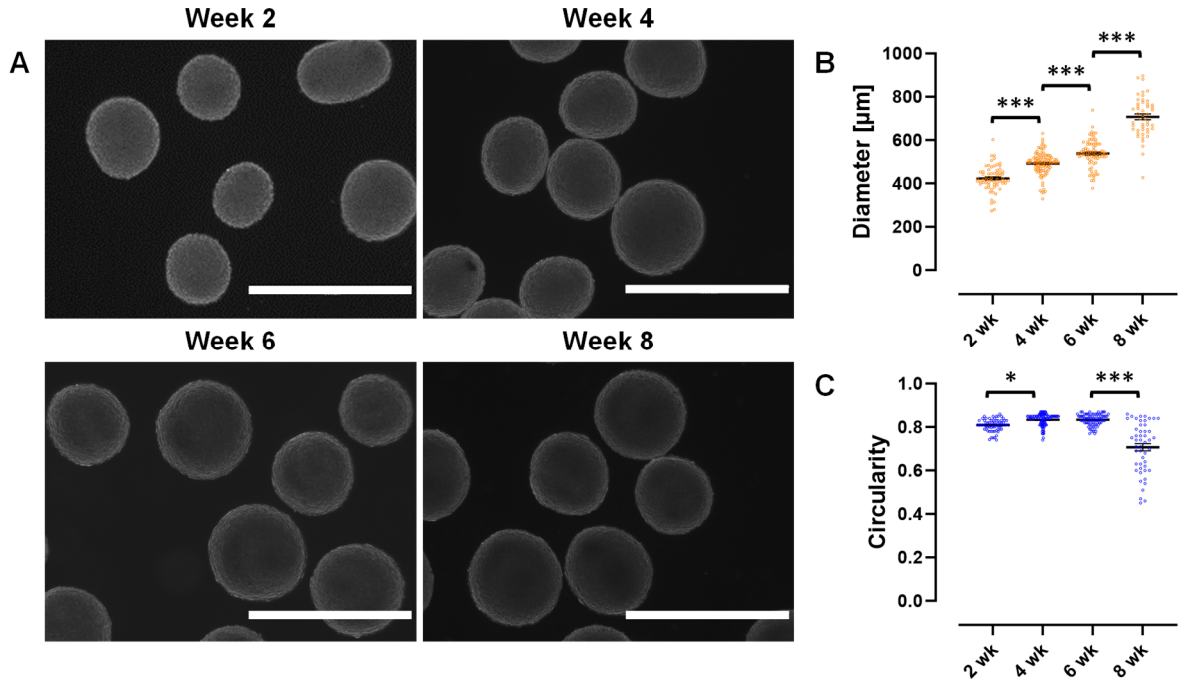

Figure 35. Circularity and diameter assessment of the KOLF2.1J neurospheres. Representative microscopy images of neurospheres. Scale bar, 1 mm **(A)**. Change of the diameter of the neurospheres over time, N>50. Black lines represent mean values. **(B)**. Change of the circularity of the neurospheres over time, N>50. Black lines represent mean values **(C)**. Data is analyzed using a one-way ANOVA. Asterisks represent the significant differences over time.

3.3.6. Electrophysiological activity of neurospheres

Immunocytochemistry confirms the presence of neurons and astroglia in the neurospheres, the two essential cell types for forming an active neuronal network. The initial assessment of electrophysiological activity has been conducted using calcium imaging. At 4 weeks of age, the electrophysiological activity has been evaluated using the calcium indicator Cal-520® and imaging. AX18 neurospheres exhibit no activity, whereas KOLF2.1J neurospheres demonstrate burst activity. (**Figure 36**).

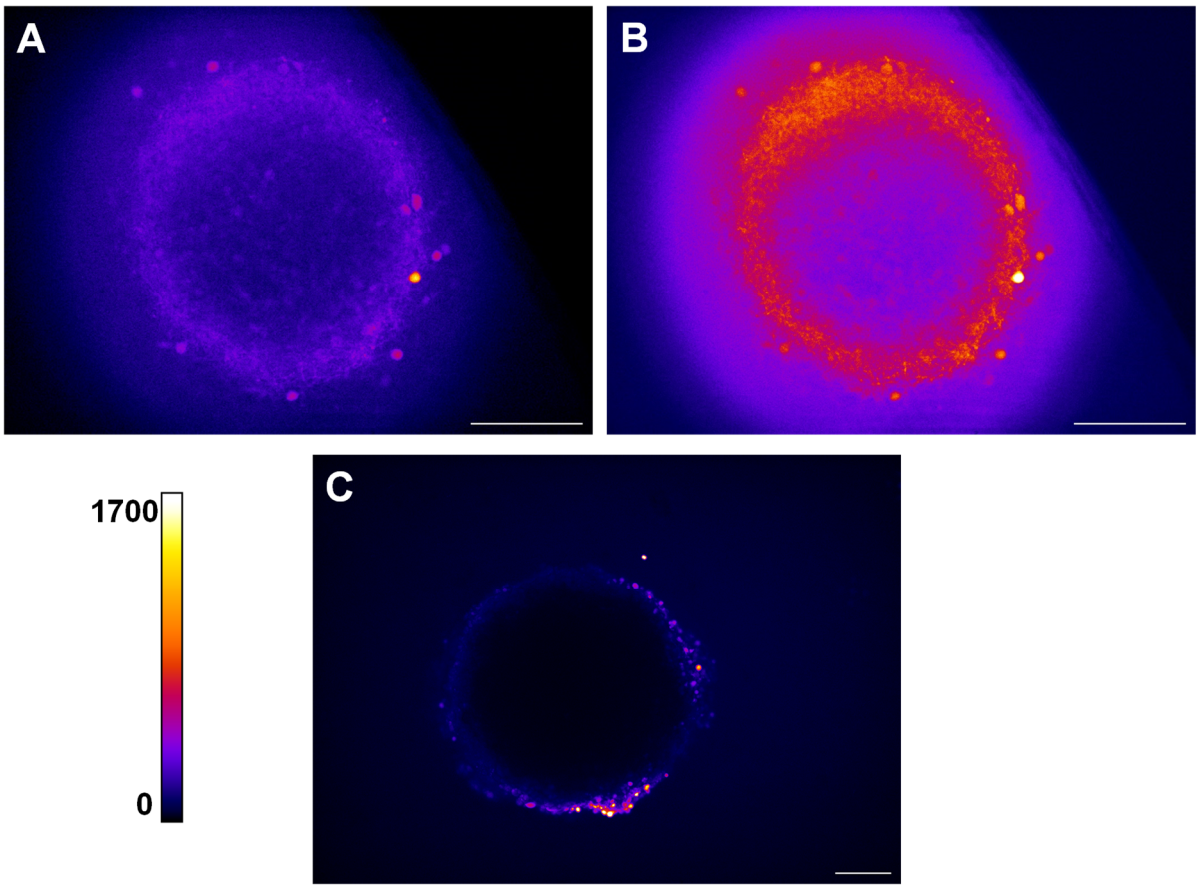

Figure 36. Calcium imaging of the AX18 and KOLF2.1J neurospheres. Neurospheres are stained with a calcium indicator dye (Cal520), and calcium influx through the neuron's voltage-gated calcium channels is monitored via imaging. The images are shown in false color for a better understanding. Representative image of the inactive and active state of the KOLF2.1J neurospheres. Representative image of non-active AX18 neurosphere. Scale bars, 100 µm.

Calcium imaging confirms that KOLF2.1J neurospheres exhibit network formation, and neurons are synaptically connected by week 4. The progression of electrophysiological activity over time was evaluated using KOLF2.1J neurospheres with NeuroMPS 2.0, focusing on mean firing rate (MFR) as the primary metric. The mean MFR values were calculated as 0.36±0.03 Hz at week 2, 3.81±0.73 Hz at week 4, 4.07±0.86 Hz at week 6, and 2.30±0.22 Hz at week 8. These results indicate that MFR increases until week 6 but decreases by week 8. (**Figure 37**).

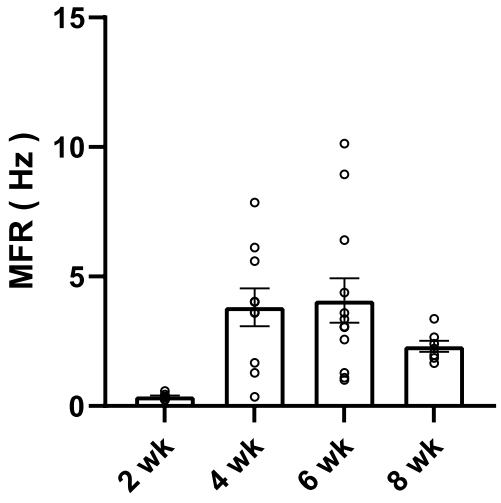

Figure 37. Electrophysiological activity development over time. Active development is assessed with KOLF2.1J neurospheres. 8-10 neurospheres are recorded per time point. Bar graphs represent mean values.

3.3.7. Validation of *NeuroMPS 2.0* for electrophysiological recordings

Neurospheres are produced with varying cell numbers to determine the optimal cell count per neurosphere for an active neuronal network. AX18 neurospheres are cultured with 3500 and 5000 cells per neurosphere, while KOLF2.1J neurospheres are cultured with 5000 and 6500 cells per neurosphere. At week 5, the neurospheres are transferred to the *NeuroMPS 2.0*, and electrophysiological activity is recorded every other day starting from day 5. The recorded data are analyzed for MFR, BFR, and NBF.

AX18 neurospheres exhibit very low MFR and BFR at both cell concentrations compared to KOLF2.1J neurospheres, and no network bursts are detected in AX18 neurospheres. In contrast, KOLF2.1J neurospheres show an increasing trend in MFR and BFR until day 9 in the *NeuroMPS 2.0*, followed by a decline starting on day 10. Additionally, KOLF2.1J neurospheres develop network burst activity, with a similar trend of increased activity observed in the NBF plot until day 9. (**Figure 38**).

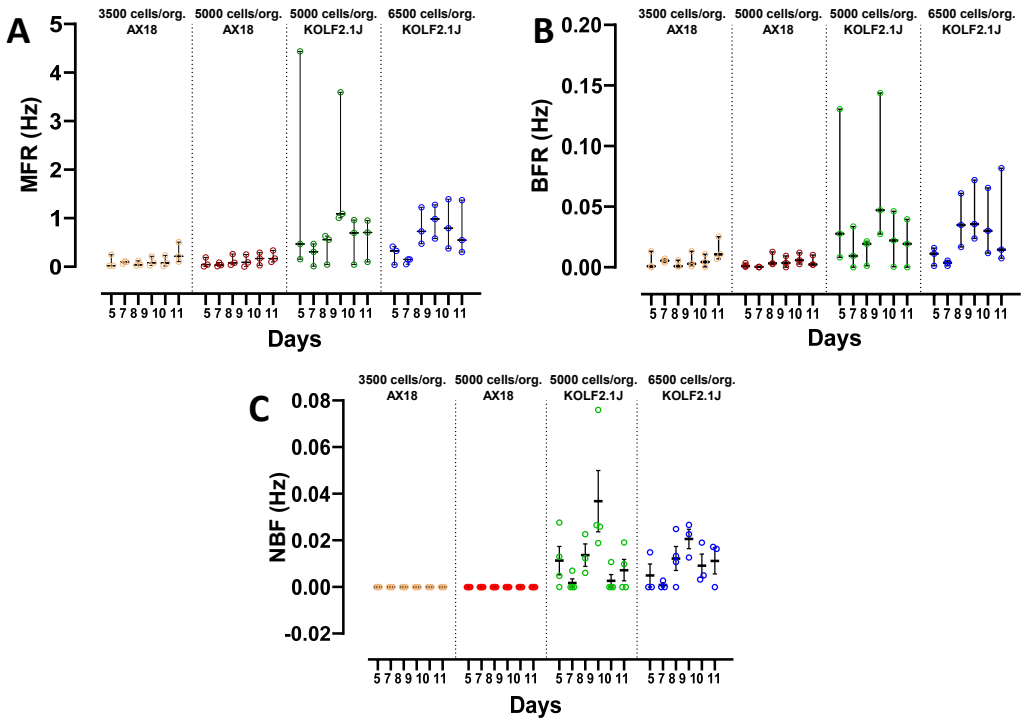

Figure 38. Validation of electrophysiological activity of AX18 and KOL2.1J neurospheres. The electrophysiological activity of AX18 neurospheres is examined under conditions of 3500 cells/neurosphere (brown) and 5000 cells/neurosphere (red), while KOLF2.1J neurospheres are analyzed under conditions of 5000 cells/neurosphere (green) and 6500 cells/neurosphere (blue). The neurospheres are plated in the *NeuroMPS 2.0* at week 5, and electrophysiological activity is recorded on days 5, 7, 8, 9, 10, and 11. The activity is analyzed for MFR (**A**), BFR (**B**), and NBF (**C**). N=3-4 neurospheres per condition. Whiskers represent the mean value for each well, horizontal lines represent the median.

*The timing of plating neurospheres into NeuroMPS 2.0 is further investigated with KOLF2.1J neurospheres. Group-1 is plated at week 4, with electrophysiological activity recorded on days 5, 7, 8, 9, and 10. Group-2 is plated at week 5, with recordings taken on the same days. The data is analyzed for MFR, BFR, %SiB, and NBF. Results indicate that the first group's values (***Figure 39***) are lower than the second group's values (***Figure 40***). Notably, NBF, an indicator of network maturation, is significantly higher in the second group (*

Table *22*).

Table 22. Numeric data of recording analysis from two different groups of KOLF2.1J neurospheres. The data shown in the table are mean values, and error values indicate SEM. Mean values are calculated from eight samples for group 1 and three for group 2.

	MFR (Hz)		BFR (Hz)	
	Group-1	**Group-2**	**Group-1**	**Group-2**
Day 5	0.26 ± 0.05	1.69 ± 1.38	0.009 ± 0.002	0.055 ± 0.037
Day 7	0.25 ± 0.06	0.26 ± 0.13	0.009 ± 0.002	0.014 ± 0.010
Day 8	0.19 ± 0.04	0.41 ± 0.18	0.007 ± 0.001	0.014 ± 0.006
Day 9	0.28 ± 0.05	1.90 ± 0.85	0.012 ± 0.003	0.073 ± 0.036
Day 10	0.54 ± 0.11	0.57 ± 0.27	0.013 ± 0.004	0.023 ± 0.013
	% SinB		**NBF (Hz)**	
	Group-1	**Group-2**	**Group-1**	**Group-2**
Day 5	17.94 ± 2.86	37.68 ± 5.39	0.003 ± 0.002	0.011 ± 0.006
Day 7	10.73 ± 2.51	17.17 ± 9.17	0	0.002 ± 0.002
Day 8	17.41 ± 4.11	21.27 ± 6.81	0	0.014 ± 0.005
Day 9	13.41 ± 2.86	49.58 ± 11.28	0.006 ± 0.004	0.037 ± 0.013
Day 10	15.44 ± 3.39	19.11 ± 9.13	0.002 ± 0.002	0.003 ± 0.003

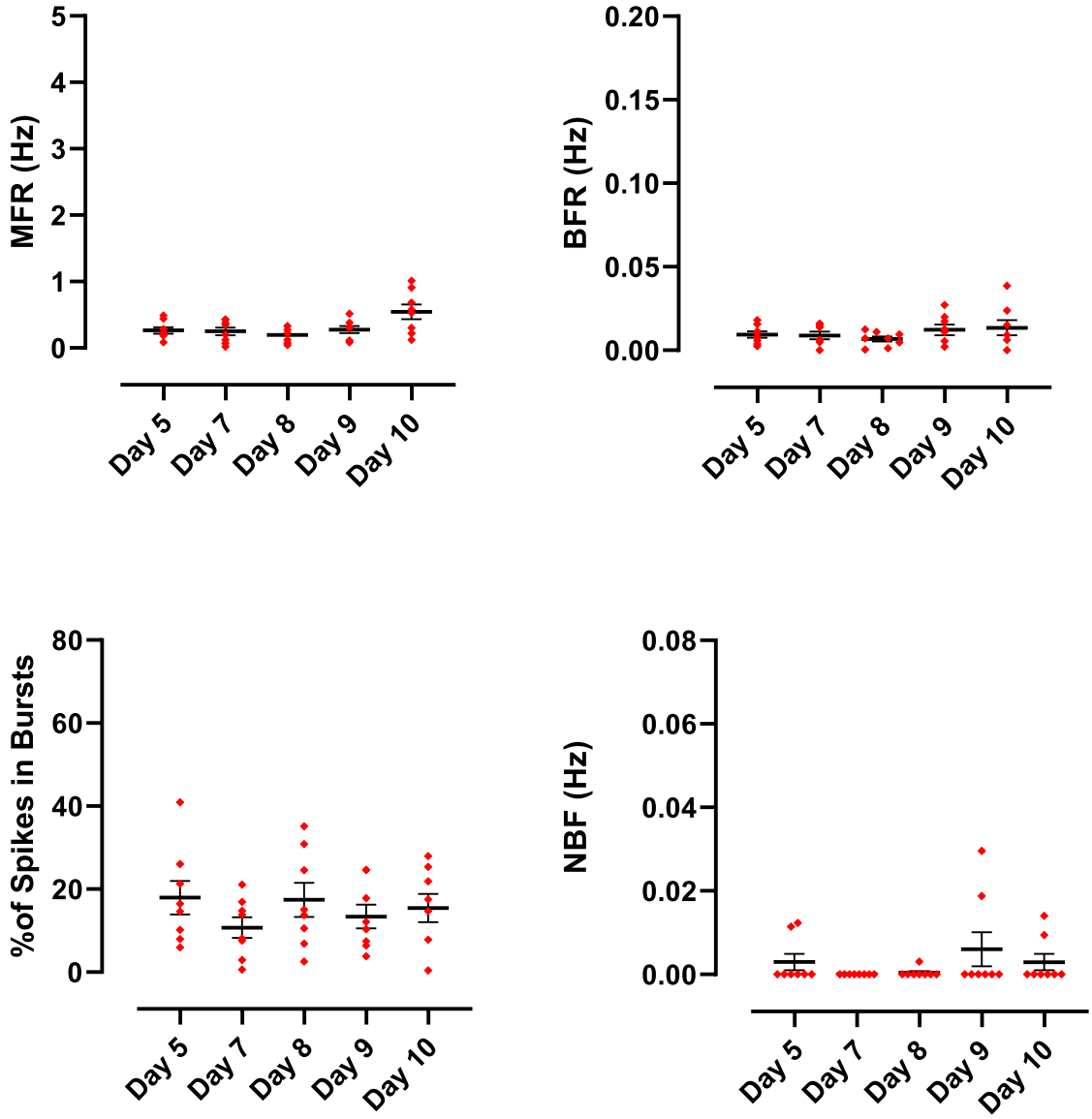

Figure 39. Recording data of the first group of KOLF2.1J neurospheres. The neurospheres are transferred into neuroMPS 2.0 at week 4, and the recordings are performed on days 5, 7, 8, 9, and 10. The data is analyzed for MFR, BFR, %SinB, and NBF. N= 8. Whiskers represent the mean value for each well. The horizontal lines represent the median.

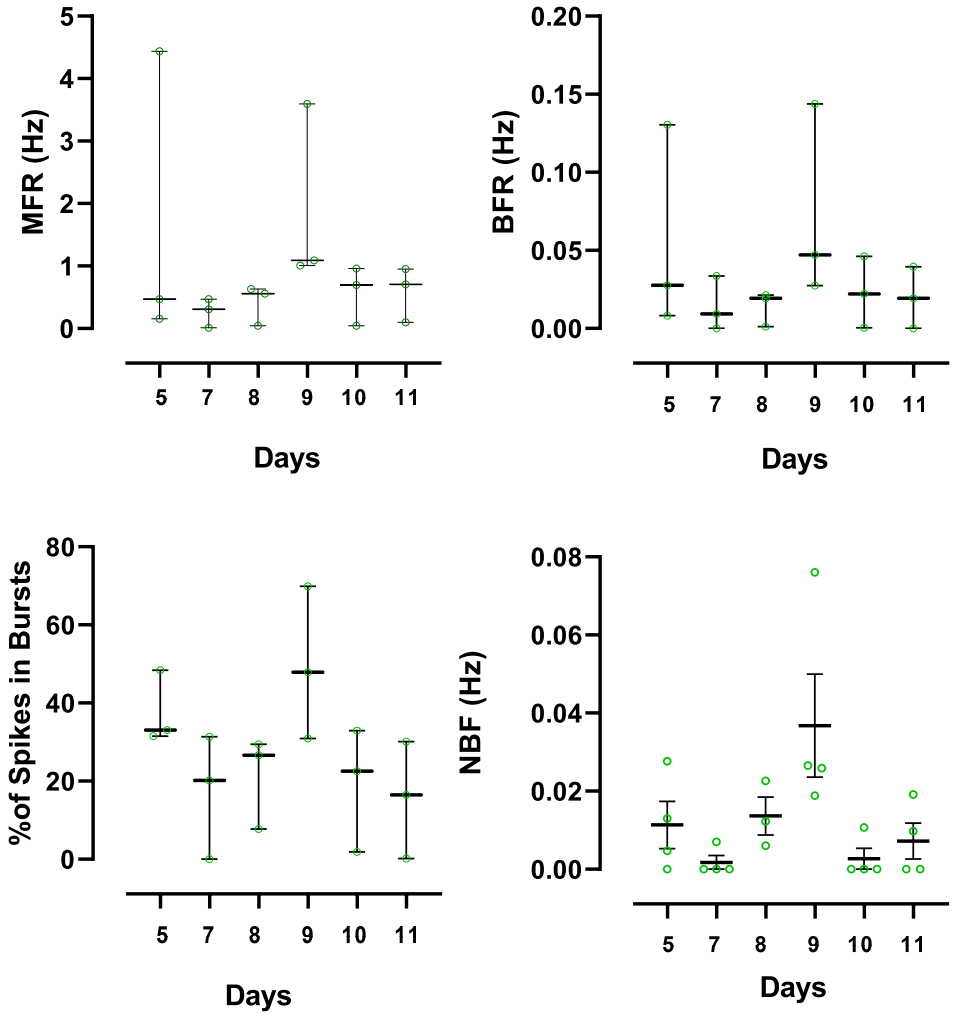

Figure 40. Recording data of the second group of KOLF2.1J neurospheres. The neurospheres are transferred into neuroMPS 2.0 at week 5, and the recordings are performed on days 5, 7, 8, 9, 10, and 11. The data is analyzed for MFR, BFR, %SinB, and NBF. N= 3-5.

The recordings confirm that plating neurospheres at week 5 results in higher electrophysiological activity. The data also indicate that the neurospheres' electrophysiological activity increases until day 9, followed by a decline on day 10. Therefore, day 9 is identified as the optimal time point for applying compounds and studying electrophysiological alterations.

3.3.8. Modulation of electrophysiological activity in the neurospheres

The brain contains both inhibitory and excitatory neurons that modulate network activity, and any disturbance to these neurons can cause widespread alterations throughout the network. In this study, different blockers are applied to assess and evaluate the resulting disturbances

in electrophysiological activity to determine if the outcomes align with expected effects. GABAergic neurons (inhibitory neurons) are blocked with either picrotoxin (PTX) or bicuculline (BIC), resulting in seizure-like activity in excitatory neurons (**Figure 41** and **Figure 42**). Both PTX and BIC disrupt the inhibitory pathway, exposing the network to triggering electrical signals. Consequently, the trains of action potentials fire at exceptionally high rates for an extended period.

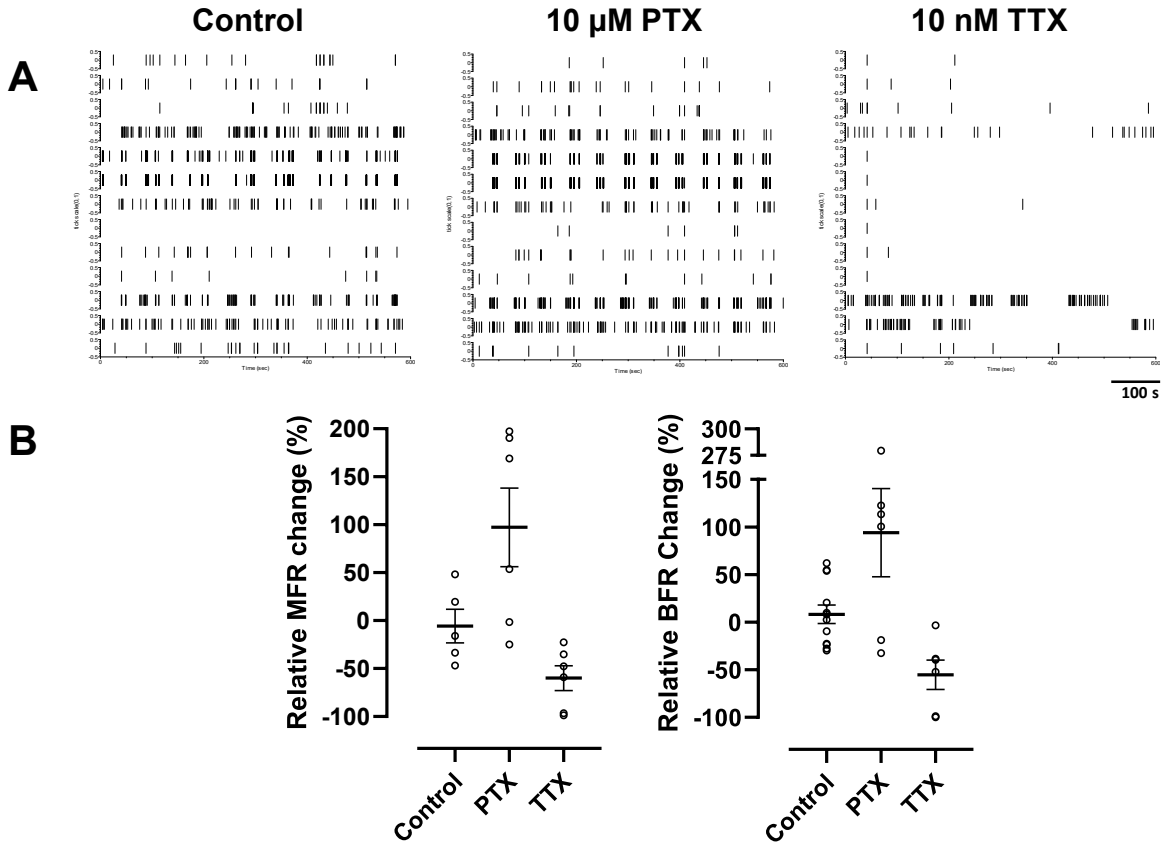

Figure 41. PTX and TTX application. Raster plots show the activity in response to PTX and TTX 10 minutes after the application; each line represents a single spike (A). The changes in MFR and BFR are plotted in graphs, horizontal lines represent mean values, and whiskers represent individual values of the recordings. N= 5-8.

Additionally, burst activity dominates throughout the recording period since the network constantly needs recovery time from a seizure-like behavior. Consequently, the inability of inhibition leads to an increase in BFR. After PTX, tetrodotoxin (TTX) - a sodium channel blocker – is applied to the neurospheres. As sodium channels are one of the critical modulators of the action potential formation[102], the entire signaling pathway is disrupted once the

channels are blocked. Therefore, a dramatic decrease in the electrical activity is observed. BIC is another GABA antagonist that blocks the inhibitory neurons, and it is paired with CNQX for this study. After BIC triggers a seizure-like activity, CNQX is applied. CNQX blocks all the excitatory pathways except the NMDA-mediated ones[103]. While BIC stops the inhibitory pathways, CNQX disrupts the majority of the excitatory signaling.

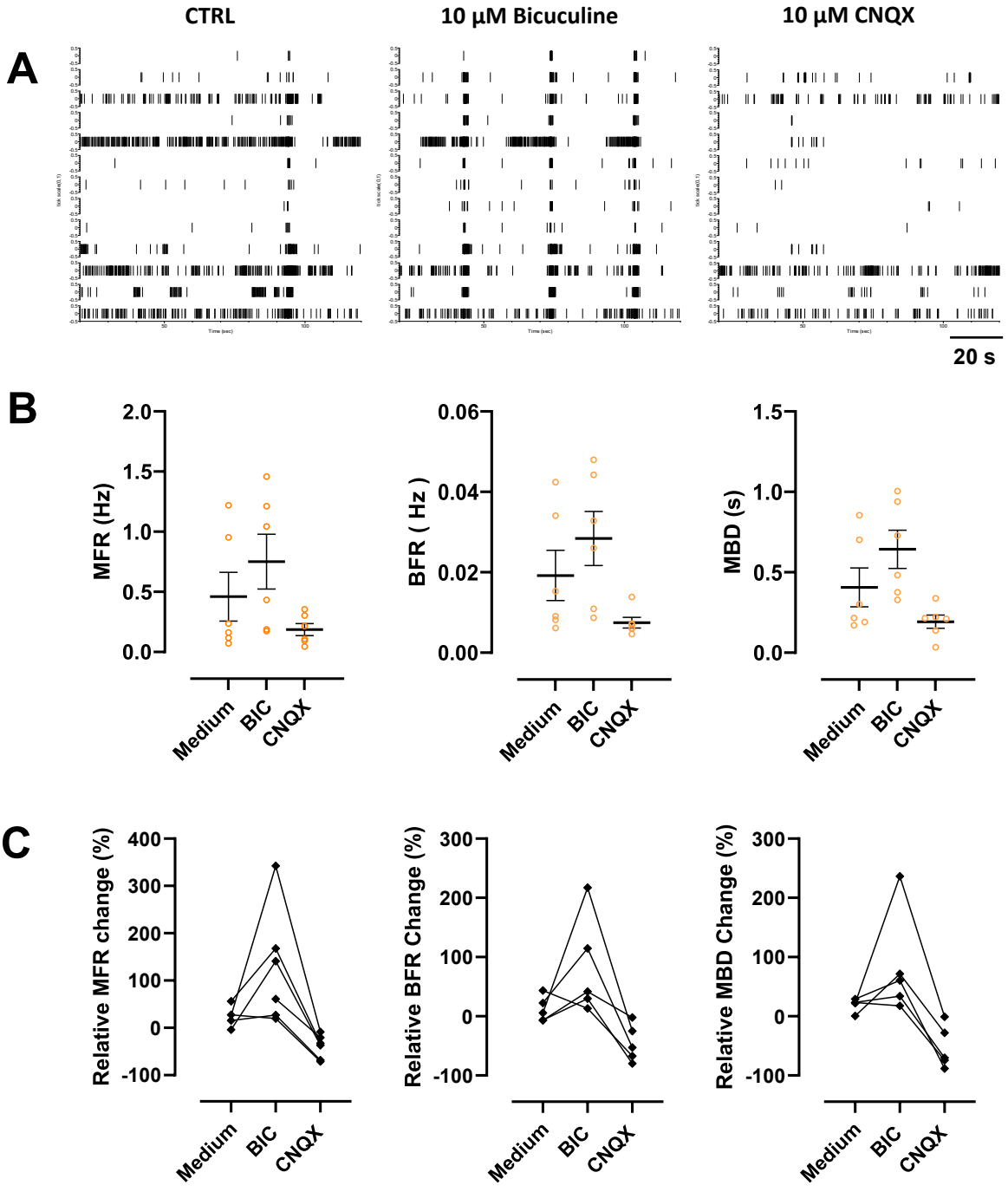

Figure 42. BIC and CNQX application. Raster plots show the response to the BIC and CNQX 10 minutes after the application **(A)**. Absolute values of the MFR, BFR, and MBD values are plotted in graphs. Horizontal lines represent the mean values; the error bars are for SEM. The whiskers show the individual values for the recordings **(B)**. Relative changes in MFR, BFR, and MBD are plotted in graphs. The lines represent the same sample responses **(C)**. N= 4-6

Consequently, the network no longer demonstrates a seizure-like activity, yet the greater part of the network is blocked. As a result, the overall network activity is reduced; expectedly, MFR, BFR, and MBD values drop significantly. BIC and CNQX are also employed to test the model's dose-response sensitivity. Five concentrations of the compounds (0.1 µM, 0.5 µM, 2.5 µM, 10 µM, and 25 µM) are applied, and the relative change of the activity is measured and plotted. The results are compared to the control condition using Welch's t-test. BIC data showed a significant change only for the 10 µM dose. Meanwhile, the neurospheres respond to CNQX doses significantly, except for the lowest dose (0.1 µM) (**Figure 43** and **Figure 43**).

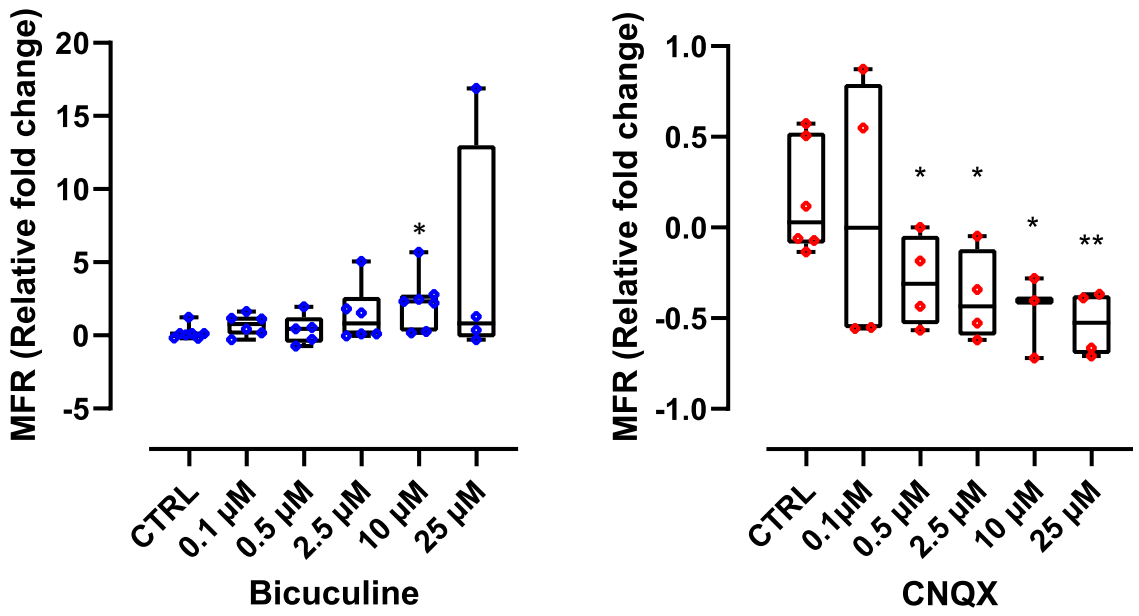

Figure 43. Dose-response to BIC and CNQX. The *NeuroMPS 2.0's* sensitivity is evaluated by applying various concentrations of BIC and CNQX. The response is recorded 10 minutes after the application. The box plots represent the median and quartiles. The data are compared to control values using Welch's t-test. Asteriks show the significance.

The neurosphere network is further tested with APV, a potent and selective NMDA receptor antagonist. NMDA-mediated synapses are inactivated with APV, and CNQX is applied, aiming

to completely cease network activity (**Figure 44**). Recordings are performed on KOLF2.1J neurospheres. A 100 µM concentration of APV is applied, and the response is recorded after 10 minutes of incubation. As anticipated, the MFR and BFR values drop due to the blocking of NMDA-mediated signaling.

Following this, network stimulation continues with the application of CNQX. A 20 µM concentration of CNQX is applied to the wells previously treated with APV, and the response is recorded after 10 minutes of incubation. As CNQX blocks non-NMDA-mediated glutamatergic responses, a greater disturbance in the network is expected. The network activity remains disrupted compared to the control; however, a recovery behavior is observed in the mean burst duration (MBD) and percentage of spikes in bursts (%SiB)(**Figure 45** and **Figure 46**).

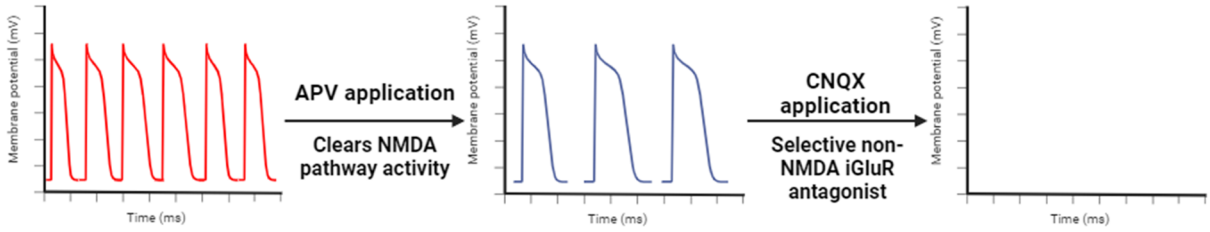

Figure 44. The schematic for APV-CNQX paired application. Created with Biorender.

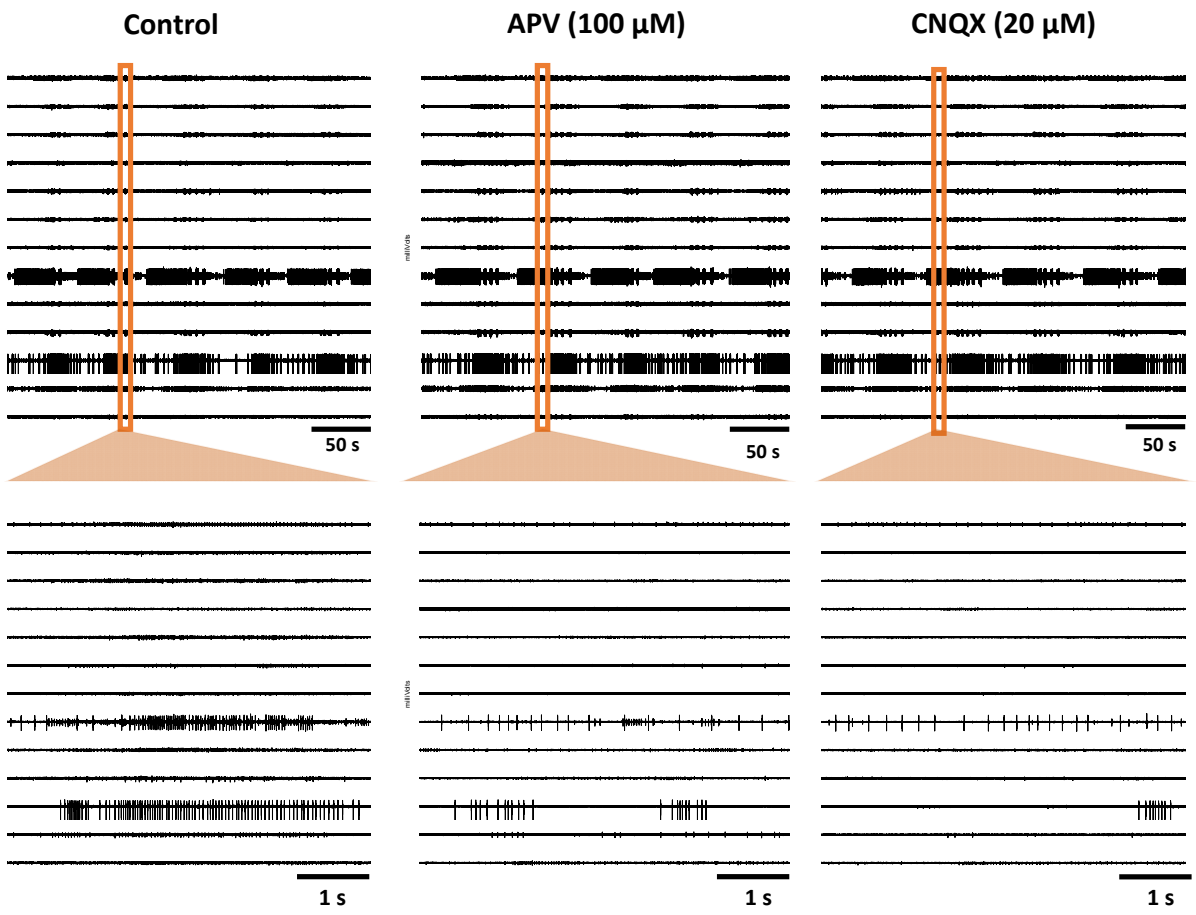

Figure 45. Traces of the recordings for APV and CNQX responses. Each line is a recording signal coming from an individual CµEs. Here, all 13 CµEs per experiment are shown.

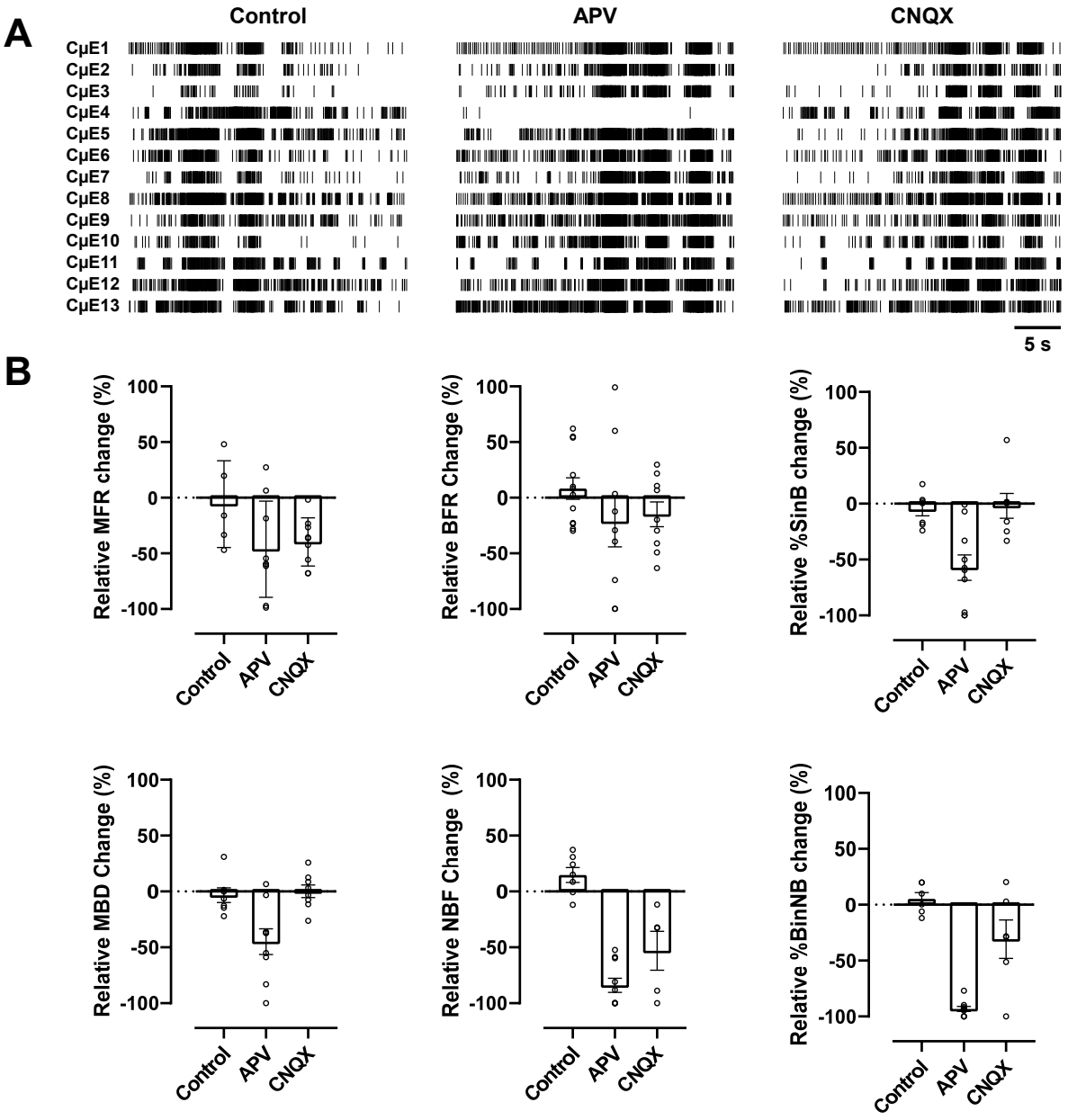

Figure 46. Response to APV and CNQX application. Raster plots show the activity in response to APV and CNQX 10 minutes after the application; each line represents a single spike, and the data represents the recordings between 30-60 seconds (A). 10 minutes of recording data is analyzed. The changes in MFR, BFR, MBD, % SinB, NBF, and %BinNB are plotted in graphs; bars represent mean values, and whiskers represent individual values of the recordings. N= 7-9.

In addition to the antagonists, a potassium channel blocker (4-AP) is applied to the neurospheres to further characterize the *NeuroMPS 2.0*. Potassium channels are crucial for depolarizing the action potential[104], and blocking these channels induces stress on the neurons. When the signal cannot depolarize, it creates a train of spikes, leading to a seizure-like phenotype. 30 µM 4-AP is applied to th eneurospheres, and the response is recorded after

10 minutes of incubation. The raster plots illustrate how the activity evolves into a train of bursts, a response also evident in the trace plots (**Figure 47** and **Figure 48**). Blocking potassium channels leads to an increase in the burst frequency rate. This, in turn, raises the percentage of bursts within a network burst. As a result, the entire network becomes stuck in a prolonged network burst state due to the inability to depolarize.

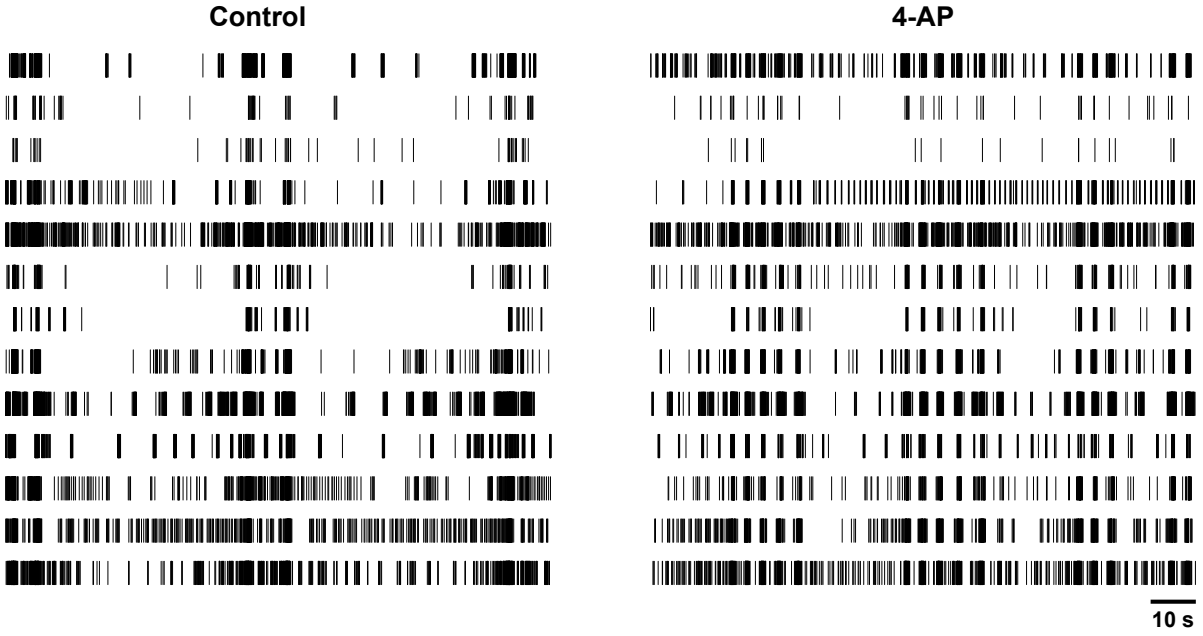

Figure 47. Raster plots for response to 4-AP. Each vertical line represents one spike. Each horizontal train of lines represents the recordings from individual electrodes.

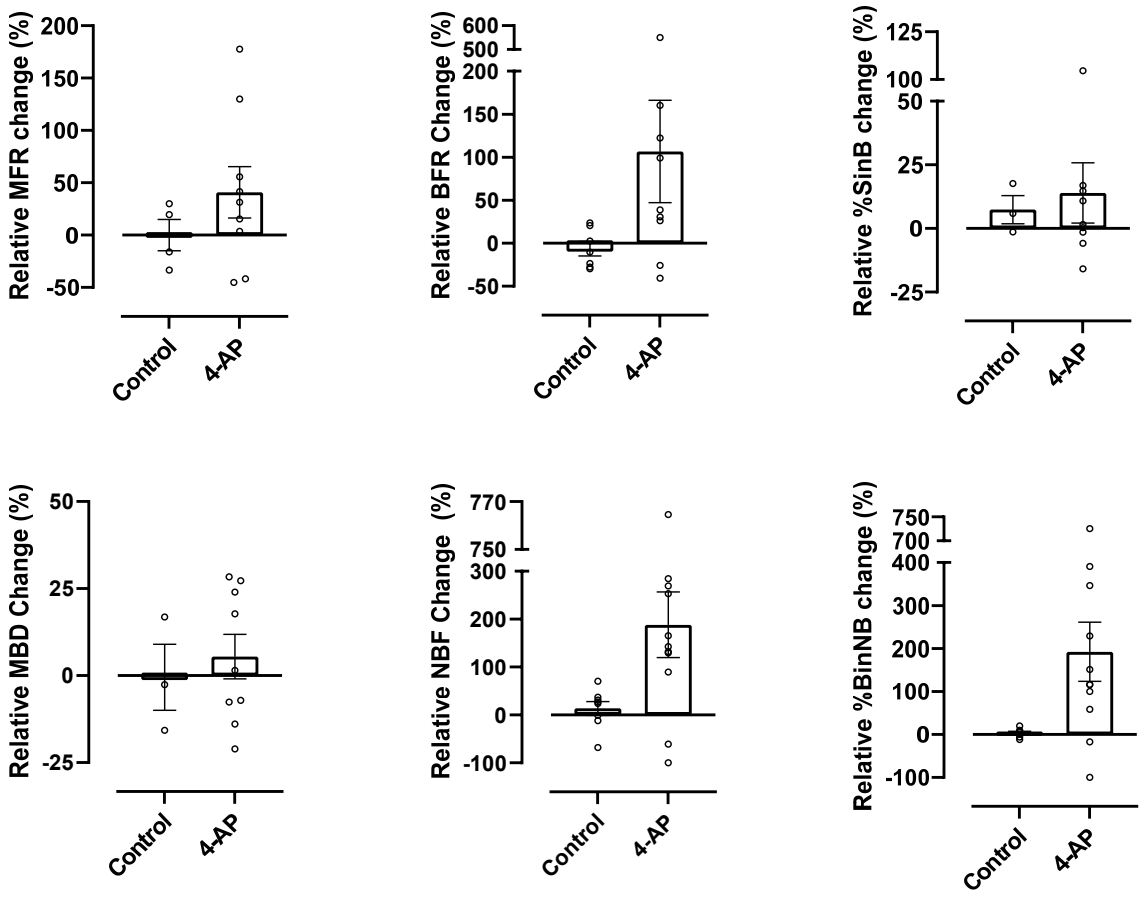

Figure 48. Response to 4-AP. Trace plots show the activity in response to 4-AP 10 minutes after the application (A). 10 minutes of recording data is analyzed. The changes in MFR, BFR, MBD, % SinB, NBF, and %BinNB are plotted in graphs; bars represent mean values, and whiskers represent individual values of the recordings. N= 7-9.

3.3.9. Toxicology

Rotenone, a pesticide known to inhibit the complex I pathway in mitochondria, induces oxidative stress and ultimately leads to apoptosis[105]. In this study, rotenone is utilized as a model neurotoxin. Neurospheres, differentiated for 6 weeks, are exposed to rotenone. The effects of rotenone are evaluated using a dynamic cytotoxicity assay, morphological observations, an ATP assay, and electrophysiological recordings.

The dynamic cytotoxicity assay is an imaging-based technique that employs a fluorescent apoptosis agent. The intensity of the fluorophore changes upon cell death. The data is analyzed against baseline and reported as fold changes. The earliest cytotoxicity effects are observed after 18 hours at higher concentrations (0.1 and 1 µM) (**Figure 49-A**).

The ATP assay serves as an indicator of cell viability. Following rotenone exposure, the assay is conducted at various time points (0h, 6h, 18h, 24h, 48h). A decrease in ATP activity is anticipated as cells undergo apoptosis due to rotenone toxicity. A drop in ATP activity is only observed after 24 hours (**Figure 49-B**).

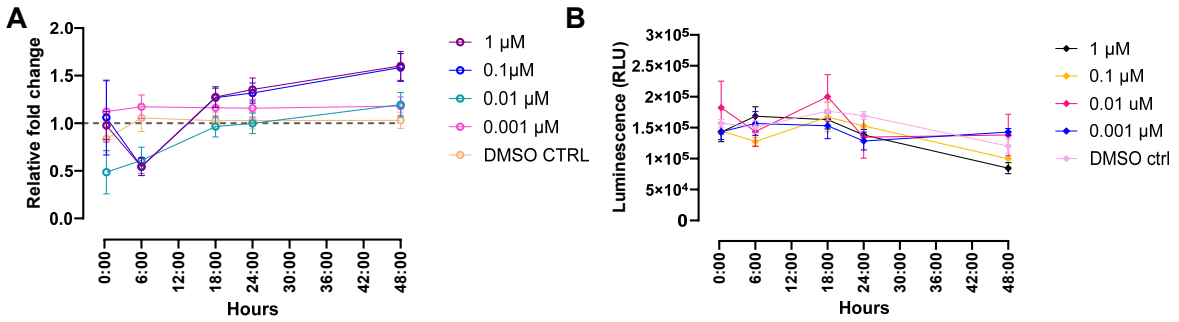

Figure 49. Metabolic response to rotenone 6-week old KOLF2.1J neurospheres. Cytotoxicity response is evaluated using a cyanine dye that binds to the DNA of the dead cells, and the images are taken at five different time points (0h, 6h, 18h, 24h, and 48h). The intensity increases over time and is demonstrated as a fold change. The effect of the rotenone on cytotoxicity is observed after 18 hours **(A)**. The ATP decrease is used as a viability indicator for the neurospheres; the measurements are employed at 0h, 6h, 18h, 24h and 48h time points. The earliest effect is detected after 24 hours **(B)**. For both assays; N=6.

Morphological assessments are performed on neurospheres transduced with green fluorescent protein (GFP). Following rotenone application, imaging is conducted at 20 minutes, 6 hours, 18 hours, 24 hours, and 48 hours. Neurite dissociation is first observed at 18 hours in wells treated with 1 µM and 0.1 µM rotenone. By 48 hours, neurite dissociation is also evident in wells treated with 0.01 µM rotenone. In contrast, no morphological changes are observed in wells treated with 0.001 µM rotenone (**Figure *50***). Higher magnification images clearly demonstrate the progressive neurite dissociation over time (**Figure 51**).

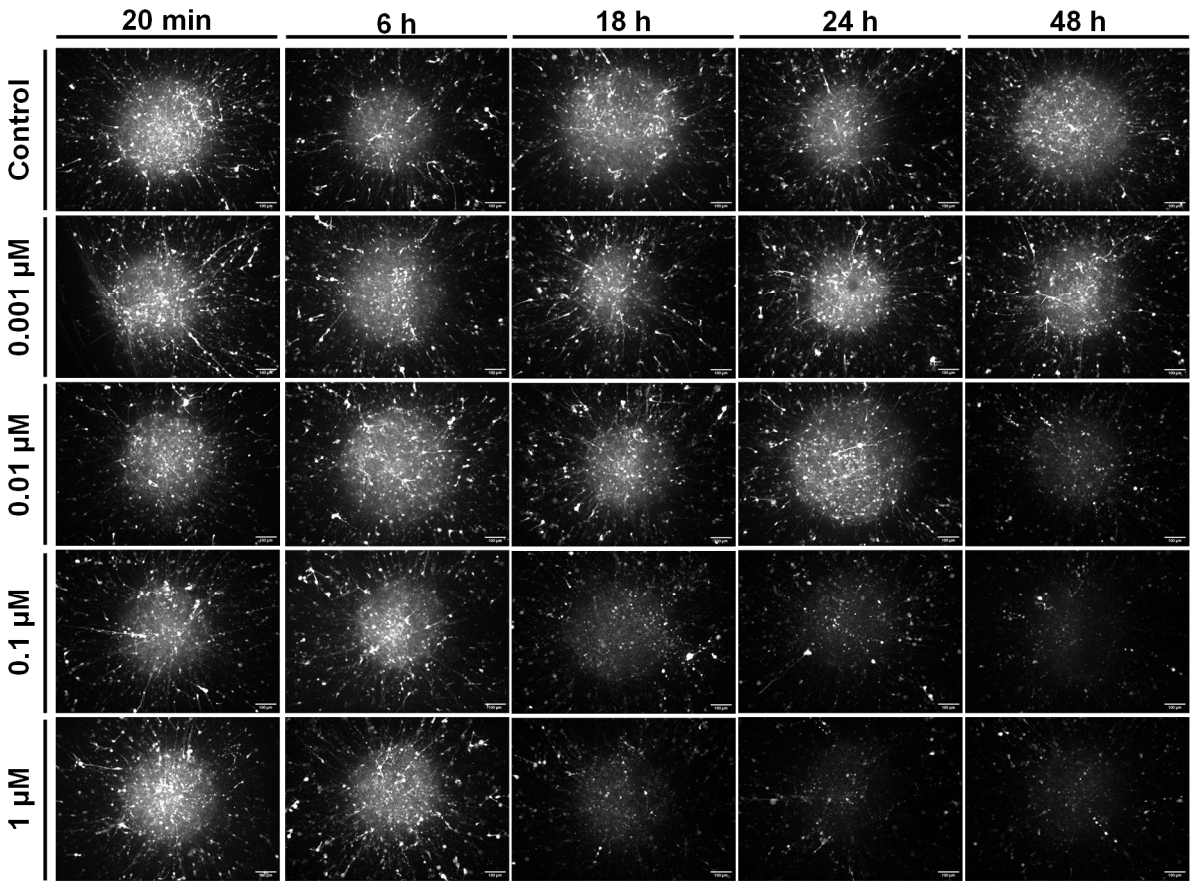

Figure 50. Morphological assessment of KOLF2.1J neurospheres' response to rotenone. GFP expressing neurospheres are treated with rotenone and imaged after 20 minutes, 6 hours, 18 hours, 24 hours and 48 hours. Z-stack imaging is employed through 300 µm thickness and images are demonstrated as MIP. Scale bars, 100 µm.

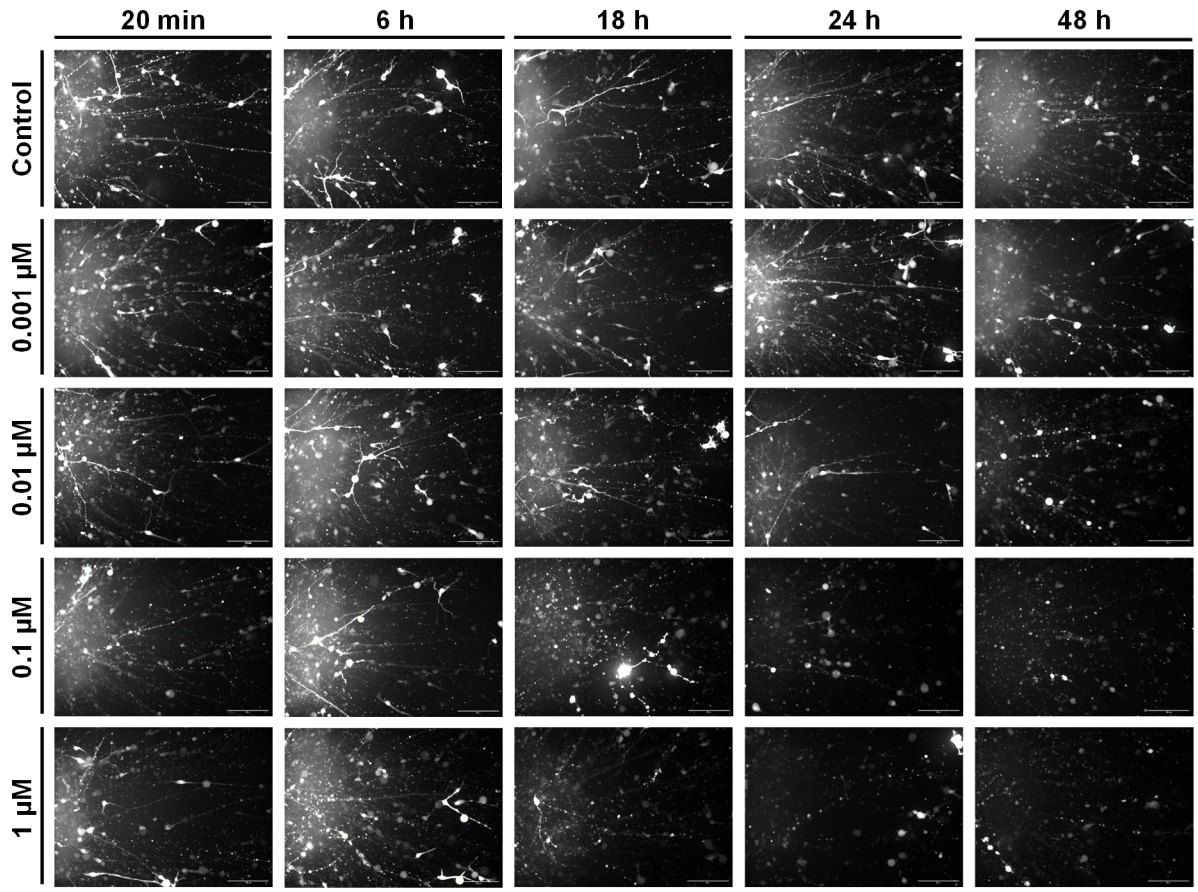

Figure 51. Neurite focused morphological assessment of KOLF2.1J neurospheres after rotenone treatment. GFP expressing neurospheres are treated with rotenone and imaged after 20 minutes, 6 hours, 18 hours, 24 hours and 48 hours. Z-stack imaging is employed through 300 µm thickness and images are demonstrated as MIP. Scale bars, 100 µm.

To evaluate the impact of rotenone on neuronal network activity, wells are treated with four different concentrations of rotenone (1 µM, 0.1 µM, 0.01 µM, and 0.001 µM). The effects are recorded for 10 minutes following a 10-minute incubation period, and the data is analyzed for MFR, BFR, MBD, %SiB, NBF, and %BinNB. In contrast to morphological and metabolic assessments, the effects of rotenone on network activity manifest rapidly, with disruptions in electrical circuits detected just 10 minutes after treatment.

The reductions in MFR, BFR, MBD, %SiB, NBF, and %BinNB are plotted in graphs, revealing a dose-dependent disruption; higher doses of rotenone result in more pronounced disruptions (**Figure 52**). Furthermore, the data indicate that rotenone treatment, particularly at higher doses, causes significant disruption in the synchronicity of network communication. This is evident in the NBF and %BinNB plots. Even the lowest concentration of rotenone compromises the synchronicity of network activity, albeit not significantly.

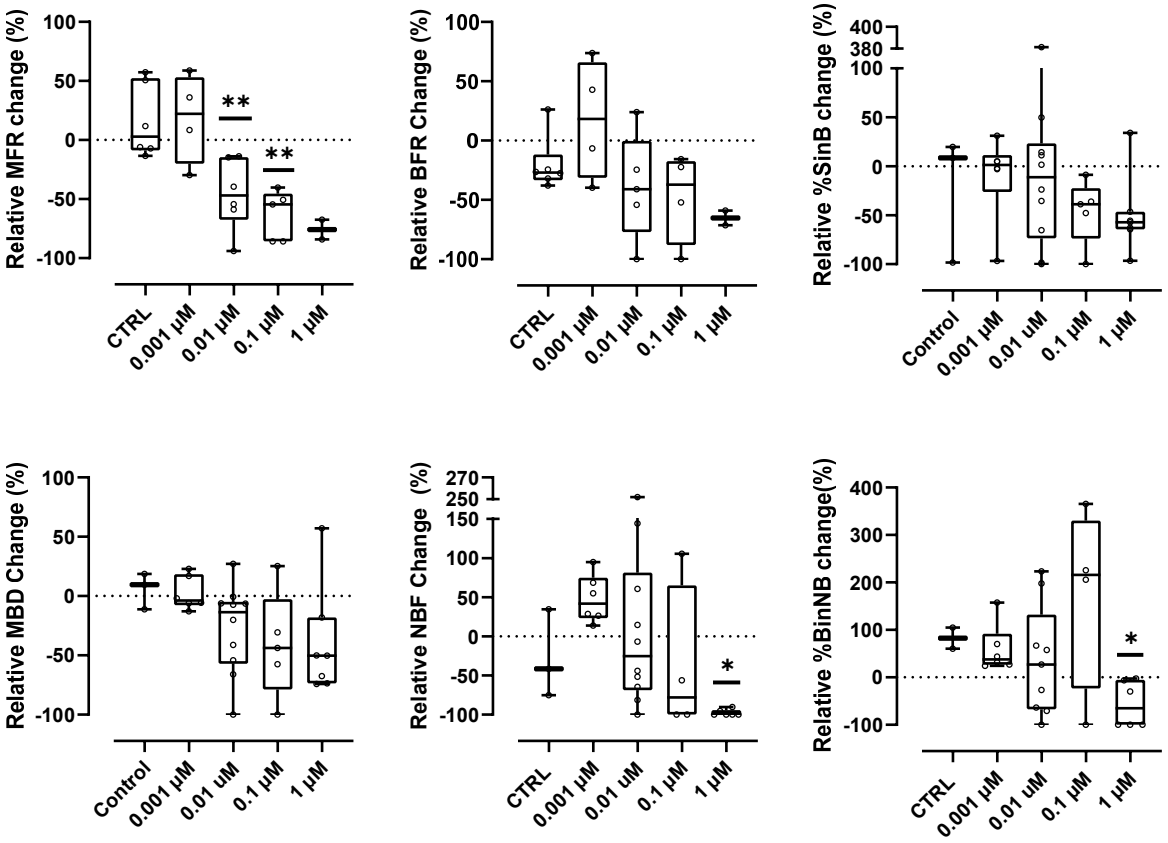

Figure 52. Electrophysiological assessment of KOLF22.1J neurospheres in response to rotenone treatment. Rotenone is applied to wells, and 10 minutes after the incubation, the recording is performed for 10 minutes. The recording data is analyzed for MFR, BFR, %SinB, MBD, NBF, and %BinNB. Sample size differs between 3 and 9 (N=3-9). Box plots demonstrate the median of each condition and its quartiles. Whiskers illustrate the individual recordings, as well as the maximum and minimum values. The data is analyzed against the control group with a non-parametric Kolmogorov-Smirnov test. Asterisks indicate significant differences between control and rotenone-treated wells

4. DISCUSSION

The human brain, with its intricate network formation and the amalgamation of electrical and metabolic activities, presents one of the most formidable challenges in in vitro modeling. Over the past decades, scientists have tirelessly dedicated their efforts to enhancing in vitro models and reducing reliance on animal studies. This shift is driven by the realization that most CNS diseases that afflict millions of people annually do not manifest in animals. The sobering reality is that the chance of a drug for neurodegenerative diseases progressing from clinical trials to FDA approval is a mere 10%[106]. The reason behind this low success rate is mostly the translation gap between human and animal research and the lack of appropriate human models to understand the mechanism of the diseases. To develop more effective drugs and treatments, it is essential to have enhanced experimental models that yield more predictive and physiologically relevant results. To create biologically representative models of the human brain in vitro, recently, stem cell-based systems have striven to replicate in vivo conditions, including the pathophysiological mechanisms observed in living organisms. This approach aims to provide more accurate and reliable systems for understanding diseases, conducting drug tests, and diagnostics. Traditional 2D cell culture systems have been invaluable for decades, offering simplified and low-cost methods for modeling CNS diseases[107].

Researchers have raised concerns that 2D models, despite their long-standing use, fail to fully replicate the human brain's intricacy. In contrast, 3D cultures offer a superior alternative, capable of recapitulating in vivo CNS architecture and providing more realistic models. These 3D models have been shown to mimic the interaction between cells and ECM, replicate cell differentiation, synaptic connections, and electrophysiological network properties in a manner more physiologically relevant than their 2D counterparts[108-110]. 3D cultures are formed either with the support of ECM-like structures such as hydrogels or cells assembled as spheroids, and they secrete their own ECM and provide cells the required support to form the 3D biological microarchitecture. The brain is a soft tissue, and to support the neuronal cells, the hydrogels should provide a specific stiffness while allowing neurite growth throughout the gel matrix. Many hydrogels have been tested, and it has been shown that the best results are achieved only with Matrigel ® (356230, Corning) due to its protein content and stiffness, which are similar to brain tissue. Unfortunately, the other hydrogels tested did not provide the conditions required for cell survival and neurite growth[78].

This research develops two models for two different 3D culture approaches. *NeuroMPS 1.0* is developed for single-cell cultures supported with Matrigel ®, and *NeuroMPS 2.0* is developed for assembled cells. Both *NeuroMPSs* are coupled with capped microelectrodes, a novel method to capture electrophysiological activity from neurites in 3D cultures.

4.1. Electrophysiological readouts in 3D cultures

Electrophysiological activity is one of the significant events in the brain, and it must be included as a readout in every study regarding CNS diseases as well as any drug or toxicology screening. There are various techniques to study electrophysiological activity, yet to this day, the best way of acquiring electrophysiological information from a mature network is using microelectrodes. Although the microelectrodes are able to record information from different neurons simultaneously, the location of the electrodes makes the recording from 3D cultures challenging. Conventional MEA systems have their electrodes on the bottom of the culture plate, which serves the purpose of 2D cultures. However, since the 2D cultures do not address the desired functions of the in vitro cultures, the traditional MEA systems face the probability issue. When the cells are in a 3D volume, the cell body suspends in the gel, and it is shown by Martinez &Jentsch et al. that the cell body should be a maximum of 15 µm away from the electrode to capture the signal. To enhance the probability of recording, electrodes are inserted into the gel matrix, which improves the percentage of recording electrodes; however, it is an invasive method and disrupts the network. On the other hand, it still does not address the need for assembled cells.

To fill the gap, the CµEs are developed. CµEs are designed for neurites to grow into their micro tunnels, so the signal is captured without disturbing the culture´s microarchitecture. The most significant advantage of CµEs is being able to record from ECM-free 3D cell organizations and ECM-supported 3D cell organizations without disturbing the cell´s network or any intervention in the culture formation. Since the network is maintained throughout the culture period, collecting information from the same culture system more than once and monitoring the effect of drugs or toxins over time is possible. CµEs are the new generation microelectrodes for MEA-based recordings of the neuronal cultures.

4.2. NeuroMPS 1.0

NeuroMPS 1.0 is developed for 3D cultures formed with hydrogel supports, and it is the first model that CµEs are utilized for neuronal cultures. The system is validated with primary murine neurons and glial cells. The cells are isolated from murine hippocampal tissue where the cell concentration is 21,000 cells per mm^3[111]. However, adapting this ratio to the in vitro system is challenging due to the network formation of the neurons. The neurites grow in all directions, and the arborization of the cells creates a force between the cell and hydrogel interface, which results in shrinkage in the culture. The cell concentration is decreased to 4,000 cells per mm^3 to address this issue. Although the concentration is five times less than the physiological conditions, the cells are kept viable in culture for 10 days. In 4 days, the burst activity is achieved, while the network formation is achieved in 7 days, and CµEs captured network burst

activity from the culture. Further morphological analysis is utilized with immunocytochemistry, and besides neuronal arborization, axonal, dendritic, and glial markers are shown for the cells cultured in *NeuroMPS 1.0.* The CμEs performed exceptionally well, and data showed two aspects of CμE recordings: i) neurite growth into micro tunnels and ii) the synaptic connection between neurons. The data demonstrated that neurites are grown into micro tunnels at day 4; however, forming a proper network requires at least 7 days in culture.

The primary purpose of developing *NeuroMPS 1.0* is to apply it for drug and toxin screenings. It has a glass bottom and glass wells, which address the compound absorption issue of polymer-based micro-physiological systems. Another advantage of glass is that it allows simultaneous imaging while recording the electrophysiological activity. Furthermore, glass is an inert material, and it is possible to wash the *NeuroMPS 1.0* with enzymatic detergents and reuse it up to 10 times[27].

A neurotoxicity assay is performed with *NeuroMPS 1.0* using a pesticide called rotenone. Complex I (NADH-ubiquinone oxidoreductase) of the electron transport chain is the molecular target for rotenone[100, 112]. The effects of rotenone include mitochondrial dysfunction (characterized by decreased ATP production and membrane potential), oxidative stress, and the accumulation of misfolded proteins[105, 113, 114]. *NeuroMPS 1.0* is utilized to study rotenone's morphological and electrophysiological effects on 3D primary murine neuronal culture. The results show that electrophysiological effects are acute compared to morphological effects, which occur as neurite dissociation after 24h at high rotenone application concentrations (0.1 μM, 0.5 μM, 1 μM). As electrophysiological alterations occur earlier, it is essential to monitor the effect of toxins and drugs at a functional level, and *NeuroMPS 1.0* offers easy, noninvasive monitoring for 3D neuronal cultures.

Additionally, *NeuroMPS 1.0* is designed according to ANSI/SLAS standards for use in automation systems. A custom adaptor is designed to accommodate two *NeuroMPS 1.0* for imaging and pipetting systems[27]. Hence, throughput increases while manual labor error is minimized with the adaption to the automation systems.

4.3. NeuroMPS 2.0

Reynold and Weiss were the first to show that multipotent immature progenitors could be isolated from the central nervous system of mice and cultured as nonadherent aggregates, termed neurospheres[115], capable of generating neurons, astrocytes, and oligodendrocytes[116]. Neurospheres become a new 3D culturing method, and since then, neuronal in vitro models have developed towards aggregates where the culture begins with neuro progenitor cells and differentiates into neuronal and glial populations in spheroidal architectures[67, 79, 117]. The discovery of induced pluripotent stem cells[118, 119] facilitated

the research on human models, and neurospheres are employed to understand the central nervous system and neurodegenerative diseases[117, 120-122].

As neurospheres have become a prominent method for 3D culturing, there is a demand for micro-physiological systems suitable for these microstructures. To address this need, *NeuroMPS 2.0* was specifically developed for neurospheres. *NeuroMPS 2.0* features a glass MEA with CμEs, and its wells are designed with pins to hold the neurospheres suspended in a gel volume. This setup allows neurites to extend from the neurosphere into the gel and reach the CμEs, enabling electrophysiological readouts to be obtained without disturbing the neurosphere.

NeuroMPS 2.0 has been validated with neurospheres generated from iPSC-derived NPCs. The differentiation protocol, based on Pamies et al.[67], reliably yields both neuronal and astroglial populations. Given the critical role of astroglia in establishing network activity in vitro[123, 124]. The reproducibility of astroglial populations within neurospheres enhances the model's dependability for examining electrophysiological alterations. In neurospheres, neuronal arborization happens in all directions, and astrocytes easily connect with axons and form tripartite synapses, which are vital for synaptic information processing[125] Ca^{+2} signaling shows that synaptic connections are built in three weeks, and recordings demonstrate that network activity is achieved in six weeks.

MFR values decrease after six weeks of differentiation, coinciding with a reduction in the circularity of the neurospheres. As the diameter of the neurospheres increases over time, nutrient transfer likely becomes insufficient for the cells at the core, leading to cell death[126]. Consequently, the compactness of the neurospheres is compromised, causing the cells to become loose and resulting in a loss of circularity. The decrease in neurosphere viability affects synaptic connections, which may explain the observed decline in MFR values after six weeks.

Compound applications are conducted with six-week-old neurospheres, which exhibit spontaneous network activity. Neurospheres respond to GABA antagonists (PTX and BIC) by increasing BFR and MFR, leading to seizure-like activity. Following PTX application, a sodium channel blocker induces an acute drop in activity. BIC application is followed by using a selective non-NMDA iGluR antagonist (CNQX), which disrupts the seizure-like activity pattern and abolishes network activity. This confirms that neurospheres contain both excitatory and inhibitory neurons and that the network responds to various compounds. *NeuroMPS 2.0* demonstrated dose sensitivity by capturing the dose-dependent effects of CNQX, with MFR values showing significant differences that *NeuroMPS 2.0* accurately detected.

A calcium channel blocker (4-AP) successfully induced a seizure-like activity profile, demonstrating that *NeuroMPS 2.0* can be used to study various phenotypes. However, discrepancies between different batches of neurosphere generations were observed when pairing APV (a selective NMDA receptor antagonist) and CNQX. Neurospheres responded to APV as expected, with decreases in all parameters, including NBF and %BinNB. However, when CNQX was applied, instead of silencing the remaining activity, no significant changes were observed in MFR, BFR, and NBF. Conversely, %SinB, MBD, and %BinNB showed a recovery behavior. As in previous batches, the neurospheres responded to CNQX as expected, with network activity disrupted and decreases in MFR and BFR values; this inconsistency could be due to a lack of non-NMDA mediated glutamatergic neurons or the absence of inhibitory neuron populations within the neurospheres.

A rotenone toxicity assay was also performed in *NeuroMPS 2.0*, examining the effects of rotenone at morphological, metabolic, and functional levels. Functional effects were observed within 10 minutes, while the earliest metabolic and morphological effects appeared after 18 hours for high concentrations of rotenone (0.1 µM and 1 µM). This confirms that functional alterations in neurospheres occur significantly earlier than metabolic and morphological changes.

In conclusion, *NeuroMPS 2.0* represents an innovative platform for neurotoxicity studies, drug screening, and disease modeling. Its transparent and ANSI/SLAS-compatible design allows for comprehensive analysis of functional, metabolic, and morphological alterations simultaneously. The versatile design of the wells supports efficient plating of neurospheres and collection of effluents, enhancing the system's utility in various research applications.

5. OUTLOOK AND PERSPECTIVES

In the last decade, numerous MEA-integrated *NeuroMPSs* have been developed, with the majority available on the market designed for 2D cultures (e.g., MEA plates from Multi Channel Systems[127], Axion BioSystems[128], Maxwell BioSystems[129]). Despite the demand for 3D *NeuroMPS*, most remain at the proof-of-concept stage and are primarily used by their developers due to the need for highly trained personnel, low production yield, or limited throughput[4, 5, 90, 130-132]. Additionally, many of these *NeuroMPS*s lack electrophysiological readouts[130, 131].

This study's primary objective is to develop a user-friendly, multi-functional *NeuroMPS* that can be utilized without advanced training and is suitable for integration into automated systems. *NeuroMPS 1.0* is designed for ECM-supported cultures and has been validated with primary murine neurons and glial cells. Additionally, iPSC-derived dopaminergic neurons have been utilized in the device, yielding both functional and morphological readouts[27]. Two devices were successfully cultured in an automated system using a custom adaptor, demonstrating the platform's compatibility with automation systems[27]. A major bottleneck in in vitro culturing platforms is the absorption of compounds by materials such as channels and perfusion tubes. This issue is addressed by designing the device entirely out of glass, which also offers the benefit of reusability. The major innovation of *NeuroMPS 1.0* lies in its ability to record from neurites using CμEs without disturbing the culture. CμEs enable non-invasive functional readouts, allowing data to be collected from the same culture over time. A custom stage incubator (Okolab, NA, Italy) ensures a controlled environment by regulating humidity, temperature, and CO_2 levels, thereby minimizing external influences on data collection.

As ECM-free 3D neuronal cultures are widely used for drug and toxicity screenings[133-135], as well as disease modeling[136-139]. *Neuro MPS 1.0* has been modified for neurospheres, resulting in *NeuroMPS 2.0*. This system has been validated with two NPCs: i) a commercially available NPC line (ax0018, AXOL Bioscience) and ii) NPCs differentiated in-house from the KOLF2.1J iPSC line. Neurospheres have been generated from both lines; however, the commercial line failed to exhibit long-term viability (over 3 weeks) and showed decreasing electrophysiological activity. Consequently, only the KOLF2.1J line was utilized for compound applications and neurotoxicity assays. *NeuroMPS 2.0* enables real-time monitoring of electrophysiological alterations in neurospheres, with CμEs facilitating non-invasive recordings.

In conclusion, two multifaceted, user-friendly platforms have been developed to monitor functional, morphological, and metabolic alterations in neuronal cultures simultaneously. Both

platforms are reusable and adaptable to automation. They have been validated with neurotoxins, demonstrating sensitive early detection of effects at the functional level.

Although the model is promising, technical challenges and potential enhancements to the biological model need to be addressed. One significant limitation is the absence of immune cells in the neurospheres; thus, integrating microglia into the model would enhance its reliability and predictive accuracy. Additionally, while the neurospheres are ECM-free culture models, they still require embedding in a gel matrix within *NeuroMPS 2.0*. Currently, Matrigel® (356230, Corning) is the only matrix that supports healthy neurite growth. Therefore, there is a need for a defined hydrogel that can adequately support neurite growth. Another limitation of the hydrogel is that as the neurites grow in all directions, the tensile forces at the gel-neurite interface cause shrinkage over time, thereby limiting the culture duration on the platform.

Furthermore, the platform is suitable for optogenetic studies and can be a valuable tool for investigating long-term potentiation, depression, and memory. The open-well design of the *NeuroMPSs* offers the advantage of easy material collection for transcriptomic analysis. Additionally, a comprehensive investigation of electrophysiological responses to compounds is necessary to further validate the utility of *NeuroMPSs* in drug and toxin screenings.

6. STATEMENT OF CONTRIBUTIONS

The following table discloses the distribution of the workload in this project and the contributions of the colleagues in different sections:

Statement of contributions	FE	PC	MvdM	LVJ	BMM	KS	LME	PL
NeuroMPS 1.0 Experimental design **(System validation)**								
NeuroMPS 2.0 Experimental design **(System validation)**								
Fabrication: NeuroMPS 1.0 design **Section 3.1**								
Fabrication: NeuroMPS 2.0 design **Section 3.1**								
Fabrication: CμE fabrication and NeuroMPS assembly **Section 3.1.1**								
Cell Culture: Primary murine cultures **Section 3.2.1**								
Cell culture: NPC formation **Section 3.3.2**								
Cell Culture: Neurosphere formation **Section 3.3.1**								
Validation: SEM images **Section 3.1**								
Validation: Morphological assessments-NeuroMPS 1.0 **Section 3.2.1**								
Validation: Electrophysiological assessments-NeuroMPS 1.0 **Section 3.2.2, 3.2.3, 3.2.4, 3.2.5, 3.2.6**								
Validation: Morphological assessments-NeuroMPS 2.0 **Section 3.3.1, 3.3.2, 3.3.3, 3.3.4, 3.3.5**								
Validation: Electrophysiological assessments-NeuroMPS 2.0 **Section 3.3.6, 3.3.7, 3.3.8, 3.3.9**								
Analysis: Electrophysiology **Section 3.3.6, 3.3.7, 3.3.8, 3.3.9, 3.2.2, 3.2.3, 3.2.4, 3.2.5, 3.2.6**								
Analysis: Statistics and data visualization **Sections 3.2 and 3.3**								

FE: Fulya Ersoy, PC: Paolo Cesare, MvdM: Matthijs van der Moolen, LVJ: Laura-Victoria Jentsch, BMM: Beatriz Martinez Molina, KS: Kathrin Stadelmann, LME: Lisa-Marie Erlandsdotter, PL: Peter Loskill. Dark brown: Significant contribution, Light brown: Less significant contribution, White: No contribution.

7. BIBLIOGRAPHY

1. Deuschl, G., et al., *The burden of neurological diseases in Europe: an analysis for the Global Burden of Disease Study 2017.* The Lancet Public Health, 2020. **5**(10): p. e551-e567.
2. Mohs, R.C. and N.H. Greig, *Drug discovery and development: Role of basic biological research.* Alzheimer's & Dementia: Translational Research & Clinical Interventions, 2017. **3**(4): p. 651-657.
3. Liu, Z., et al., *Two decades of new drug discovery and development for Alzheimer's disease.* RSC advances, 2017. **7**(10): p. 6046-6058.
4. Shin, H., et al., *3D high-density microelectrode array with optical stimulation and drug delivery for investigating neural circuit dynamics.* Nature communications, 2021. **12**(1): p. 492.
5. Soscia, D.A., et al., *A flexible 3-dimensional microelectrode array for in vitro brain models.* Lab on a Chip, 2020. **20**(5): p. 901-911.
6. Park, J., et al., *A 3D human triculture system modeling neurodegeneration and neuroinflammation in Alzheimer's disease.* Nature neuroscience, 2018. **21**(7): p. 941-951.
7. Ramón y Cajal, S., *Degeneration and regeneration of the nervous system.* 1928.
8. Golgi, C., *Sulla fina anatomia degli organi centrali del sistema nervoso: studi*. 1886: Ulrico Hoepli.
9. Bennett, M.R., *The early history of the synapse: from Plato to Sherrington.* Brain research bulletin, 1999. **50**(2): p. 95-118.
10. Foster, M.a.S., C. S., *Textbook of physiology*. 7th edition ed. Vol. 3. 1897: London:Macmillan.
11. Von Bartheld, C.S., J. Bahney, and S. Herculano-Houzel, *The search for true numbers of neurons and glial cells in the human brain: A review of 150 years of cell counting.* Journal of Comparative Neurology, 2016. **524**(18): p. 3865-3895.
12. Zeng, H. and J.R. Sanes, *Neuronal cell-type classification: challenges, opportunities and the path forward.* Nature Reviews Neuroscience, 2017. **18**(9): p. 530-546.
13. Siegel, A. and H.N. Sapru, *Essential neuroscience*. 2006: Lippincott Williams & Wilkins.
14. Gurney, K., *An introduction to neural networks*. 2018: CRC press.
15. Kandel, E.R., et al., *Principles of neural science*. Vol. 4. 2000: McGraw-hill New York.
16. Purves, D., et al., *Neurosciences*. 2019: De Boeck Supérieur.
17. Purves, D., et al., *Neurotransmission in the visceral motor system*, in *Neuroscience. 2nd edition*. 2001, Sinauer Associates.
18. Uddin, M.S., et al., *Neurochemistry of neurochemicals: messengers of brain functions.* J. Intellect. Disabil. Diagnosis Treat, 2018. **5**: p. 137-151.
19. Deutch, A.Y. and R.H. Roth, *Neurochemical systems in the central nervous system.* Neurobiology of mental illness, 1999: p. 10-25.
20. Paredes, R.M., et al., *Chemical calcium indicators.* Methods, 2008. **46**(3): p. 143-151.
21. Wei, Z., et al., *A comparison of neuronal population dynamics measured with calcium imaging and electrophysiology.* PLoS computational biology, 2020. **16**(9): p. e1008198.
22. Scanziani, M. and M. Häusser, *Electrophysiology in the age of light.* Nature, 2009. **461**(7266): p. 930-939.
23. Hodgkin, A.L. and A.F. Huxley, *A quantitative description of membrane current and its application to conduction and excitation in nerve.* Bulletin of mathematical biology, 1990. **52**: p. 25-71.
24. Johnstone, A.F., et al., *Microelectrode arrays: a physiologically based neurotoxicity testing platform for the 21st century.* Neurotoxicology, 2010. **31**(4): p. 331-350.
25. Jones, P.D., et al., *A microphysiological system for parallelized morphological and electrophysiological read-out of 3D neuronal cell culture.* Lab on a Chip, 2024. **24**(6): p. 1750-1761.

26. Kraushaar, U., E. Guenther, and D. Hess, *Addressing functional neurotoxicity using the microelectrode array (MEA).* Stem cell-derived models in toxicology, 2017: p. 293-309.
27. Molina-Martínez, B., et al., *A multimodal 3D neuro-microphysiological system with neurite-trapping microelectrodes.* Biofabrication, 2022. **14**(2): p. 025004.
28. Lee, S.Y., et al., *Optogenetic control of iPS cell-derived neurons in 2D and 3D culture systems using channelrhodopsin-2 expression driven by the synapsin-1 and calcium-calmodulin kinase II promoters.* Journal of tissue engineering and regenerative medicine, 2019. **13**(3): p. 369-384.
29. Ting, J.T., et al., *Acute brain slice methods for adult and aging animals: application of targeted patch clamp analysis and optogenetics.* Patch-clamp methods and protocols, 2014: p. 221-242.
30. Kim, C.K., A. Adhikari, and K. Deisseroth, *Integration of optogenetics with complementary methodologies in systems neuroscience.* Nature Reviews Neuroscience, 2017. **18**(4): p. 222-235.
31. Lowe, R., et al., *Transcriptomics technologies.* PLoS computational biology, 2017. **13**(5): p. e1005457.
32. Close, J.L., B.R. Long, and H. Zeng, *Spatially resolved transcriptomics in neuroscience.* Nature methods, 2021. **18**(1): p. 23-25.
33. Okaty, B.W., K. Sugino, and S.B. Nelson, *Cell type-specific transcriptomics in the brain.* Journal of Neuroscience, 2011. **31**(19): p. 6939-6943.
34. Tasic, B., *Single cell transcriptomics in neuroscience: cell classification and beyond.* Current opinion in neurobiology, 2018. **50**: p. 242-249.
35. Bagyinszky, E., V.V. Giau, and S.A. An, *Transcriptomics in Alzheimer's disease: Aspects and challenges.* International journal of molecular sciences, 2020. **21**(10): p. 3517.
36. Zhou, Y., et al., *Human and mouse single-nucleus transcriptomics reveal TREM2-dependent and TREM2-independent cellular responses in Alzheimer's disease.* Nature medicine, 2020. **26**(1): p. 131-142.
37. Fores-Martos, J., et al., *Transcriptomic and genetic associations between Alzheimer's disease, Parkinson's disease, and cancer.* Cancers, 2021. **13**(12): p. 2990.
38. Fernandes, H.J., et al., *Single-cell transcriptomics of Parkinson's disease human in vitro models reveals dopamine neuron-specific stress responses.* Cell Reports, 2020. **33**(2).
39. He, Y., et al., *An integrated transcriptomic analysis of autism spectrum disorder.* Scientific reports, 2019. **9**(1): p. 11818.
40. Quesnel-Vallières, M., et al., *Autism spectrum disorder: insights into convergent mechanisms from transcriptomics.* Nature Reviews Genetics, 2019. **20**(1): p. 51-63.
41. Pickard, B.S., *Schizophrenia biomarkers: translating the descriptive into the diagnostic.* Journal of Psychopharmacology, 2015. **29**(2): p. 138-143.
42. Roussos, P., et al., *A system-level transcriptomic analysis of schizophrenia using postmortem brain tissue samples.* Archives of general psychiatry, 2012. **69**(12): p. 1205-1213.
43. Ajalik, R.E., et al., *Human organ-on-a-chip microphysiological systems to model musculoskeletal pathologies and accelerate therapeutic discovery.* Frontiers in Bioengineering and Biotechnology, 2022. **10**: p. 846230.
44. Li, R., et al., *Microphysiological Systems: Bridging Human and Animal Research: Proceedings of a Workshop—in Brief.* 2021.
45. Roth, A. and M.-W. Berlin, *Human microphysiological systems for drug development.* Science, 2021. **373**(6561): p. 1304-1306.
46. Wang, Y.I., et al., *Multiorgan microphysiological systems for drug development: strategies, advances, and challenges.* Advanced healthcare materials, 2018. **7**(2): p. 1701000.
47. Maulana, T.I., et al., *Solid tumor-on-chip model for efficacy and safety assessment of CAR-T cell therapy.* bioRxiv, 2023: p. 2023.07. 13.548856.

48. Maulana, T.I., et al., *Breast cancer-on-chip for patient-specific efficacy and safety testing of CAR-T cells.* Cell Stem Cell, 2024.
49. Ronaldson-Bouchard, K., et al., *A multi-organ chip with matured tissue niches linked by vascular flow.* Nature Biomedical Engineering, 2022. **6**(4): p. 351-371.
50. Skardal, A., et al., *Multi-tissue interactions in an integrated three-tissue organ-on-a-chip platform.* Scientific reports, 2017. **7**(1): p. 8837.
51. Shroff, T., et al., *Studying metabolism with multi-organ chips: new tools for disease modelling, pharmacokinetics and pharmacodynamics.* Open Biology, 2022. **12**(3): p. 210333.
52. Sances, S., et al., *Human iPSC-derived endothelial cells and microengineered organ-chip enhance neuronal development.* Stem cell reports, 2018. **10**(4): p. 1222-1236.
53. Vatine, G.D., et al., *Human iPSC-derived blood-brain barrier chips enable disease modeling and personalized medicine applications.* Cell stem cell, 2019. **24**(6): p. 995-1005. e6.
54. Bernardin, A.A., et al., *Impact of neurons on patient-derived cardiomyocytes using organ-on-A-chip and iPSC biotechnologies.* Cells, 2022. **11**(23): p. 3764.
55. van der Moolen, M., et al., *Cancer-mediated axonal guidance of sensory neurons in a microelectrode-based innervation MPS.* Biofabrication, 2024. **16**(2): p. 025013.
56. Koo, Y., B.T. Hawkins, and Y. Yun, *Three-dimensional (3D) tetra-culture brain on chip platform for organophosphate toxicity screening.* Scientific reports, 2018. **8**(1): p. 2841.
57. Defranchi, E., et al., *Feasibility assessment of micro-electrode chip assay as a method of detecting neurotoxicity in vitro.* Frontiers in neuroengineering, 2011. **4**: p. 6.
58. Schneider, M.R., et al., *Applicability of organ-on-chip systems in toxicology and pharmacology.* Critical Reviews in Toxicology, 2021. **51**(6): p. 540-554.
59. de Rus Jacquet, A., et al., *The contribution of inflammatory astrocytes to BBB impairments in a brain-chip model of Parkinson's disease.* Nature Communications, 2023. **14**(1): p. 3651.
60. Park, J., et al., *Three-dimensional brain-on-a-chip with an interstitial level of flow and its application as an in vitro model of Alzheimer's disease.* Lab on a Chip, 2015. **15**(1): p. 141-150.
61. Suntsova, M.V. and A.A. Buzdin, *Differences between human and chimpanzee genomes and their implications in gene expression, protein functions and biochemical properties of the two species.* BMC genomics, 2020. **21**(Suppl 7): p. 535.
62. Batzoglou, S., et al. *Human and mouse gene structure: comparative analysis and application to exon prediction*. in *Proceedings of the fourth annual international conference on Computational molecular biology*. 2000.
63. Heikkilä, T.J., et al., *Human embryonic stem cell-derived neuronal cells form spontaneously active neuronal networks in vitro.* Experimental neurology, 2009. **218**(1): p. 109-116.
64. Ylä-Outinen, L., et al., *Three-dimensional growth matrix for human embryonic stem cell-derived neuronal cells.* Journal of tissue engineering and regenerative medicine, 2014. **8**(3): p. 186-194.
65. Takahashi, K., et al., *Induction of pluripotent stem cells from adult human fibroblasts by defined factors.* cell, 2007. **131**(5): p. 861-872.
66. Nakagawa, M., et al., *Generation of induced pluripotent stem cells without Myc from mouse and human fibroblasts.* Nature biotechnology, 2008. **26**(1): p. 101-106.
67. Pamies, D., et al., *A human brain microphysiological system derived from induced pluripotent stem cells to study neurological diseases and toxicity.* Altex, 2017. **34**(3): p. 362.
68. Brown, J.A., et al., *Metabolic consequences of inflammatory disruption of the blood-brain barrier in an organ-on-chip model of the human neurovascular unit.* Journal of neuroinflammation, 2016. **13**: p. 1-17.
69. Volpato, V. and C. Webber, *Addressing variability in iPSC-derived models of human disease: guidelines to promote reproducibility.* Disease models & mechanisms, 2020. **13**(1): p. dmm042317.

70. Pan, L., et al., *Propagation of action potential activity in a predefined microtunnel neural network.* Journal of neural engineering, 2011. **8**(4): p. 046031.
71. Peyrin, J.-M., et al., *Axon diodes for the reconstruction of oriented neuronal networks in microfluidic chambers.* Lab on a Chip, 2011. **11**(21): p. 3663-3673.
72. Renault, R., et al., *Combining microfluidics, optogenetics and calcium imaging to study neuronal communication in vitro.* PloS one, 2015. **10**(4): p. e0120680.
73. LaPlaca, M.C., et al., *Three-dimensional neuronal cultures.* Methods in bioengineering: 3D tissue engineering, 2010: p. 187-204.
74. Kim, Y.H., et al., *A 3D human neural cell culture system for modeling Alzheimer's disease.* Nature protocols, 2015. **10**(7): p. 985-1006.
75. Tekin, H., et al., *Effects of 3D culturing conditions on the transcriptomic profile of stem-cell-derived neurons.* Nature Biomedical Engineering, 2018. **2**(7): p. 540-554.
76. Chandrasekaran, A., et al., *Comparison of 2D and 3D neural induction methods for the generation of neural progenitor cells from human induced pluripotent stem cells.* Stem cell research, 2017. **25**: p. 139-151.
77. Jentsch, L.-V., *Novel neuro-microphysiological system (nMPS) for multiple characterisations of 3D neuronal networks co-cultured with astrocytes and microglia*. 2022, Universität Tübingen.
78. Molina Martinez, B., *Development of a novel 3D microphysiological system for functional and morphological assessment of neuronal networks*, in *Biologie*. 2022, University of Tuebingen: Tuebingen.
79. Lancaster, M.A. and J.A. Knoblich, *Generation of cerebral organoids from human pluripotent stem cells.* Nature protocols, 2014. **9**(10): p. 2329-2340.
80. Bagley, J.A., et al., *Fused cerebral organoids model interactions between brain regions.* Nature methods, 2017. **14**(7): p. 743-751.
81. Jo, J., et al., *Midbrain-like organoids from human pluripotent stem cells contain functional dopaminergic and neuromelanin-producing neurons.* Cell stem cell, 2016. **19**(2): p. 248-257.
82. Tieng, V., et al., *Engineering of midbrain organoids containing long-lived dopaminergic neurons.* Stem cells and development, 2014. **23**(13): p. 1535-1547.
83. Smits, L.M. and J.C. Schwamborn, *Midbrain organoids: a new tool to investigate Parkinson's disease.* Frontiers in Cell and Developmental Biology, 2020. **8**: p. 359.
84. Takemuro, T., et al., *Polydimethylsiloxane microfluidic films for in vitro engineering of small-scale neuronal networks.* Japanese Journal of Applied Physics, 2020. **59**(11): p. 117001.
85. Bae, M., et al., *Microphysiological systems for neurodegenerative diseases in central nervous system.* Micromachines, 2020. **11**(9): p. 855.
86. Blau, A., et al., *Flexible, all-polymer microelectrode arrays for the capture of cardiac and neuronal signals.* Biomaterials, 2011. **32**(7): p. 1778-1786.
87. Holloway, P.M., et al., *Advances in microfluidic in vitro systems for neurological disease modeling.* Journal of Neuroscience Research, 2021. **99**(5): p. 1276-1307.
88. Johnson, B.N., et al., *3D printed nervous system on a chip.* Lab on a Chip, 2016. **16**(8): p. 1393-1400.
89. Nelson, M.D., N. Ramkumar, and B.K. Gale, *Flexible, transparent, sub-100 μm microfluidic channels with fused deposition modeling 3D-printed thermoplastic polyurethane.* Journal of Micromechanics and Microengineering, 2019. **29**(9): p. 095010.
90. McDonald, M., et al., *A mesh microelectrode array for non-invasive electrophysiology within neural organoids.* Biosensors and Bioelectronics, 2023. **228**: p. 115223.
91. Park, Y., et al., *Three-dimensional, multifunctional neural interfaces for cortical spheroids and engineered assembloids.* Science advances, 2021. **7**(12): p. eabf9153.
92. Kaech, S. and G. Banker, *Culturing hippocampal neurons.* Nature protocols, 2006. **1**(5): p. 2406-2415.
93. Poindron, P., P. Piguet, and E. Förster, *New methods for culturing cells from nervous tissues*. Vol. 1. 2005: Karger Medical and Scientific Publishers.

94. Garcia-Agudo, L.F., et al., *Genetically induced brain inflammation by Cnp deletion transiently benefits from microglia depletion.* The FASEB Journal, 2019. **33**(7): p. 8634-8647.
95. Reinhardt, P., et al., *Derivation and expansion using only small molecules of human neural progenitors for neurodegenerative disease modeling.* PloS one, 2013. **8**(3): p. e59252.
96. Quiroga, R.Q., Z. Nadasdy, and Y. Ben-Shaul, *Unsupervised spike detection and sorting with wavelets and superparamagnetic clustering.* Neural Comput, 2004. **16**(8): p. 1661-87.
97. Cotterill, E., et al., *A comparison of computational methods for detecting bursts in neuronal spike trains and their application to human stem cell-derived neuronal networks.* Journal of neurophysiology, 2016. **116**(2): p. 306-321.
98. Legendy, C. and M. Salcman, *Bursts and recurrences of bursts in the spike trains of spontaneously active striate cortex neurons.* Journal of neurophysiology, 1985. **53**(4): p. 926-939.
99. Suzumura, A. and K. Ikenaka, *Neuron-glia interaction in neuroinflammation*. Vol. 7. 2013: Springer.
100. Lindahl, P. and K. Öberg, *The effect of rotenone on respiration and its point of attack.* Experimental Cell Research, 1961. **23**(2): p. 228-237.
101. Liu, D.D., et al., *Purification and characterization of human neural stem and progenitor cells.* Cell, 2023. **186**(6): p. 1179-1194. e15.
102. Tukker, A.M., et al., *Mixture effects of tetrodotoxin (TTX) and drugs targeting voltage-gated sodium channels on spontaneous neuronal activity in vitro.* Toxicology Letters, 2023. **373**: p. 53-61.
103. Li, Q. and B.D. Burrell, *CNQX and AMPA inhibit electrical synaptic transmission: a potential interaction between electrical and glutamatergic synapses.* Brain research, 2008. **1228**: p. 43-57.
104. Jan, L.Y. and Y.N. Jan, *Voltage-gated potassium channels and the diversity of electrical signalling.* The Journal of physiology, 2012. **590**(11): p. 2591-2599.
105. Bisbal, M. and M. Sanchez, *Neurotoxicity of the pesticide rotenone on neuronal polarization: a mechanistic approach.* Neural Regeneration Research, 2019. **14**(5): p. 762-766.
106. Hay, M., et al., *Clinical development success rates for investigational drugs.* Nature biotechnology, 2014. **32**(1): p. 40-51.
107. Centeno, E.G., H. Cimarosti, and A. Bithell, *2D versus 3D human induced pluripotent stem cell-derived cultures for neurodegenerative disease modelling.* Molecular neurodegeneration, 2018. **13**: p. 1-15.
108. Hopkins, A.M., et al., *3D in vitro modeling of the central nervous system.* Progress in neurobiology, 2015. **125**: p. 1-25.
109. Edmondson, R., et al., *Three-dimensional cell culture systems and their applications in drug discovery and cell-based biosensors.* Assay and drug development technologies, 2014. **12**(4): p. 207-218.
110. Antoni, D., et al., *Three-dimensional cell culture: a breakthrough in vivo.* International journal of molecular sciences, 2015. **16**(3): p. 5517-5527.
111. Keller, D., C. Erö, and H. Markram, *Cell densities in the mouse brain: a systematic review.* Frontiers in neuroanatomy, 2018. **12**: p. 83.
112. Grivennikova, V.G., et al., *Interaction of the mitochondrial NADH-ubiquinone reductase with rotenone as related to the enzyme active/inactive transition.* Biochimica et Biophysica Acta (BBA)-Bioenergetics, 1997. **1319**(2-3): p. 223-232.
113. Keane, P., et al., *Mitochondrial dysfunction in Parkinson' s disease.* Parkinson's disease, 2011. **2011**(1): p. 716871.
114. Terron, A., et al., *An adverse outcome pathway for parkinsonian motor deficits associated with mitochondrial complex I inhibition.* Archives of Toxicology, 2018. **92**: p. 41-82.

115. Reynolds, B.A. and S. Weiss, *Generation of neurons and astrocytes from isolated cells of the adult mammalian central nervous system.* science, 1992. **255**(5052): p. 1707-1710.
116. Reynolds, B.A. and S. Weiss, *Clonal and population analyses demonstrate that an EGF-responsive mammalian embryonic CNS precursor is a stem cell.* Developmental biology, 1996. **175**(1): p. 1-13.
117. Chiaradia, I. and M.A. Lancaster, *Brain organoids for the study of human neurobiology at the interface of in vitro and in vivo.* Nature Neuroscience, 2020. **23**(12): p. 1496-1508.
118. Inoue, H., et al., *iPS cells: a game changer for future medicine.* The EMBO journal, 2014. **33**(5): p. 409-417.
119. Yamanaka, S., *Induced pluripotent stem cells: past, present, and future.* Cell stem cell, 2012. **10**(6): p. 678-684.
120. Grenier, K., J. Kao, and P. Diamandis, *Three-dimensional modeling of human neurodegeneration: brain organoids coming of age.* Molecular psychiatry, 2020. **25**(2): p. 254-274.
121. Moors, M., et al., *Human neurospheres as three-dimensional cellular systems for developmental neurotoxicity testing.* Environmental health perspectives, 2009. **117**(7): p. 1131-1138.
122. Cosset, E., et al., *Human neural organoids for studying brain cancer and neurodegenerative diseases.* JoVE (Journal of Visualized Experiments), 2019(148): p. e59682.
123. Fellin, T., *Communication between neurons and astrocytes: relevance to the modulation of synaptic and network activity.* Journal of neurochemistry, 2009. **108**(3): p. 533-544.
124. Halassa, M.M. and P.G. Haydon, *Integrated brain circuits: astrocytic networks modulate neuronal activity and behavior.* Annual review of physiology, 2010. **72**: p. 335-355.
125. Perea, G., M. Navarrete, and A. Araque, *Tripartite synapses: astrocytes process and control synaptic information.* Trends in neurosciences, 2009. **32**(8): p. 421-431.
126. Bell, H., et al., *The development of necrosis and apoptosis in glioma: experimental findings using spheroid culture systems.* Neuropathology and applied neurobiology, 2001. **27**(4): p. 291-304.
127. *In vitro MEA-Systems from Multi Channel Systems*. [cited 2024 26.06.2024]; Available from: https://www.multichannelsystems.com/products/vitro-mea-systems.
128. *MEA Plates from Axion BioSystems*. [cited 2024 26.06.2024]; Available from: https://www.axionbiosystems.com/resources/product-brochure/mea-plates-brochure.
129. *MEA Systems from MAXWELL Biosystems*. [cited 2024 26.06.2024]; Available from: https://www.mxwbio.com/products/.
130. Taylor, A.M., et al., *A microfluidic culture platform for CNS axonal injury, regeneration and transport.* Nature methods, 2005. **2**(8): p. 599-605.
131. Irons, H.R., et al., *Three-dimensional neural constructs: a novel platform for neurophysiological investigation.* Journal of neural engineering, 2008. **5**(3): p. 333.
132. Liu, R., et al., *High density individually addressable nanowire arrays record intracellular activity from primary rodent and human stem cell derived neurons.* Nano letters, 2017. **17**(5): p. 2757-2764.
133. Kobolak, J., et al., *Human induced pluripotent stem cell-derived 3D-neurospheres are suitable for neurotoxicity screening.* Cells, 2020. **9**(5): p. 1122.
134. Silva, M.C. and S.J. Haggarty, *Human pluripotent stem cell–derived models and drug screening in CNS precision medicine.* Annals of the New York Academy of Sciences, 2020. **1471**(1): p. 18-56.
135. Strong, C.E., et al., *Functional brain region-specific neural spheroids for modeling neurological diseases and therapeutics screening.* Communications Biology, 2023. **6**(1): p. 1211.

136. Pillat, M.M., et al., *Differentiated embryonic neurospheres from familial Alzheimer's Disease Model Show Innate Immune and glial cell responses.* Stem Cell Reviews and Reports, 2023. **19**(6): p. 1800-1811.
137. da Silva Siqueira, L., et al., *Neurospheres: a potential in vitro model for the study of central nervous system disorders.* Molecular Biology Reports, 2021. **48**: p. 3649-3663.
138. Iefremova, V., et al., *An Organoid-Based Model of Cortical Development Identifies Non-Cell-Autonomous Defects in Wnt Signaling Contributing to Miller-Dieker Syndrome.* Cell Reports, 2017. **19**(1): p. 50-59.
139. Ogawa, J., et al., *Glioblastoma Model Using Human Cerebral Organoids.* Cell Reports, 2018. **23**(4): p. 1220-1229.